

MANUFACTURING AND TESTING OF COMPOSITE MACHINE TOOL STRUCTURES

by

Dai Gil Lee

B.S., Seoul National University, Korea
(1975)

M.S., Korea Advanced Institute of Science, Korea
(1977)

SUBMITTED TO THE DEPARTMENT OF
MECHANICAL ENGINEERING
IN PARTIAL FULFILLMENT OF THE REQUIREMENTS
FOR THE DEGREE OF

DOCTOR OF PHILOSOPHY IN MECHANICAL ENGINEERING

at the

MASSACHUSETTS INSTITUTE OF TECHNOLOGY

June 1985

© Massachusetts Institute of Technology, 1985

Signature of Author.....
Department of Mechanical Engineering
June 28, 1985

Certified by.....
Professor Nam P. Suh
Thesis Supervisor

Accepted by.....
Professor Ain A. Sonin
Chairman, Departmental Committee on Graduate Studies
Department of Mechanical Engineering

Archives
MASSACHUSETTS INSTITUTE
OF TECHNOLOGY

OCT 02 1985

LIBRARIES

MANUFACTURING AND TESTING OF COMPOSITE MACHINE TOOL STRUCTURES

by

Dai Gil Lee

Submitted to the Department of Mechanical Engineering
on June 28, 1985 in partial fulfillment of the
requirements for the Degree of Doctor of Philosophy in
Mechanical Engineering

ABSTRACT

The important characteristics of a machine tool structure for metal cutting are high static stiffness and high damping: these ensure the production of workpieces of the required geometries with acceptable surface finish at as high a rate of production as economically feasible.

To increase static stiffness and damping as well as thermal stability, a graphite epoxy composite spindle bearing system and a composite bed structure are constructed and tested. The composite bed structure is composed of polymer concrete, epoxy adhesive and sand. The vibrational and thermal characteristics of the graphite epoxy composite spindle bearing system are compared to those of a comparable steel spindle bearing system which has the same static stiffness as the graphite epoxy composite spindle bearing system. In machining an AISI 1045 steel bar, the graphite epoxy composite spindle bearing system allowed for an increase of 23 % in the width of cut compared to that of the steel spindle bearing system, before the onset of chatter.

In order to further improve the performance of the graphite epoxy composite spindle bearing system, the dynamic characteristics of a spindle bearing system are modelled mathematically in order to determine which parameters of the machine tool affect the system performance. The mathematical model predicts the first and second natural frequencies as well as the damping at the first mode, but is less effective for predicting the damping at the second mode.

Using the mathematical model, the optimal design procedure of a spindle bearing system is developed. The optimal design procedure indicates that the graphite epoxy composite spindle bearing system is suitable for a high speed machine tool which has a small spindle nose mass, because the natural frequency of a spindle bearing system is dependent on the spindle nose mass as well as the spindle mass. Moreover, because of its zero longitudinal thermal expansion coefficient, the graphite epoxy composite spindle bearing system eliminates the need for a temperature compen-

sation mechanism found in high precision spindle bearing systems.

The static stiffness of the composite bed was 50 % higher than that of a similar cast iron bed using a box type rather than an I beam type of bed structure. The damping of the composite bed increased more than 50 % over that of the cast iron bed, and the natural frequency of the composite bed was also increased significantly.

Thesis supervisor : Nam P. Suh
Title : Professor of Mechanical Engineering

ACKNOWLEDGEMENTS

I would like to express my gratitude to Professor Nam P. Suh for his supervision of this research and for his interest and encouragement. I am also indebted to the doctoral committee members.

The financial support of the research by Daewoo Heavy Industries in Korea is gratefully acknowledged.

I would also like to thank Dr. Hyo-Chol Sin, Dr. George Chryssolouris, Mr. Fred Cote, Ms. Theresa Harrisson and Ms. Anne Diamond.

A special thanks goes to my mother, mother-in-law and father-in-law in Korea.

A final word of thanks goes to my wife Og Heui and my son Dong Gyu, their loves, supports and endurances enabled me to keep working.

TABLE OF CONTENTS

| | Page |
|----------------------------------------------------------------------------------|------|
| TITLE PAGE | 1 |
| ABSTRACT | 2 |
| ACKNOWLEDGEMENTS | 4 |
| TABLE OF CONTENTS | 5 |
| LIST OF FIGURES | 9 |
| LIST OF TABLES | 13 |
| 1 INTRODUCTION | 14 |
| 1.1 The Nature of Problem | 14 |
| 1.2 A Review of the Previous Manufacturing Work of the Machine Tool Structure | 16 |
| 1.3 A Review of the Previous Theories of Machine Tool Structure | 19 |
| 1.4 The Scope of Research | 21 |
| 2 THE MANUFACTURING OF THE GRAPHITE EPOXY COMPOSITE SPINDLE | 27 |
| 2.1 Introduction | 27 |
| 2.2 The Graphite Epoxy Composite Used for the Spindle | 30 |
| 2.3 The Manufacturing Method of the Graphite Epoxy Composite Spindle | 35 |
| 3 THE PERFORMANCE TESTS OF THE SPINDLE BEARING SYSTEM | 46 |
| 3.1 Introduction | 46 |

| TABLE OF CONTENTS (CONTINUED) | | Page |
|-------------------------------|-----------------------------------------------------------------|------|
| 3.2 | The Bearing Preload Characteristics | 46 |
| 3.3 | The Metal Cutting Test | 50 |
| 3.3.1 | MTIRA Method | 50 |
| 3.3.2 | The Metal Cutting Test Used In This Work | 52 |
| 3.4 | The Vibration Characteristics of the Spindle Bearing Systems | 56 |
| 4 | THE ANALYSIS OF THE SPINDLE BEARING SYSTEM | 61 |
| 4.1 | Introduction | 61 |
| 4.2 | The Static Analysis | 62 |
| 4.3 | The Dynamic Analysis | 68 |
| 4.4 | The Numerical Values | 71 |
| 4.4.1 | The First Mode | 71 |
| 4.4.2 | The Second Mode | 75 |
| 4.5 | Damping Estimation | 86 |
| 4.5.1 | The Source of Damping of the Spindle Bearing System | 86 |
| 4.5.2 | The Calculation of the Damping Factor | 97 |
| 5 | THE OPTIMAL DESIGN OF A SPINDLE BEARING SYSTEM | 102 |
| 5.1 | Introduction | 102 |
| 5.2 | Optimal Design Procedure for a Spindle Bearing System | 103 |

| TABLE OF CONTENTS (CONTINUED) | | Page |
|-------------------------------|-----------------------------------------------------------------------------------|------|
| 5.2.1 | Preliminary Specifications | 103 |
| 5.2.2 | The Selection of a Lubrication Method | 104 |
| 5.2.3 | The Selection of Bearings | 106 |
| 5.2.4 | The Relationships Among the Properties of an Optimal Spindle Bearing System | 109 |
| 5.2.5 | The Calculation of the Natural Frequency of the Spindle Bearing System | 114 |
| 5.3 | The Example of the Optimal Design Procedure of a Milling Machine | 117 |
| 6 | THE MANUFACTURING OF THE COMPOSITE BED | 135 |
| 6.1 | Introduction | 135 |
| 6.2 | The Manufacturing Method of the Composite Bed Structure | 135 |
| 6.3 | The Dynamic Test Results of the Composite Bed | 141 |
| 7 | DISCUSSIONS AND CONCLUSIONS | 149 |
| | REFERENCES | 153 |
| | APPENDIX : | |
| A | Definitions of Damping Parameters | 163 |
| B | Calculation of the Material Properties of the Graphite Epoxy Composite Spindle | 165 |

TABLE OF CONTENTS (CONTINUED)

| | Page |
|----------------------------------------------------------------------------------------------------|------|
| C Calculation of the Power and Torque Capability of Adhesive Bonded Joint | 172 |
| D Properties of Hysol EA 9309.2 Adhesive | 178 |
| E Dependence of the Metal Cutting Performance on the Damping and Stiffness of a Machine Tool | 179 |
| BIOGRAPHY | 183 |

LIST OF FIGURES

| Figure | Page |
|-----------------------------------------------------------------------------------------------------|------|
| 2.1 Specific Modulus of Several Materials | 28 |
| 2.2 Steel Sleeves for Bearing Mounting and Power Transmission | 36 |
| 2.3 Steel Sleeves and Graphite Epoxy Composite Shaft Bonded by Epoxy Adhesive | 37 |
| 2.4 Final Shape of the Graphite Epoxy Composite Shaft | 39 |
| 2.5 Five Angular Contact Bearings Used in the Spindle Bearing System | 40 |
| 2.6 Five Angular Contact Ball bearings, Bearing Accessories and Spindle Case | 41 |
| 2.7 Some Dimensional Characteristics of the Graphite Epoxy Composite Spindle Bearing System | 42 |
| 2.8 Preload Spring for the Spindle Bearing System | 43 |
| 2.9 Some dimensional Characteristics of the Steel Spindle Bearing System | 45 |
| 3.1 Experimental Set-up for the Metal Cutting Test of the Manufactured Spindle Bearing System | 54 |
| 3.2 Steel Bar Workpiece Used in the Metal Cutting Test | 55 |

LIST OF FIGURES (CONTINUED)

| Figure | Page |
|-----------------------------------------------------------------------------------------------------------------|------|
| 3.3 Transfer Functions of the Spindle Bearing Systems Obtained by the HP5423A Structural Dynamic Analyzer | 60 |
| 4.1 Mathematical Model of the Spindle Bearing System | 63 |
| 4.2 Damping Ratio vs. Frequency in Graphite/Epoxy [± 45] _{2s} | 87 |
| 4.3 Damping Factor Possessed by Unfilled Plasticized Polyvinyl Acetate | 87 |
| 4.4a Steel Shaft Used in the Vibration Test | 90 |
| 4.4b Steel Shaft with the Epoxy Bonded Steel Sleeves Used in the Vibration Test | 90 |
| 4.5 Graphite Epoxy Composite Shaft with the Epoxy Bonded Steel Sleeves Used in the Vibration Test | 91 |
| 4.6 Transfer Function of the Steel Shaft | 92 |
| 4.7 Transfer Function of the Steel Shaft with the Epoxy Bonded Steel Sleeves | 93 |
| 4.8 Transfer Function of the Graphite Epoxy Composite Shaft with the Epoxy Bonded Steel Sleeves | 94 |
| 5.1 Basic Principles of Bearings : (a) Angular Contact Bearing ; (b) Tapered Roller Bearing | 107 |

LIST OF FIGURES (CONTINUED)

| Figure | Page |
|-------------------------------------------------------------------------------------------------------------------------|------|
| 5.2 Relationships Between the Compliance C and the Bearing Span Length ℓ | 111 |
| 5.3 Relationships Between the Minimum Compliance C_{min} and the Optimal Bearing Span Length ℓ_o | 112 |
| 5.4 Several Limitations on the Optimal Bearing Span Length ℓ_o | 115 |
| 5.5 Schematic Drawing of the Optimally Designed Graphite Epoxy Composite Spindle Bearing System | 133 |
| 6.1 Composite Bed Structure : (a) Overview ; (b) Cross Section | 138 |
| 6.2 Composite Bed Model on Which the Graphite Epoxy Composite Spindle Bearing System is Mounted | 140 |
| 6.3 Data Acquisition System Used in Measuring the Vibration of the Composite Bed | 142 |
| 6.4 Cross Sections of the Beds : (a) Cast Iron Bed ; (b) Composite Bed | 143 |
| 6.5 Vibration Test Method of the Composite Bed | 144 |
| 6.6 Vibration of the Beds : (a) Composite Bed (0.2 lb-in Kinetic Energy) ; (b) Cast Iron Bed (0.1 lb-in Kinetic Energy) | 146 |

LIST OF FIGURES (CONTINUED)

| Figure | page |
|---------------------------------------------------------------------------------------------------------------|------|
| 6.7 Fast Fourier Transform Results of the Vibration of the Beds : (a) Composite Bed ; (b) Cast Iron Bed | 147 |
| C.1 Theoretical Model of the Epoxy Adhesive Bonded Joint | 173 |
| C.2 Shear Stress Distribution in Tubular Lap and Scarf Joints Subjected to Torque | 175 |
| E.1 Geometry of an Idealized Dynamic Cutting Process | 180 |
| E.2 Force Relationships for Vibrating Machine Tool | 180 |

LIST OF TABLES

| Table | Page |
|--------------------------------------------------------------------------------------------------------------------------------------------------------------------|------|
| 1.1 Modulus and Damping of Several Materials | 24 |
| 2.1 Some Material Properties of the Graphite Epoxy Composite Used in the Spindle | 33 |
| 4.1 Design Values of the Spindle Bearing System | 73 |
| 4.2 Frequency and Damping Data of Fig. 4.4 | 92 |
| 4.3 Frequency and Damping Data of Fig. 4.5 | 93 |
| 4.4 Frequency and Damping Data of Fig. 4.6 | 94 |
| 5.1 Maximum Speed for Oil Lubrication and Grease Lubrication | 105 |
| 5.2 Comparison of the Properties of the Manufactured and the Optimally Designed Graphite Epoxy Composite Spindle Bearing Systems | 131 |
| 5.3 Comparison of the Properties of the Optimally Designed Graphite Epoxy Composite Spindle Bearing System and the Optimally Designed Steel Spindle Bearing System | 132 |
| 6.1 Properties of Polymer Concrete | 136 |
| B.1 Young's Moduli of the Piles with Several Winding Angles | 168 |

1. INTRODUCTION

1.1 The Nature of Problem

The basic function of a machine tool is to produce a workpiece of the required geometric form with an acceptable surface finish at as high a rate of production as is economically possible [1]. High cutting speeds and feeds are essential requirements of a machine tool structure to accomplish this basic function. In fact, general purpose machine tools, CNC lathes and machining centers are designed to cope with low cutting speeds with high cutting forces as well as high cutting speeds with low cutting forces.

During the past fifty years, many new cutting tool materials have been developed, which range from high-speed cutting steels (HSS) to diamond cutting tools. These tools enabled higher and higher cutting speeds and chip removal rates, which are remarkable compared to the development of a machine tool structure. These new cutting tool materials, which are hard and usually brittle require that the machine tool structure have a high static and dynamic stiffness.

The spindle bearing system is the main source of the total cutting point compliance [2]. The other sources of compliance come from the bed, slides and joints of the machine tool structure. The compliance of the slides and joints is difficult to control in many situations.

Therefore, the machine tool structure can be stiffened through the use of proper materials for the spindle and bed even if we cannot completely control the slide and joint properties.

Self-excited vibration or chatter occurs when the width of cut or cutting speed exceeds the stability limit of the machine tool [3,4]. The chatter is a nuisance to the metal cutting process and can occur on any chip-producing machine tool. The effects of chatter are all adverse, affecting surface finish, dimensional accuracy, tool life and machine life [5]. When the machine tool is operated without any vibration or chatter, the damping of the machine tool plays no important role in machining. However, the machine tool structure has several resonant frequencies because of its continuous structural elements. If the damping is too small to dissipate the vibrational energy of the machine tool, the resonant vibration occurs when the frequency of the machining operation approaches one of the natural frequencies of the machine tool structure.

According to the theory of machine tool dynamics (See Appendix E), the maximum width of cut that can be taken without expectation of chatter is approximately proportional to the static stiffness and damping of a machine tool.

Therefore, the material for the machine tool structure should have high static stiffness and damping in its property to improve both the static and dynamic performance.

Sometimes high specific stiffness (E/ρ) is more important than stiffness to increase the natural frequency of the vibration of the machine tool structure in high speed machining [6].

The static stiffness of a machine tool can be increased by using either higher modulus material or more material in the structure of a machine tool. However, it is difficult to increase the dynamic stiffness of a machine tool with these methods because the damping of the machine tool structure cannot be increased by increasing the static stiffness. Often the most economical way of improving a machine tool with high resonance peaks is to increase the damping rather than the static stiffness even though it is not easy to increase the damping of the machine tool structure [6].

1.2 A Review of the Previous Manufacturing Work of the Machine Tool Structure

In recent years, many efforts have been made to increase the material damping of the machine tool bed structures especially in precision machining area. Cranfield Institute of Technology in England has reported the successful use of the synthetic granite material in the bed of the vertical axis precision lathe [7]. George Fisher Company in Switzerland used reinforced concrete in its NC lathe to

Increase the material damping of the bed structure [8]. There are other examples of using the polymer concrete material, which is composed of conventional concrete and several kinds of polymeric material, in the bed structure of a machine tool to exploit its better dynamic properties than those of concrete and polymeric material [9, 10].

Tuned dampers have been also used as auxiliary dampers for machine tools. Tuned dampers should be tuned whenever the machine tool mass or workpiece is changed. Moreover the mass of the auxiliary system is usually limited by dimensional considerations. This is a real limitation, because the equivalent mass of the main system is greatly influenced by the mass of the workpiece [11].

Friction damping method to increase the structural damping of a machine tool has been also attempted [12]. The principles of this damper are the selection of optimal values of tuning by analog computer simulation of regenerative chatter.

Chowdhury [13] used epoxy resin as a bonding material between structural components of a milling machine to increase joint damping. It was reported that the bonded overarm of milling machine performed much better than those of the welded and the cast iron.

Also many attempts have been made to increase the damping of the machine tool spindles [11]. The simple method used to increase the damping and static stiffness of the

bearing of a spindle was to preload the bearing. However, preloading the bearing does not always increase the damping of the bearing, while it always increases the static stiffness of the bearing [14]. Furthermore, the excessive preloading of the spindle bearing will cause the bearing failure at the start of the operation of the machine tool because the heat produced by the excessive preloaded bearing at the start makes the ununiform expansions of the bearing and spindle and may induce a very large load on the bearing.

Peters [11] has presented the viscous damper in the spindle bearing structure. The viscous damper in the spindle has very good damping characteristics, but has such undesirable characteristics as power dissipation and temperature rise in the spindle bearing structure. The power dissipation and temperature rise are very critical to the high speed bearing and the precision bearing.

Several attempts to use high damping materials in the spindle structure have been also conducted. High damping materials used in the spindle material are usually divided into two groups : organic systems and metallic systems. The high damping organic materials which have visco-elastic properties, are usually constrained between two stiff plates to induce large shear strain in the organic materials. Hammill has attempt to use this method in the spindle structure [15]. However, the visco-elastic damping coatings are easily contaminated by their environment (oil, water, etc.)

and they are useful only over limited frequency and temperature ranges. Also the manufacturing of the constrained layer is limited by the geometric and boundary conditions. Many theories of the constrained layer damping method are addressed in several papers [16-27].

Instead of visco-elastic materials, James [28] suggested using high damping metals as a spindle material. Vandeurzen [29] used high damping metals in additive layer treatment which was the similar method of the sandwiched visco-elastic damping coating. However, this method is not very effective because even the highest damping metal has less damping compared to other polymeric material. Furthermore, this method is limited by the geometric constraint, lubrication and bearing mountings.

A successful use of anaerobic adhesive, which cures by polymerization in the absence of air by cross-linking of monomer chains to form a hard structure, to bond bearing and spindle was reported [30]. This method increases much the static stiffness of the spindle bearing system, but decreases a little the dynamic stiffness because bonding the bearings and the spindle with adhesive decreases the loose joint surfaces.

1.3 A Review of the Previous Theories of Machine Tool Structure

Many investigators tried to determine the static and dynamic compliance between tool and workpiece, which governs cutting accuracy [2]. Tool-workpiece compliance is the sum of the compliances of all components in the tool workpiece loop. The components are composed of bearings, workpiece, spindle, bed and several joints. Several attempts also have been made to analyze the dynamics of the machine tool structure incorporating the properties of the joint dynamics [31]. However, none of these theories clearly predict the dynamic performance of a machine tool in the design stage.

Japanese researchers [32] used finite element method to determine the stiffness of the machine tool structure. This method requires the data of the joint to analyze the stiffness of the spindle bearing system. However, the theories of joint mechanics [33-41] are seldom complete rather than the empirical observation of a particular joint although many researchers have attempted to predict it.

Sometimes the analysis was concentrated only on the spindle bearing structure of a machine tool because the spindle bearing structure is the largest single source of compliance among the components of the machine tool.

Indeed, the dynamic analysis of the spindle bearing system should be completed before proceeding further to the analysis of the overall machine tool structure.

Shuzi [42] analyzed statically the cutting point compliance of the spindle bearing system and suggested the

optimal bearing span length. Singhvi [43] also presented the data of optimal design of spindle bearing system based on static analysis. However, the dynamic properties of the spindle bearing system is different from the static properties and the statically better spindle bearing system is not always the dynamically better spindle bearing system [6,30]. Some looseness in bearing or joint might improve dynamic stiffness even though it lowers the static stiffness [2,30]. Therefore, the analysis of the spindle bearing structure should be performed dynamically rather than statically.

The dynamic analysis of the spindle bearing system is also very difficult because the data of the stiffness and damping of the bearing is very few [2,14]. If the chuck or workpiece is engaged in the spindle, the analysis becomes even more complicated because of the increase of joint surfaces[44]. Some investigators tried to model and predict the dynamic characteristics of the spindle bearing system [2], but the result is not as satisfactory as can be used in predicting the resonant frequencies and the damping of the spindle bearing system in the design stage.

1.4 The Scope of Research

As reviewed in the previous sections, the spindle bearing system and the bed are the main sources of the total

cutting point compliance.

The spindle bearing system of a machine tool usually has two dominant natural frequencies: one is the rigid body motion of a spindle in bearings and the other is the bending motion of a spindle in the bearing span (See Fig. 3.3). The natural frequency of the bending of a spindle bearing system is usually higher than that of the rigid body motion because the weakest stiffness usually comes from bearings. From this fact, the natural frequency of the rigid body motion of a spindle should be increased in order to obtain chatter free machining performance. The damping of the rigid body motion of a spindle comes largely from bearings while the damping of the bending motion of a spindle comes from joints and slides of bearing mountings. Also some damping of the bending motion comes from material damping of the spindle. Since the damping of a bearing in lateral motion is proportional to the frequency (See Chapter 4), high frequency range for the rigid body motion is desired in order to increase damping.

The spindle material should have high specific stiffness to increase the natural frequency of the rigid body motion of a spindle. If the spindle material has high damping, it will increase the damping of the bending motion of the spindle bearing system. Spindles with high damping properties are especially important for high speed bearings such as magnetic or air bearings. This is because high

speed bearings have low damping characteristics. The spindle material should also have low thermal expansion coefficient for machining accuracy and bearing preload.

The requirement of high specific stiffness material in the bed structure of a machine tool is not as critical as the requirement of damping, because the bed structure can be stiffened by changing the design of the bed or by using more material in the bed structure. Such alterations are feasible because the weight and space limitations of bed structures are not so strict. In fact, it is more cost effective to increase the stiffness of a structure which is composed of high damping material than to increase the damping of a structure which is composed of high stiffness material.

Usually the specific stiffness of a conventional material is not high. Also, it is difficult to increase both the stiffness and the damping of a conventional material because statically stiff conventional material usually has low damping and vice versa (See Table 1.1).

Some filamentary composite materials, on the other hand, can be made to have both high specific stiffness and damping. This is normally done with composite materials that is composed of two materials : very high modulus fiber and high damping polymeric matrix material. The resulting performance will reflect the best characteristics of each material.

Other composite materials which are used in the bed

Table 1.1 Modulus and Damping of Several Materials

| Material | Young's Modulus | Damping Factor (Appendix A) |
|------------------|--------------------------|-----------------------------|
| 1018 Steel | 207 GPa (30 Mpsi) | 0.0001 (500 Hz) [46,47] |
| 1018 Steel | 207 GPa (30 Mpsi) | 0.001 (100 Hz) [46,47] |
| Cast Iron | 172-193 GPa (25-28 Mpsi) | 0.003 [48] |
| Aluminum | 69 GPa (10 Mpsi) | 0.002 (100 Hz) [47] |
| Aluminum | 69 GPa (10 Mpsi) | 0.0002 (500 Hz) [47] |
| Graphite Epoxy | 138-207 GPa (20-30 Mpsi) | 0.01 [49] |
| PVC | 2.1 GPa (0.3 Mpsi) | 0.2 [27] |
| Polymer Concrete | 35 GPa (5.3 Mpsi) | 0.02 |

structure can be made to have high damping and moderate specific stiffness by mixing high damping material with moderate stiffness material. The product of the damping and the specific stiffness of such composite materials is usually larger than that of conventional materials.

One objective of this study is to manufacture and test the composite spindle of a machine tool. From the many composite materials available, high modulus graphite epoxy composite material [45] has been selected as a spindle material. The high modulus graphite epoxy composite material has very high specific stiffness, high damping and near-zero thermal expansion coefficient in longitudinal direction. The static and dynamic model of the spindle bearing system is investigated and the result of dynamic analysis is compared to the test result. Also the optimal design method of the spindle bearing system is developed using the static and dynamic model.

The other objective of this study is to manufacture and test the composite bed composed of polymer concrete [10] and some damping material.

The manufacturing method of the graphite epoxy composite spindle bearing system is explained in chapter 2. In chapter 3, the metal cutting test results and the metal cutting method used are explained. And the thermal stability of the graphite spindle bearing system is discussed. Also the vibration test results, which are performed by the

structural dynamic analyzer, are presented in this chapter. In chapter 4, the results of the static and dynamic analysis of the spindle bearing system are explained. The optimal design method of the spindle bearing system is presented in chapter 5. The manufacturing method and the dynamic test results of the polymer concrete bed are explained in chapter 6. Finally, based on these investigations, discussions and conclusions are given in chapter 7.

2. THE MANUFACTURING OF THE GRAPHITE EPOXY COMPOSITE SPINDLE

2.1 Introduction

In recent years, graphite epoxy composite has been used widely as a structural element because it has better properties than conventional materials [50]. High modulus graphite epoxy composite has a specific modulus of elasticity (E/ρ) that is 4 times greater than steel (See Fig. 2.1). To utilize this superior property, many parts of commercial and military airplanes are made of graphite epoxy composite. A recent report by MacDonnel Douglas [51] indicates that the Company uses the graphite epoxy composite in more than 25 % of the structure of Harrier Two. As a result, the plane which can land or take off vertically, can go twice as far or carry twice as much as earlier models could. Another example is the Sikorsky helicopter whose structure is made of graphite and Kevlar epoxy composite [52].

Since the natural frequency of the flexural vibration of a shaft is proportional to the square root of the specific modulus of elasticity [53], the natural frequency of the flexural vibration of the graphite epoxy composite shaft can be more than twice that of a steel shaft of the same flexural rigidity.

Successful attempts have been made to replace the steel

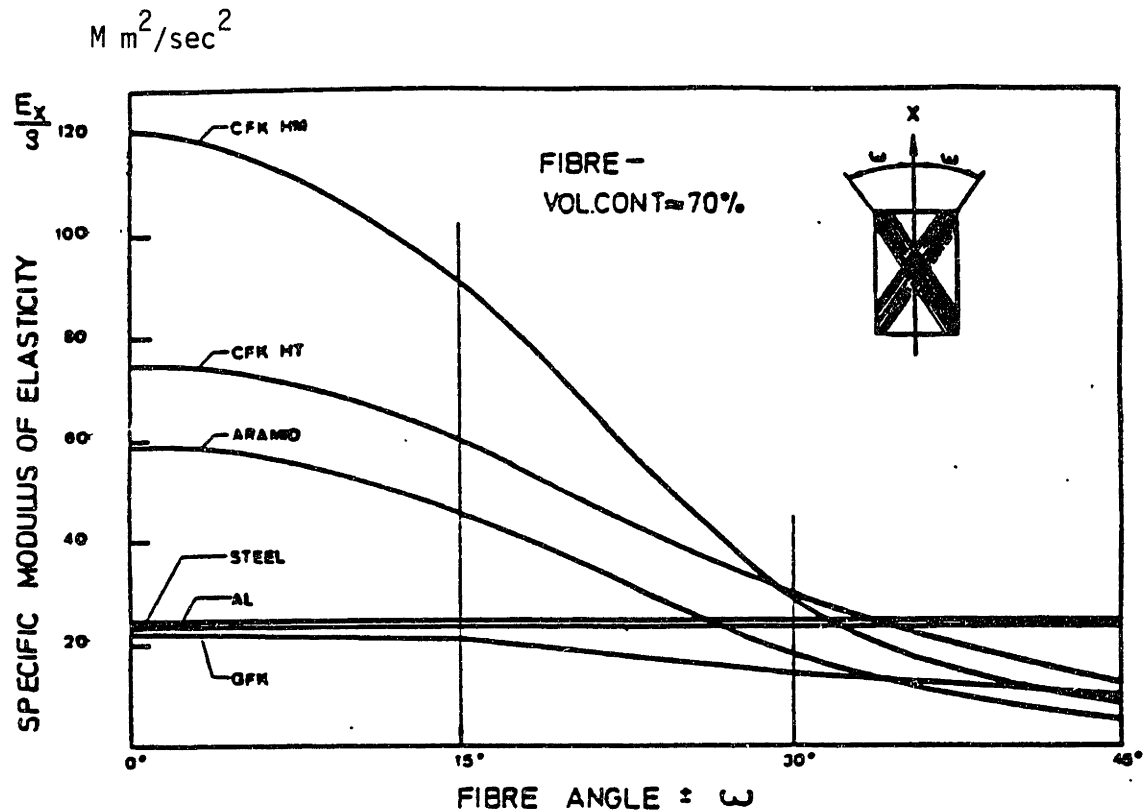


Fig. 2.1 Specific Modulus of Several Materials [45]

drive shaft of an automobile with a graphite epoxy composite shaft [45]. Most cars have drive shafts within about 1.25 m and 1.75 m of length. Assuming a limiting diameter of 7 cm and length of 1.5 m, the fundamental natural frequency of the flexural vibration of a steel or aluminum drive shaft is about 7,200 rpm, which is just the critical limit of the rotational speed of an automobile. Therefore, in this case the usual two-piece drive shaft is the only solution to avoid the flexural vibrations. If we use the graphite epoxy composite shaft for the drive shaft, we can increase the fundamental natural frequency of the flexural vibration to 14,000 rpm, which is far beyond the critical frequency of an automobile. Moreover, we can eliminate the middle bearing and additional yokes to reduce weight and cost.

In the metal cutting operations, the self-excited vibration or chatter phenomenon, which is induced by the flexural vibration of the spindle, is similar to the drive shaft vibration of an automobile. If the frequency of the cutting operation, which is usually originated from a regenerative chatter, reaches the natural frequency of the flexural vibration of the spindle, the self-excited vibration occurs. Therefore, the self-excited vibration which occurs at lower natural frequency can be eliminated if we make the spindle of a machine tool with a graphite epoxy composite shaft.

The graphite epoxy composite is known as a good materi-

al in high speed as well as intermittently operating machine components. Because of its light weight and low rotational moment of inertia, the acceleration and deceleration time can be reduced significantly. The decrease of the acceleration time and deceleration time will obviously increase the productivity in automated factories.

The high damping characteristics of graphite epoxy composite, whose damping is about 10 times higher than that of steel (See Table 1.1), has been taken advantage of in many fields. Tennis rackets and fishing rods are manufactured using graphite epoxy composite because of its high damping property as well as its high specific modulus. Also golf club shafts, sailboat components, bicycles (one of which was used by an U.S. athlete who won the gold medal in the 1984 L.A. Olympics), skis and etc. are manufactured using the graphite epoxy composite [54].

In spite of these superior properties, no attempt has been made to use the graphite epoxy composite as the spindle of a machine tool. Therefore, it is determined as a material for a machine tool spindle.

2.2 The Graphite Epoxy Composite Used for the Spindle

The graphite fiber used for the spindle is high modulus Cellon G-50 : its tensile modulus is 50 Mpsi. The epoxy

used in making the composite is Fiberite 9481. The tensile modulus of the composite, when 40 % epoxy resin is added, is 30 Mpsi.

This unidirectional graphite epoxy composite material has a large Young's modulus in the longitudinal direction, but small shear modulus. If the shear modulus is small, the power and torque transmission capabilities of the shaft which is made of the graphite epoxy composite material, are also small. In addition, the adhesive bonded joint described in Section 2.3 has limited power and torque transmission capabilities (See Appendix B and C).

To improve the power and torque transmission capabilities, the graphite epoxy fiber should be wound at some angle from the longitudinal direction of the spindle. A winding angle which is greater than 15 degrees is not desirable because the longitudinal Young's modulus drops very quickly for the winding angles in excess of this value (See Fig. 2.1).

If we select $[\pm 15]_s$ as the winding angle of the graphite fiber, the longitudinal Young's modulus decreases from 30 Mpsi to 23.2 Mpsi and the shear modulus increases from 0.65 Mpsi to 2.4 Mpsi. Also the thermal expansion coefficient changes from $-0.3 \times 10^{-6} / ^\circ\text{F}$ to $-1.1 \times 10^{-6} / ^\circ\text{F}$.

If we select $[\pm 10]_s$ as the winding angle of the graphite fiber, the longitudinal Young's modulus is 27.3 Mpsi and the shear modulus is 1.49 Mpsi. The thermal expansion

sion coefficient is then $-0.68 \times 10^{-6} / ^\circ\text{F}$.

From the above results, we can see that the shear modulus and absolute thermal expansion coefficient both decrease as the winding angle of the graphite fiber decreases, but the longitudinal Young's modulus increases. If the shear modulus is too small, the natural frequency of bending of the graphite epoxy composite shaft decreases because of shear deformation (See Chapter 4).

For the machine tool spindle application, the composite is pre-preg laid-up with a winding angle of $[\pm 15]^\circ$ s from the axis of the shaft in order to obtain a moderate shear modulus without severely impairing the longitudinal Young's modulus. Table 2.1 shows the composite properties calculated by classical composite laminate theory (See Appendix B for details).

Since the spindle of a machine tool is designed for stiffness rather than strength, it is usually under low levels of stress. Therefore, a winding angle of $[\pm 10]^\circ$ s may be used in future applications in order to increase the longitudinal Young's modulus and decrease the absolute value of the thermal expansion coefficient. In using a smaller winding angle, the decrease of the bending natural frequency due to shear deformation should be checked despite the fact that the increase in the longitudinal Young's modulus may offset some part of the decrease of the natural frequency of bending.

Table 2.1 Some Material Properties of the Graphite Epoxy Composite Used in the Spindle

(Fiber: Celion G-50, Resin: Fiberite 9481)

| Ply Values | Laminate Values | Steel Values |
|--------------------------------------------------------|-----------------------------------------------------------------|----------------------------------------------|
| $\alpha_{11}^* = -0.3 \times 10^{-6}/^{\circ}\text{F}$ | $\alpha_{11}^{\text{L}} = -1.1 \times 10^{-6}/^{\circ}\text{F}$ | |
| $\alpha_{22}^* = 14 \times 10^{-6}/^{\circ}\text{F}$ | $\alpha_{22}^{\text{L}} = 12.4 \times 10^{-6}/^{\circ}\text{F}$ | |
| $\alpha_{12}^* = 0$ | $\alpha_{12}^{\text{L}} = 0$ | $\alpha = 7 \times 10^{-6}/^{\circ}\text{F}$ |
| $G_{\text{LT}} = 0.65 \times 10^6 \text{ psi}$ | $G_{\text{LT}}^{\text{L}} = 2.4 \times 10^6 \text{ psi}$ | $G = 10 \times 10^6 \text{ psi}$ |
| $E_{\text{L}} = 30 \times 10^6 \text{ psi}$ | $E_{\text{L}}^{\text{L}} = 23.2 \times 10^6 \text{ psi}$ | |
| $E_{\text{T}} = 1.14 \times 10^6 \text{ psi}$ | $E_{\text{T}}^{\text{L}} = 1.18 \times 10^6 \text{ psi}$ | $E = 30 \times 10^6 \text{ psi}$ |
| $\rho = 1.6 \text{ g/cm}^3$ | $\rho = 1.6 \text{ g/cm}^3$ | $\rho = 7.8 \text{ g/cm}^3$ |

+ The subscript L refers to longitudinal direction,
 subscript T refers to transverse direction,
 superscript L refers to laminate values

* refers to ply values

α = the thermal expansion coefficient

ρ = the density

E = the Young's modulus

G = the shear modulus

Data on material damping is scarce and there are even discrepancies among them. Moreover, the method of measuring damping is not well established. The difficulties in damping measurement are isolating the air damping and the joint damping. The fact that the material damping is dependent on the stress level and the vibrational frequency makes damping measurement even more difficult.

Recently, Vorlicek [47] measured the damping property of the graphite epoxy composite in a vacuum to eliminate air damping. In order to remove the clamping damping of the specimen, he used the freely falling specimen in a vacuum after giving impulse to the center of the specimen to excite the fundamental mode of the vibration of specimen. The vibrational signal was picked up by a strain gage which limits the frequency below 100 Hz.

Crawley [49] improved the experimental apparatus of Vorlicek and measured the damping factor to be about 0.01 of the graphite epoxy composite. Crawley also showed that the damping of the graphite epoxy composite was almost constant with respect to frequency.

The damping of graphite epoxy composites comes largely from epoxy because the graphite fiber essentially has no damping. The damping characteristics of epoxy or polymeric material is not sensitive to the frequency applied compared to the inorganic materials [55]. This fact might explain the independence of the damping of the graphite epoxy compo-

site on the frequency applied. Therefore, we can estimate the damping factor, which is twice the damping ratio (See Appendix A), as about 0.01. The damping properties of the graphite epoxy composite is more extensively discussed in Chapter 4.

The material damping of metals is a function of frequency[46,47]. The damping factors of steel and cast iron usually decrease with frequency and are less than 0.001 when the frequency is greater than 100 Hz. Therefore, the damping factor of the graphite epoxy composite is at least 10 times greater than that of the cast iron or steel where the vibrational frequency is higher than 100 Hz.

2.3 The Manufacturing Method of the Graphite Epoxy Composite Spindle

Two steel sleeves for bearing mounting and power transmission were manufactured (See Fig. 2.2). The graphite epoxy composite shaft was manufactured by the pre-preg lay-up method and was cured at 250°F. After grinding the graphite epoxy composite to the final dimensions, the two steel sleeves and the graphite epoxy composite shaft were bonded together by epoxy adhesive (See Fig. 2.3).

After bonding the graphite epoxy composite shaft to the two steel sleeves, the outer surfaces of the steel sleeves

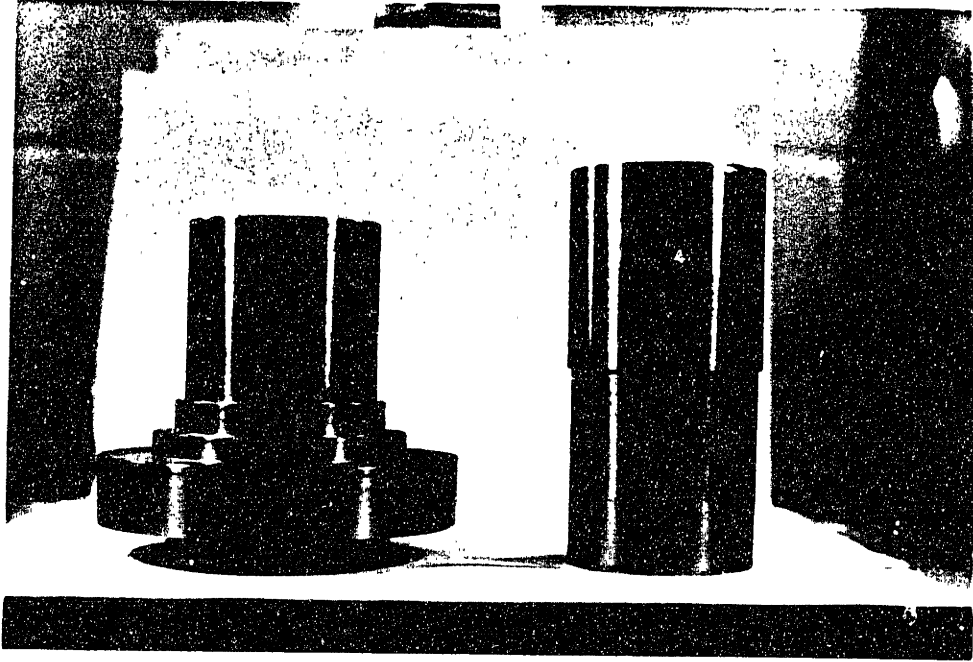


Fig. 2.2 Steel Sleeves for Bearing Mounting and Power Transmission

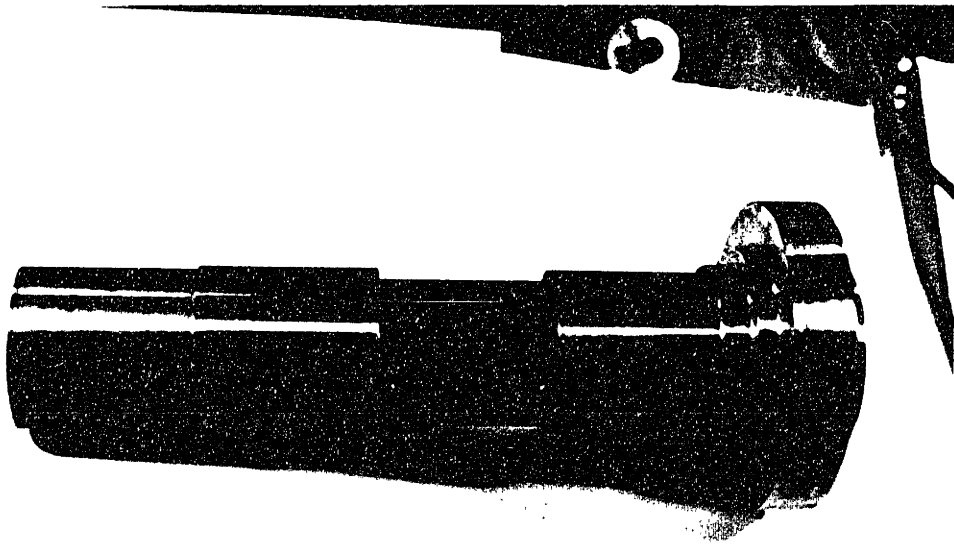


Fig. 2.3 Steel Sleeves and Graphite Epoxy Composite Shaft Bonded by Epoxy Adhesive

were ground to match the dimensions of the bearings (See Fig. 2.4). Five angular contact ball bearings, which were manufactured by SNFA, were mounted on the surfaces of the steel sleeves (See Fig. 2.5, Fig. 2.6). The specification of the bearings is SEB 70, which has 70 mm bearing bore diameter and 15 degree contact angle.

Three bearings were installed in the front of the spindle. Two of them were installed tandemly and one of them was installed as a back-to-back to resist a back thrust (See Fig. 2.7).

Two bearings were installed in the rear of the spindle tandemly in the opposite direction of the tandemly installed front bearing. The average preload of each tandemly installed bearing is 180 lb. Therefore, the total preload of the bearings is 360 lb, which was produced by compressing 3/16 inch of the preload springs (See Fig. 2.8).

The spindle bearing assembly was sealed in the spindle case after grease lubrication. After this operation, the spindle bearing system was dynamically balanced. The proper mounting of the bearings was checked by measuring the bearing temperature increase after running one hour at 2,000 rpm.

The weak part of the composite spindle is the epoxy bonded area. Therefore, a new bonding method was devised to ensure bonding reliability. As shown in Fig. 2.7, each steel sleeve has a step on its inner surface. One step has



Fig. 2.4 Final Shape of the Graphite Epoxy Composite Spindle

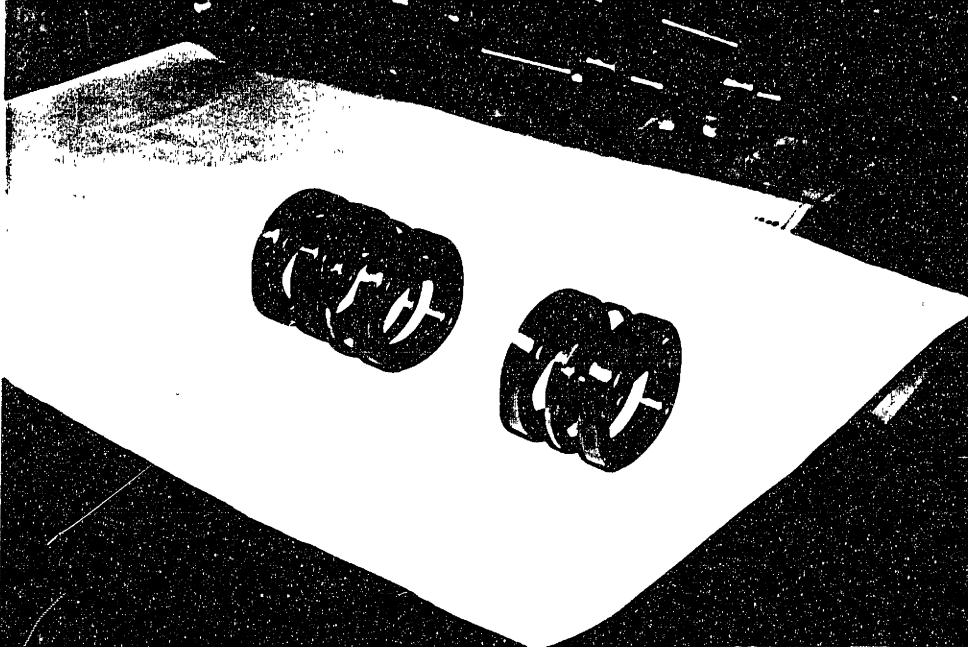


Fig. 2.5 Five Angular Contact Ball Bearings Used in the Spindle Bearing System

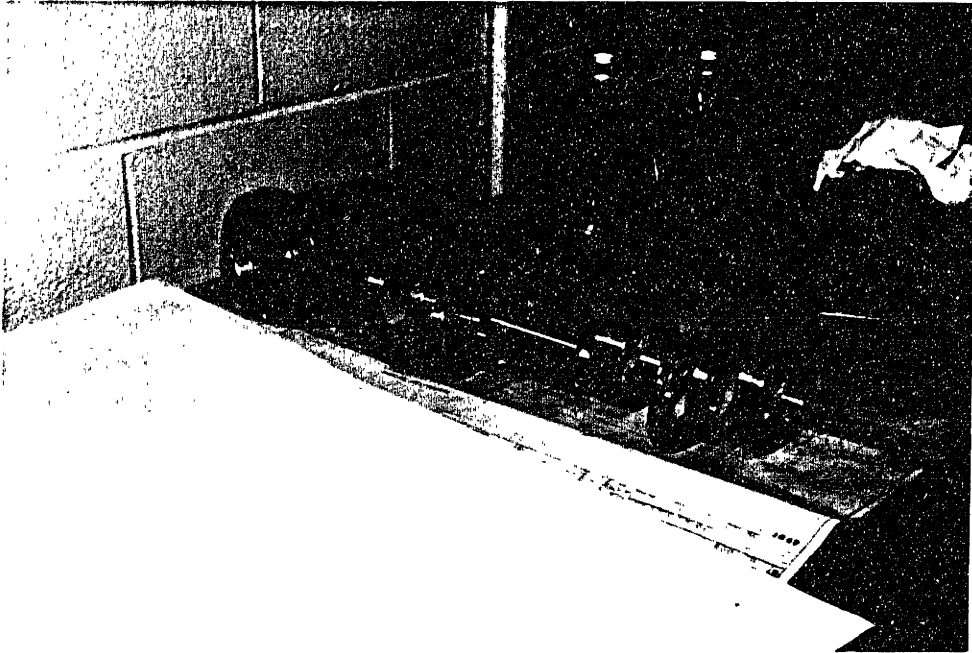


Fig. 2.6 Five Angular Contact Ball Bearings, Bearing Accessories and Spindle Case

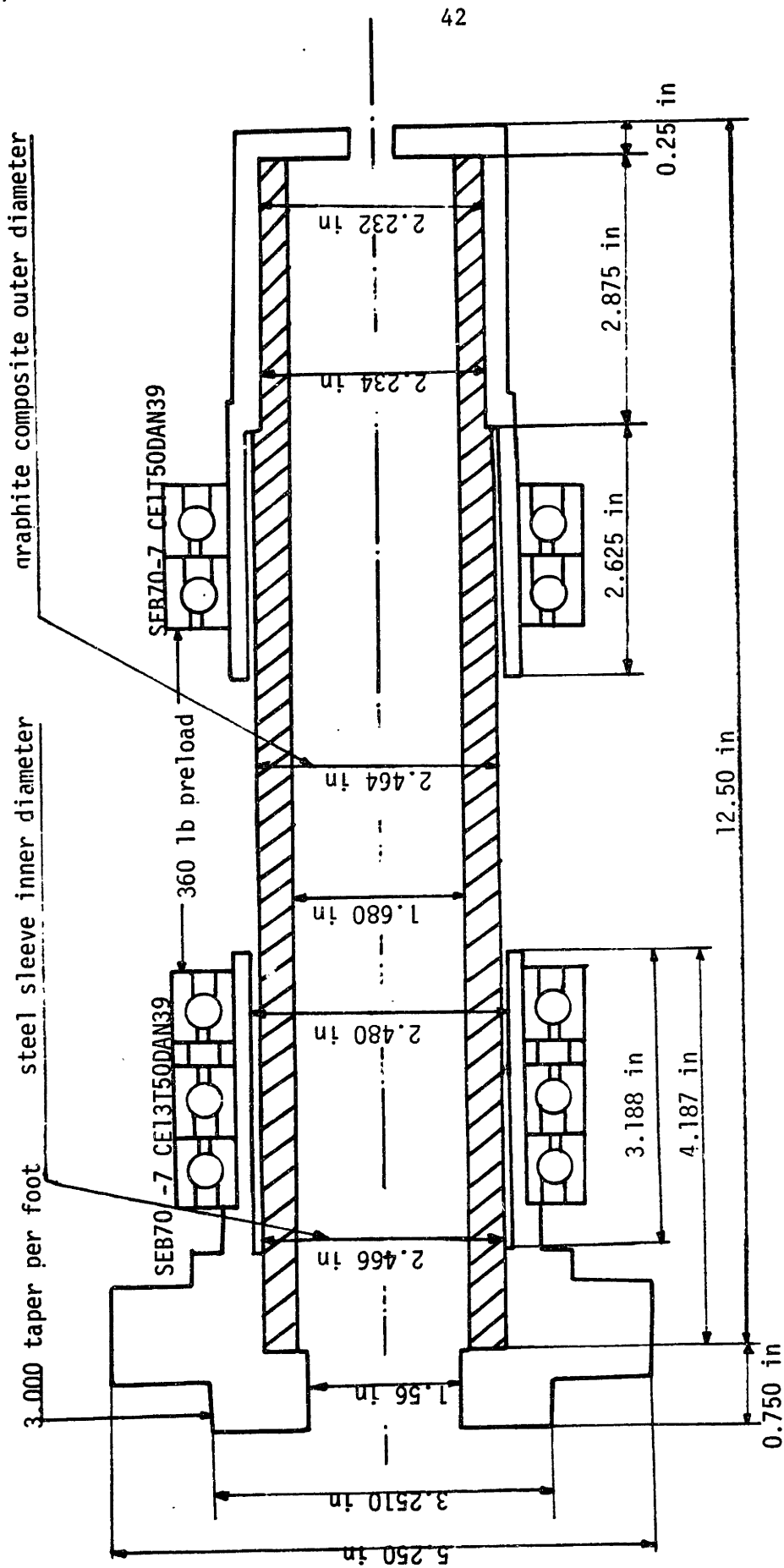


Fig. 2.7 Some Dimensional Characteristics of the Graphite Epoxy Composite Spindle Bearing System

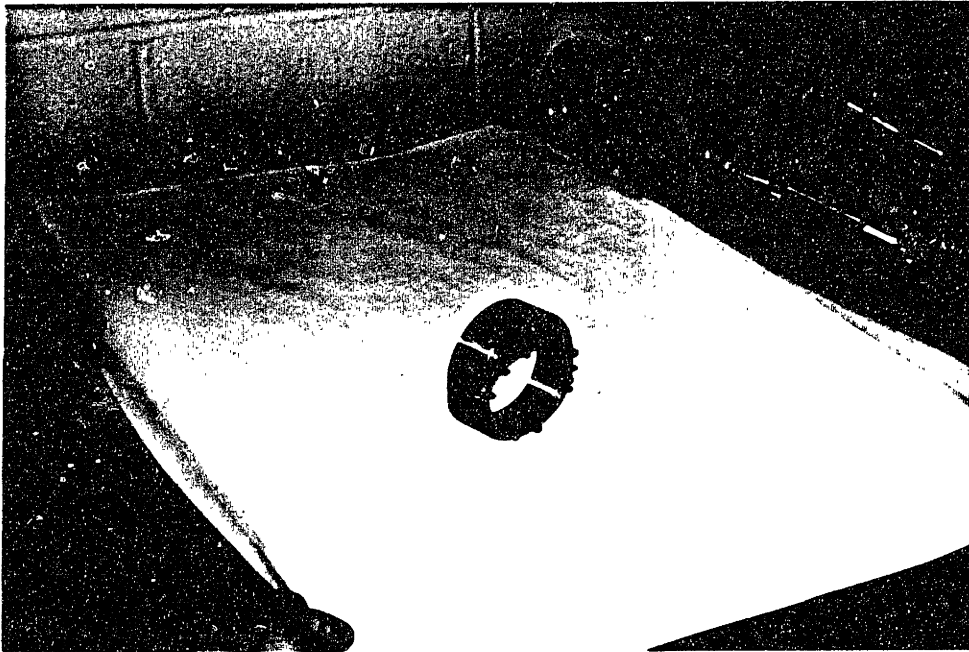


Fig. 2.8 Preload Spring for the Spindle Bearing System

a very tight tolerance of 0.001 inch to maintain concentricity between the composite shaft and the steel sleeve in bonding ; the other has a tolerance of 0.008 inch to be filled with epoxy adhesive. The torque transmitting capability of the epoxy bonded joint was calculated by Adams' method (See Appendix C). Since the adhesive used in bonding is Hysol EA 9309.2 (See Appendix D), which has a lap shear strength of 5000 psi at 77°F, the torque capability is 970 lb-ft at 77°F. If the rotational speed is 1,000 rpm, the power that can be transmitted is about 185 HP.

The manufactured spindle bearing system was inserted in the thick cast iron housing mounted on the bed of the 10 HP Monarch lathe, for the cutting test.

In addition, one steel spindle, which has the same dimensions as the graphite epoxy composite spindle except the inner diameter, has been manufactured (See Fig. 2.9). The inner diameter of the steel spindle was changed to give the same flexural rigidity (EI) as the graphite epoxy composite spindle. The same housing which was used for the graphite epoxy composite spindle was also used for the steel spindle in the cutting and vibration tests.

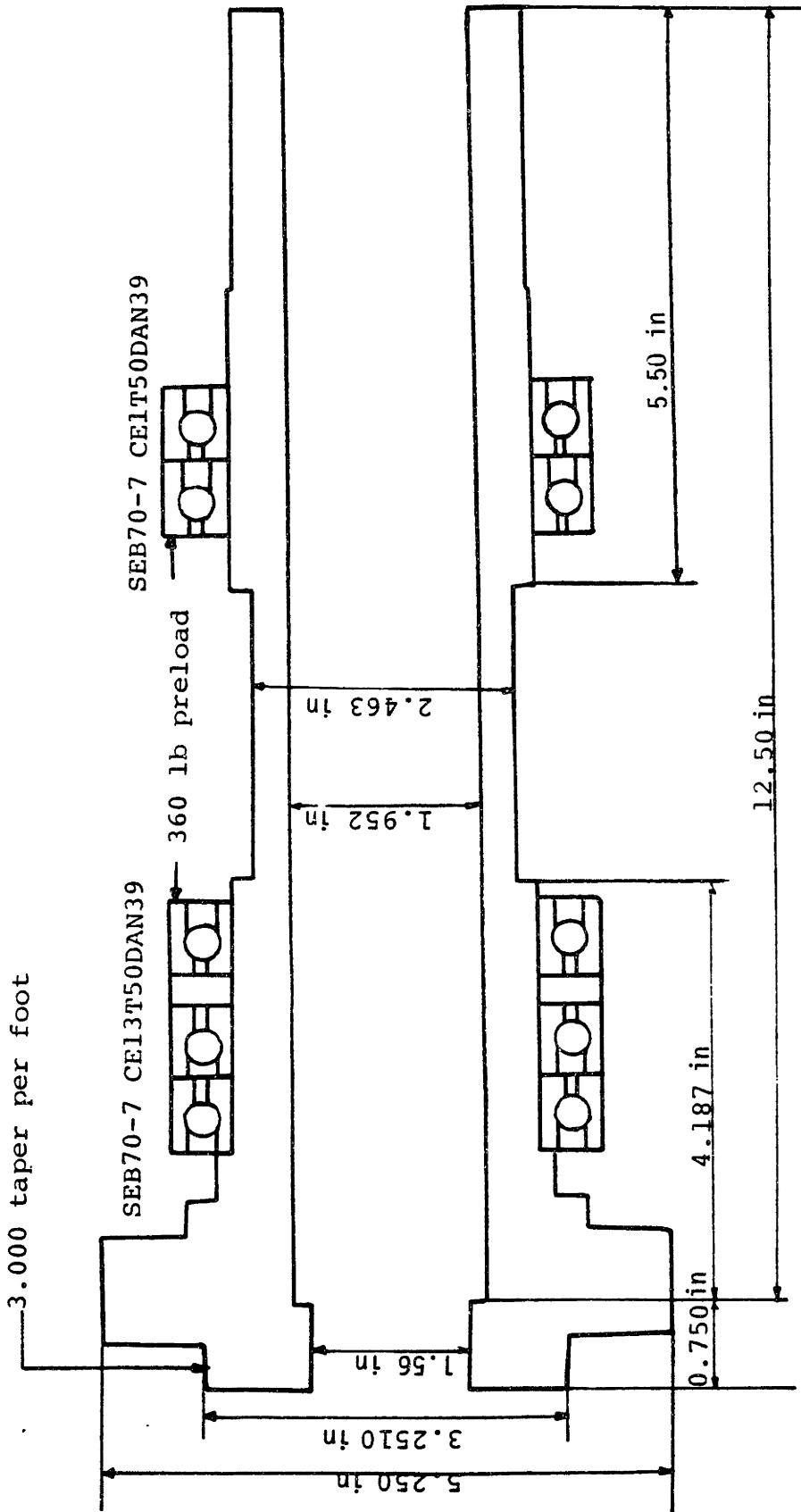


Fig. 2.9 Some Dimensional Characteristics of the Steel Spindle Bearing System

3. THE PERFORMANCE TESTS OF THE SPINDLE BEARING SYSTEM

3.1 Introduction

In this chapter the performance test results of the graphite epoxy composite spindle bearing system are compared to those of the steel spindle bearing system.

In section 3.2, The bearing preload characteristics of the graphite spindle bearing system are compared to those of the steel spindle bearing system.

In section 3.3, the method for the metal cutting test to investigate the performances of a machine tool is discussed. Also, the metal cutting performances of the graphite epoxy composite spindle bearing system are compared to those of the steel spindle bearing system in this section.

In section 3.4, the vibration characteristics of the graphite epoxy composite spindle bearing system and the steel spindle bearing system are compared.

3.2 The Bearing Preload Characteristics

It has been found that the dynamic stiffness of a machine tool changes for up to two hours after starting to

run the spindle bearing system [1]. This is due to the rolling contacts in the bearing which generate heat and expand the bearings, spindle and spindle housing.

In order to ensure that the bearings and the spindle have expanded sufficiently, a warm-up time of one hour at $2/3$ maximum speed is recommended by MTIRA [1]. The machine tool will then be in a normal running condition if the heat generated from the machining process does not transfer to the machine tool.

In the real metal cutting process, the heat generated between the workpiece and the cutting tool can transfer to the spindle and the spindle bearings through the workpiece and the chuck. Therefore, the bearing and the spindle temperatures of the steel spindle bearing system can be higher than those of the graphite epoxy composite spindle bearing system because of the low thermal conductivity of the graphite epoxy composite material.

All the machine tool bearings are preloaded to increase their stiffness and reduce their deflection under the action of externally applied loads.

The temperature increase in the spindle gives an adverse effect to the bearing preload [56]. For ordinary spindles where speeds are low, or for intermittent motion with high speed rotation of very short duration and comparatively long periods between rotations, a straightforward solution is possible with simple bearing mountings.

With very high speed spindles, the solution is not so simple. When a spindle is started up to attain a high speed, heat is generated rapidly in the bearing parts, even with anti-friction bearings. The inner bearing race and the rolling components heat up first and a rapid radial expansion of those parts occurs. Heat transfer is not instantaneous and since time is required for heat to be transferred to the outer parts and released to the surroundings, the preload of the bearings is rapidly increased. Therefore, the bearing may have suffered irreparably, in spite of good lubrication if the initial preload is too large.

However, the preload of the steel spindle can not be too small to compensate for the thermal expansion of the spindle in order to do accurate machining.

The SEB bearing, which is manufactured by SNFA, has the following axial deflection characteristics with applied preload [57].

$$\delta a = 2 \times 10^{-3} \cdot F^{2/3} \cdot Z^{2/3} \cdot d^{-1/3} \cdot \sin^{-5/3} \alpha$$

Where

δa = axial deflection (mm)

F = Preload (10 N)

Z = number of balls

d = ball diameter (mm)

α = contact angle (degrees)

With the numerical values of SEB 70 bearings ($F = 800 \text{ N} = 180 \text{ lbs}$, $Z = 22$, $d = 9.52 \text{ mm}$, $\alpha = 15 \text{ degrees}$), the axial deflection is 0.0212 mm .

If the temperature difference between the spindle and the housing is 14 K and the bearing span length is 127 mm (5 inches), the axial deflection of the steel spindle bearing system is (the thermal expansion coefficient of steel = $12.6 \cdot 10^{-6} / \text{K}$)

$$\begin{aligned} \text{Axial Deflection} &= 12.6 \cdot 10^{-6} / \text{K} \cdot 127 \text{ mm} \cdot 14 \text{ K} \\ &= 0.0224 \text{ mm} \end{aligned}$$

Therefore, the axial preload of the steel spindle bearing system disappears if the temperature difference between the spindle and the housing is larger than 14 K , while the graphite epoxy composite spindle housing system has almost the same preload with a temperature rise because of its almost zero longitudinal thermal expansion coefficient (See Table 2.1). There is no need to give a large preload to the graphite epoxy composite spindle bearing in order to compensate the thermal expansion of the spindle.

The preload of the graphite epoxy composite spindle will increase slightly because the spindle case expands slightly as the heat is transferred from the bearings to the

spindle case. There is less chance of bearing failure of the graphite epoxy composite spindle at the start of the machining because the necessary preload of the graphite epoxy composite is less than that of the steel spindle with the same machining accuracy.

3.3 The Metal Cutting Test

3.3.1 MTIRA Method [1]

The surface finish and the metal removal rate depend largely on the dynamic stiffness of a machine tool and useful information relating to these characteristics can be obtained by measuring the dynamic performance of machine tools. To date, however, there are neither established methods to certify the dynamic performance of machine tools nor are there any testing standards. Realizing this problem, The Machine Tool Industry Research Association (MTIRA) of England has devised a cutting test that could be used as a test of dynamic performance for lathes and other turning machines.

The MTIRA cutting test for a lathe is to compare the chatter-free machining performance of two or more lathes by cutting the tapered workpiece. This procedure enables the determination of the limiting width of cut at which chatter

commences on each lathe to be compared.

Several important conditions of the MTIRA cutting test for a lathe are described below.

(a) All bolted joints, and sliding elements not required to be in motion during the test must be locked or clamped.

(b) Before any test or series of tests the spindle or table must be run at two-thirds maximum speed for one hour.

(c) The ambient temperature must have been kept within ± 5 °C of a mean ambient temperature, which is recommended as 20 °C, for at least 12 hours before the tests are commenced.

(d) The outer 5 mm of the stock as supplied must be removed before the workpiece is manufactured and all workpieces for use in any one set of comparative tests must be manufactured from the same bar.

(e) For sintered carbide tips, the normal rake angle should be ± 6 degrees.

(f) The geometry of the chip breaker and its position relative to the cutting edge must be the same for each comparative test.

(g) The cutting edge angle should be 0, 60 or 75 degrees.

Though the MTIRA method is very practical, it has a

problem that the scatter of data obtained through its procedures even for the same type of machine are so wide that those standardizations of the cutting test are far from perfect. The MTIRA method failed to consider some important chucking conditions, e.g. the chucking force, the chucking length, the relative shape of the inner face of jaws with respect to the testpiece specification and the number of jaws [58].

The slipping of the testpiece from the jaw face and the stalling of the machine were experienced by the author of this thesis when the 2 HP Rockwell lathe was used to perform MTIRA cutting test.

The detection of the exact position of the chatter threshold was another problem because the position of chatter was not always clear due to the eccentricity of the workpiece which was slipped from the jaws.

3.3.2 The Metal Cutting Test Used In This Work

Since the purpose of this experiment is to investigate the effects of the spindle properties on the metal cutting performance, it was necessary to eliminate the effect of the bed as much as possible. For this purpose, the housing of the spindle bearing system was mounted on the bed of an existing Monarch 12 inch lathe, which has 5 times the power

capacity of the manufactured spindles (See Fig. 3.1).

The power was delivered to the Monarch lathe by a 10 HP D.C. motor to change the cutting speed steplessly. The power of the manufactured spindle bearing system was delivered from the chuck of the Monarch lathe to the rear sleeves of the manufactured spindle by a flexible coupling (Love Joy No.1-150) to avoid aligning problems with the shafts.

Before the metal cutting test, the spindle bearing system was run at 1280 rpm, the maximum speed of the monarch lathe, for one hour. The ambient temperature was kept within $20 \pm 2^\circ\text{C}$ more than 24 hours before the tests.

The workpiece material in the cutting test was the AISI 1045 carbon steel. The workpieces were made from the same bar and the outer 5mm of the bar stock as supplied was removed before the workpieces were made. The shape of the workpiece was cylindrical and the cutting experiment was conducted when the workpiece diameter was within 2.0 - 2.2 inch (See Fig. 3.2).

The cutting tool material was the throw-away carbide tip SNMP-432E manufactured by TRW. The tool shank used has a 1 inch x 1 inch cross sectional dimension and an approach angle (cutting edge angle) of 45 degrees was used. The tool overhang was maintained at 2.0 inch and the tool center height was kept within ± 0.01 times of the workpiece diameter. The surface cutting speed was maintained at 330 ± 5

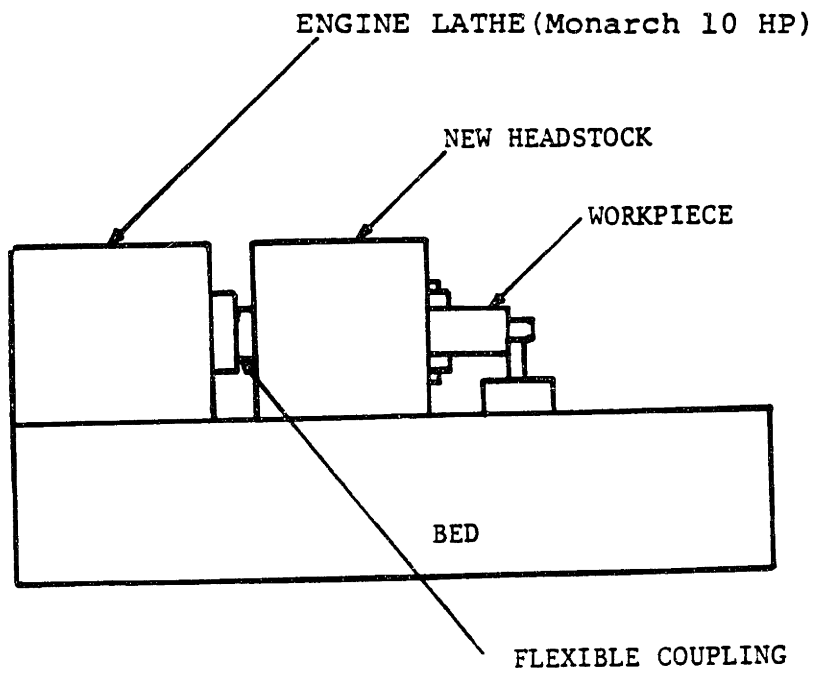


Fig. 3.1 Experimental Set-up for the Metal Cutting Test of the Manufactured Spindle Bearing Systems

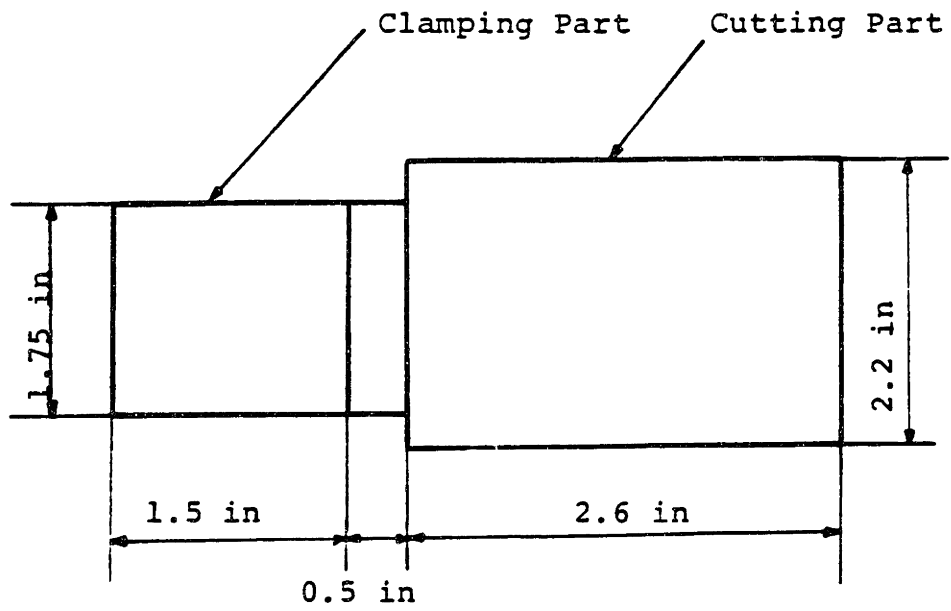


Fig. 3.2 Steel Bar Workpiece Used in the Metal Cutting Test

ft/min and the feed rate was maintained at 0.008 inch/rev. The chuck clamping torque was maintained at 30 ft-lb by the torque wrench.

In the cutting operation, the cutting tool edge was engaged from the right end of the workpiece. The cutting tool edge was used for only one cut. The width of cut was increased by the dial gage of the Monarch lathe. If the width of cut is close to the critical value, the spindle bearing system becomes unstable and chatter begins after one revolution of the workpiece. The width of cut at chatter initiation could be detected within 0.0025 inch accuracy by this method.

At the onset of chatter, the width of the cut of the graphite epoxy composite spindle was a 0.04 ± 0.0025 inch. While it was a 0.0325 ± 0.0025 inch for the steel spindle. Therefore, the increase in the width of cut of the graphite epoxy composite spindle was 23 %.

3.4 The Vibration Characteristics of the Spindle Bearing Systems

It is necessary to obtain the dynamic characteristics of the machine tool structure to predict the onset of the machine tool chatter. Since the main contributing part of the dynamics of the machine tool structure is the spindle

bearing system [2], it is important to know the dynamics of the spindle bearing system.

For this purpose, it is necessary to obtain the transfer function of the spindle bearing system in the working frequency range instead of the simple time history of the vibration of the spindle bearing system.

Several researchers have attempted to obtain the transfer function of the machine tool structure by both theoretical and experimental methods [5,59,60,61]. However, attempts to obtain the transfer function by both methods in the range of the cutting force and the cutting frequency have not been successful because of the difficulties of the high frequency vibration pick-up [59] and the large vibration exciting force which is usually order of thousand pounds in an engine lathe.

The two common methods of vibration pick-up use either an accelerometer to obtain acceleration or an electromagnetic device to obtain velocity [59]. Accelerometers generate a voltage proportional to the acceleration of the mechanical vibration and have a high natural frequency response. Velocity pick-ups generate a voltage proportional to the velocity and have a low natural frequency response. The disadvantage of accelerometers is that noise can cause erroneous signals and also two integrations are necessary to get displacement signals, which are of great importance in machine-tool vibrations. In addition, the voltage output is

small compared with the voltage output of velocity pick-ups. The disadvantages of velocity pick-ups are that it should be mounted in a rigid structure and costs much more compared to the accelerometer.

The two common methods of vibration excitation are to use either a vibration exciter or an impulse hammer.

There are two basic types of the exciter, the electromagnetic exciter and the hydraulic exciter. The electromagnetic exciter has a high frequency characteristics but has a small force amplitude which is usually few pounds. The hydraulic exciter has a large force amplitude but has a low frequency characteristics.

Since the damping properties of the machine tool is nonlinear, it is necessary to give the same magnitude of the exciting force and frequency in order to get a transfer function which gives reliable natural frequencies and damping of the machine tool. However, this is practically impossible because the natural frequencies of the machine tool structure ranges from a few hundred to a few thousand Hz and the maximum cutting force of a medium size lathe is a few thousand pounds.

Another method of vibration excitation is to use impulse signal. This method was widely used in the area of measurements and instrumentation to get the transfer function of a structure after the publication of the Cooley-Turkey algorithm for the fast Fourier transform in

1965 [53]. However, this method can not predict accurately the damping of the machine tool structure because this method should sample the time history of the vibration for a some period. It will give the average damping value in the decay of the vibration curve.

Since the impulse method is very easy to use, the impulse signal was used to test the dynamic characteristics of the spindle bearing system in this experiment although it has some disadvantages as mentioned previously.

Fig. 3.3 is the transfer function obtained by the HP 5423A Structural Dynamic Analyzer. The impulse was given to the upper part of the spindle nose by the impulse hammer and the acceleration was picked up at the lower part of the spindle nose by the BBN 507 LF/HS accelerometer. There are two dominant natural frequencies of the spindle bearing system. The first natural frequencies of the graphite epoxy composite spindle bearing system was increased about 16 % compared to that of the steel spindle bearing system. The second mode of the graphite epoxy composite spindle has two adjacent frequencies. From Fig. 3.3, we can see that the graphite epoxy composite spindle bearing system at the second vibration mode has more damping than the steel spindle bearing system.

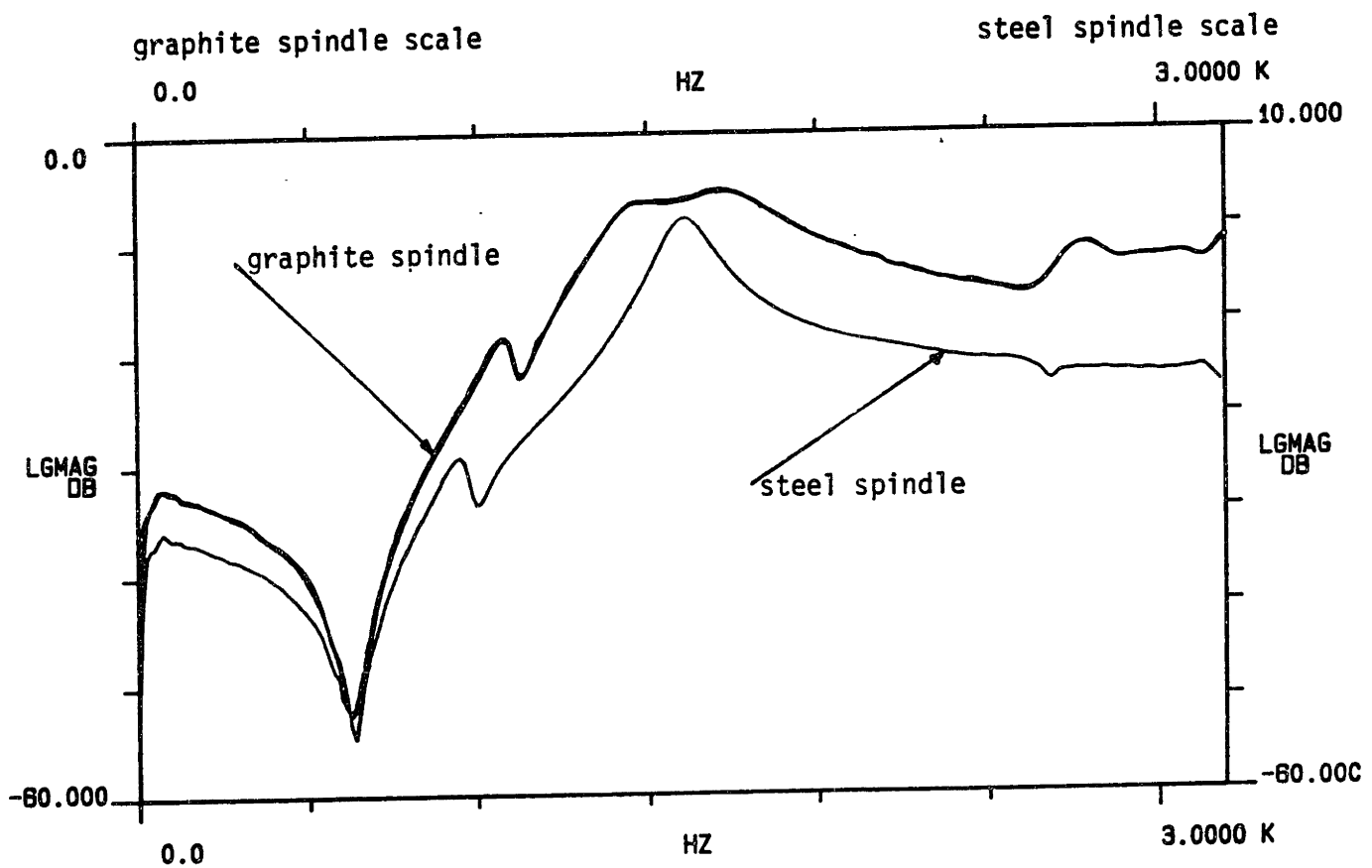
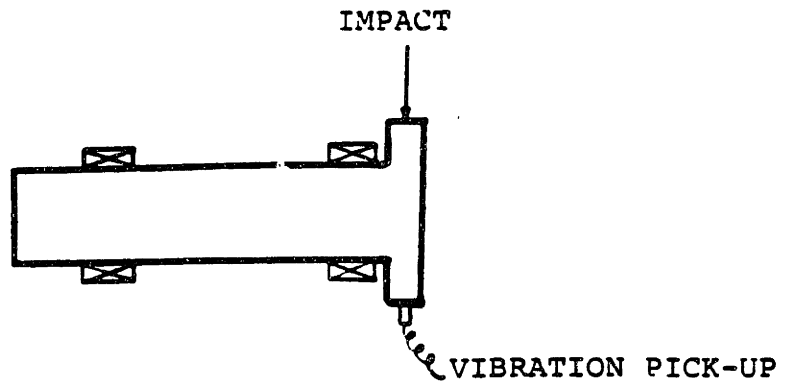


Fig. 3.3 Transfer Functions of the Spindle Bearing Systems Obtained by the HP5423A Structural Dynamic Analyzer

4. THE ANALYSIS OF THE SPINDLE BEARING SYSTEM

4.1 Introduction

The static stiffness is one of the most important properties of machine tools because the static stiffness and damping determine the dynamic performance of the machine tools. Static stiffness is defined as the ability to resist deflection under the action of static cutting force [42].

Therefore, in Section 4.2 the equations of the static stiffness are derived through the elastic bending model and applied to the manufactured spindle bearing systems in order to calculate its deflection characteristics. Also the method chosen to estimate the static stiffness of the bearing is discussed in this section.

With the increase in performance of high speed rotating machinery, many theoretical predictions of rotating machinery have been attempted. Many results are available in the rotor bearing systems [62,63].

However, the dynamics of the spindle bearing system of the machine tool is seldom complete because the spindle bearing systems have several components whose dynamic characteristics are too complex to be analyzed. Several investigators have attempted to predict theoretically and experimentally the dynamics of the spindle bearing system

[2,14].

The dynamics of the spindle bearing system is more complicated if the workpiece is engaged in the chuck because of the joints between these elements. The stiffness and damping of a joint are difficult to predict because the damping and stiffness are governed by the surface phenomena and clamping forces of the joint [33-41]. A workpiece dynamics without including the spindle bearing characteristics was attempted by Ismail[44]. This workpiece dynamics calculates natural frequencies accurately but not the damping values.

In section 4.3, the dynamics of the spindle bearing system, without taking into consideration of the chuck and workpiece, is investigated. In section 4.4, the natural frequencies of the manufactured spindle bearing system are calculated using the developed dynamic model and the calculated natural frequencies are compared to those obtained by the structural dynamic analyzer in Chapter 3. In section 4.5, the damping estimation method of the spindle bearing system is discussed.

4.2 The Static Analysis

Fig. 4.1 shows the model of the spindle bearing system with following assumptions :

(a) The front three bearings which are placed near the head

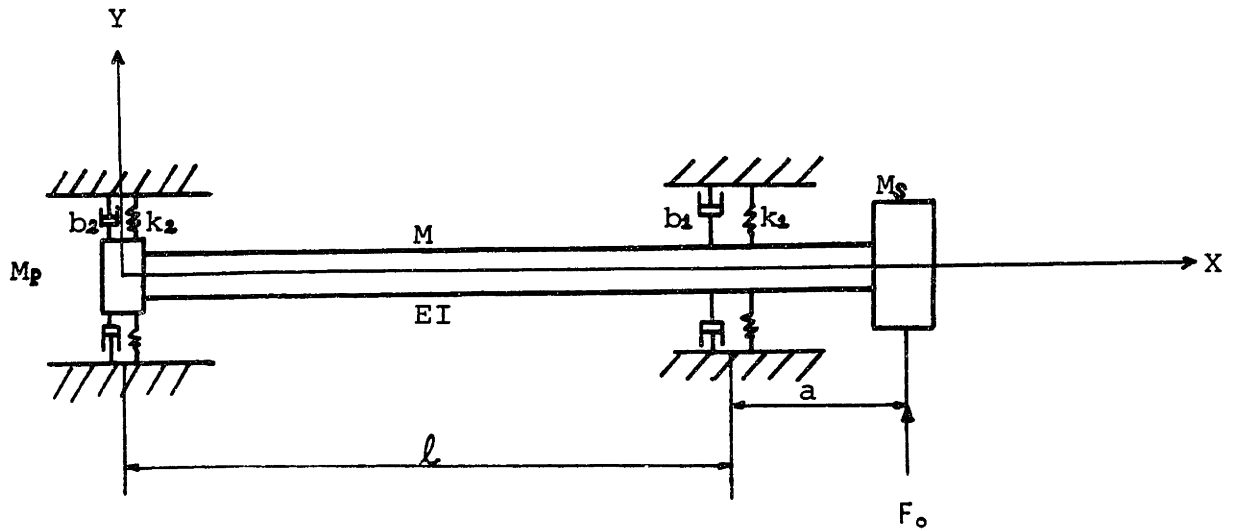


Fig. 4.1 Mathematical Model of the Spindle Bearing System

stock of a spindle bearing system, are simplified as a spring with spring constant k_1 and a viscous damper with viscous damping coefficient b_1 .

(b) The rear two bearings are simplified as a spring with spring constant k_2 and a viscous damper with viscous damping coefficient b_2 .

(c) The flexural rigidity (EI) of the spindle is assumed to be constant for simplicity

(d) The mass of the spindle nose (M_s), which includes the masses of the inner races of the front bearings, and the mass of the power transmission sleeve (M_p), which includes the masses of the inner races of the rear bearings, are modelled as lumped masses acting at $x = 0$ and $x = \ell + a$ respectively.

Under the static force having magnitude $F_0 a^+$ the spindle nose, the moment-curvature relations are

$$EI \frac{d^2 y}{d x^2} = - k_2 y_0 x - k_1 y_\ell \langle x - \ell \rangle \quad (4.1)$$

where

ℓ = bearing span

EI = flexural rigidity

k_1, k_2 = static stiffness of the front and rear bearings, respectively

y_0, y_ℓ = deflection at $x = 0$ and $x = \ell$, respectively

$\langle \quad \rangle$ = singularity function [64]

Integrating Equation (4.1) twice, the deflection equation becomes

$$EI y = -\frac{k_2 y_0}{6} x^3 - \frac{k_1 y_\ell}{6} (x - \ell)^3 + A_1 x + A_2 \quad (4.2)$$

From the force and momentum equilibrium condition, y_0 and y_ℓ can be calculated as follows.

$$y_0 = -\frac{a}{k_2 \ell} F_0 \quad (4.3)$$

$$y_\ell = \frac{\ell + a}{k_1 \ell} F_0 \quad (4.4)$$

From the boundary conditions $y = y_0$ at $x = 0$ and $y = y_\ell$ at $x = \ell$, A_1 and A_2 of Equation (4.3) can be calculated as

$$A_1 = \left[\frac{EI}{\ell^2} \left(\frac{\ell + a}{k_1} + \frac{a}{k_2} \right) - \frac{a\ell}{6} \right] F_0 \quad (4.5)$$

$$A_2 = -\frac{EI a}{k_2 \ell} F_0 \quad (4.6)$$

where

a = length between the front bearing and the spindle nose

The static compliance C , which is the inverse of the static stiffness K at the spindle nose, is obtained from equation (4.2).

$$C = 1/K = \frac{1}{3EI} (a^2 l + a^3) + \frac{1}{k_1} \left(1 + \frac{a}{l}\right)^2 + \frac{1}{k_2} \left(\frac{a}{l}\right)^2 = \frac{y_l + a}{F_o} \quad (4.7)$$

All the spindle bearings are preloaded to give high static stiffness and better accuracy. In order to estimate the static radial stiffness k_o of the preloaded bearing, the following empirical equation [2] is used.

$$k_o = 2.2 \cdot 10^6 \cdot \cot \alpha \cdot (\sin \alpha)^{5/3} \cdot F^{1/3} \cdot Z^{2/3} \cdot d^{1/3} \quad (\text{N/m}) \quad (4.8)$$

where

F = bearing preload (N)

d = the ball diameter (mm)

Z = the number of balls

α = the contact angle between the ball and race

The bearing data of SEB 70 which was used in the manufactured machine tools are following.

$F = 800 \text{ N} = 180 \text{ lb}$

$d = 9.52 \text{ mm}$

$Z = 22$

$\alpha = 15 \text{ degree}$

Then the static stiffness of the SEB 70 bearing is

$$k_o = 1.34 \cdot 10^8 \text{ (N/m)} = 7.66 \cdot 10^5 \text{ (lb/in)} \quad (4.9)$$

Stone [14] gives the stiffness data of several kinds of machine tool bearings. The static stiffness data of similar ball bearings with 60 mm bore diameter in the Stone's paper was reported to be about $1.5 \cdot 10^8$ (N/m). Stone's data is almost identical to that calculated above, if we take into consideration the different preload values between the two machine tool bearings. Therefore, the calculated values of the static stiffness of the bearings are used with confidence in estimating the static and dynamic stiffness of the spindle bearing systems.

The manufactured spindle bearing systems have three front bearings, one is not preloaded and the two rear bearings which are preloaded. The stiffness of the unpreloaded bearing has zero value if we use Equation (4.8). However, this is not reasonable because the bearing without any clearance between the bearing race and the ball of a bearing will produce some static stiffness even if there is no axial preload. In Stone's paper [14], the radial static stiffness of the unpreloaded bearing was given about the half value of the preloaded bearing instead of zero value.

Therefore, in this thesis the static stiffness of the unpreloaded bearing was assumed to be half the value of the preloaded bearing. Then the static stiffness k_1 and k_2 are

$$k_1 = 3.36 \cdot 10^8 \text{ (N/m)} = 1.92 \cdot 10^6 \text{ (lb/in)} \quad (4.10)$$

$$k_2 = 2.68 \cdot 10^8 \text{ (N/m)} = 1.53 \cdot 10^6 \text{ (lb/in)} \quad (4.11)$$

The design values of the both spindles are

$$EI = 35.0 \cdot 10^6 \text{ lb}\cdot\text{in}^2$$

$$a = 2.5 \text{ in}$$

$$l = 5.0 \text{ in}$$

Then the compliance of the spindle bearing system at the spindle nose is computed from Equation (4.7) as :

$$\begin{aligned} C &= 4.46 \cdot 10^{-7} \text{ (from the bending of the spindle)} \\ &+ 1.34 \cdot 10^{-6} \text{ (from the deflections of the bearings)} \\ &= 1.79 \cdot 10^{-6} \text{ (in/lb)} = 1.0 \cdot 10^{-8} \text{ (m/N)} \end{aligned}$$

The bearings produced 75 % of the total compliance of the spindle bearing system in this case.

4.3 The Dynamic Analysis

Machine tool structures are continuous systems and are described by partial differential equations. These are for-

midable equations with complex boundary conditions, nonlinear damping and complicated constraints. The number of the natural frequencies of the machine tool structures are infinite. However, the first two natural modes of the spindle bearing system are usually dominant. Therefore, the first two natural modes of the vibration of the spindle bearing system were investigated in this analysis.

In order to calculate the first two natural frequencies of the spindle bearing system, the Rayleigh-Ritz method was used because the damping factor of the spindle bearing system is usually less than 0.2. Then the error from neglecting the damping will be less than 1 %.

The first mode of the lateral vibration of the spindle bearing system was assumed to be the rigid body motion of the spindle between the bearing span. The deflection of the spindle is expressed as the following equation if we give force F_0 at the spindle nose :

$$y/F_0 = -\frac{a}{k_2 l} + \left[\frac{a}{l^2} \left(\frac{1}{k_1} + \frac{1}{k_2} \right) + \frac{1}{k_1 l} \right] x \quad (4.12)$$

Therefore, the lateral deflection $y(x,t)$ at the first mode is assumed as follows :

$$y(x,t) = P_1(t) \left[-\frac{a}{k_2 l} + \left\{ \frac{a}{l^2} \left(\frac{1}{k_1} + \frac{1}{k_2} \right) + \frac{1}{k_1 l} \right\} x \right] \quad (4.13)$$

and the second mode of the lateral vibration was assumed to

be the bending vibration between the bearing span. If we subtract Equation (4.12) from Equation (4.2) to get the pure bending motion without rigid body motion, the deflection shape is expressed as following :

$$y/F_0 = \frac{1}{EI} \left(\frac{a}{6l} x^3 - \frac{l+a}{6l} \langle x-l \rangle^3 - \frac{al}{6} x \right) \quad (4.14)$$

The above equation is valid only if the bearing support has a point contact. However, spindle bearings have some length and can produce clamped condition. Therefore, $y(x,t)$ at the second mode is expressed as :

$$y(x,t) = P_2(t) \left(\frac{a}{6l} x^3 - \frac{l+a}{6l} \langle x-l \rangle^3 - \frac{al}{6} x \right) + P_3(t) \cos \frac{\pi}{l} x \quad (4.15)$$

where $P_1(t)$, $P_2(t)$ and $P_3(t)$ are assumed arbitrary time functions. The cosine function represents the clamping condition because its derivatives are zero at $x = 0$ and $x = l$.

From these two assumed modes, the kinetic energy T and the potential energy U of the lateral vibration of the spindle bearing system can be calculated (See Fig. 4.1) as follows :

$$T = \frac{\rho}{2} \int_0^{l+a} \left(\frac{\partial y}{\partial t} \right)^2 dx + \frac{M_p}{2} \left(\frac{\partial y}{\partial t} \right)_0^2 + \frac{M_s}{2} \left(\frac{\partial y}{\partial t} \right)_{l+a}^2 \quad (4.16)$$

$$U = \frac{EI}{2} \int_0^{l+a} \left(\frac{\partial^2 y}{\partial x^2} \right)^2 dx + \frac{k_2}{2} y_0^2 + \frac{k_1}{2} y_l^2 \quad (4.17)$$

where

ρ = mass density per unit length of the spindle

M_p = mass of the power transmission sleeve

M_s = mass of the spindle nose

In deriving Equation (4.16) and (4.17), the masses of the spindle nose and the power transmitting sleeve are modelled as lumped masses acting at $x = 0$ and $x = \ell + a$ respectively. Also the gravity is neglected in deriving the potential energy.

4.4 The Numerical Values

4.4.1 The First Mode

With Equations (4.13), (4.16) and (4.17), the kinetic energy T and the potential energy U at the first mode were calculated as follows :

$$T = \dot{p}_1^2 \frac{\rho}{2} \int_0^{\ell+a} \left[-\frac{a}{k_2 \ell} + \left\{ \frac{a}{\ell^2} \left(\frac{1}{k_1} + \frac{1}{k_2} \right) + \frac{1}{k_1 \ell} \right\} x \right]^2 dx$$

$$+ \dot{p}_1^2 \left[\frac{1}{2} M_p \left(\frac{a}{k_2 \ell} \right)^2 + \frac{1}{2} M_s \left\{ \frac{1}{k_1} \left(1 + \frac{a}{\ell} \right)^2 + \left(\frac{a}{\ell} \right)^2 \frac{1}{k_2} \right\} \right]$$

or

$$\begin{aligned}
T = & \dot{p}_1^2 \cdot \frac{\rho}{2} \left[\frac{a^2}{k_2^2 l^2} (\ell + a) - \frac{a}{k_2 l} \left\{ \frac{a}{k_1} \left(\frac{1}{k_1} + \frac{1}{k_2} \right) + \frac{1}{k_1 l} \right\} (\ell + a)^2 \right. \\
& + \frac{(\ell + a)^3}{3} \left\{ \frac{a}{l^2} \left(\frac{1}{k_1} + \frac{1}{k_2} \right) + \frac{1}{k_1 l} \right\}^2 \left. \right] + \dot{p}_1^2 \left[\frac{1}{2} M_p \left(\frac{a}{k_2 l} \right)^2 \right. \\
& \left. + \frac{1}{2} M_s \left\{ \frac{1}{k_1} \left(1 + \frac{a}{l} \right)^2 + \left(\frac{a}{l} \right)^2 \frac{1}{k_2} \right\} \right] \quad (4.16a)
\end{aligned}$$

and

$$\begin{aligned}
U = & \frac{p_1^2}{2} \left[k_2 \left(\frac{a}{k_2 l} \right)^2 + k_1 \left(\frac{l}{k_1 l} \right)^2 \right] \\
= & \frac{p_1^2}{2} \left[\frac{a^2}{k_2 l^2} + \frac{(\ell + a)^2}{k_1 l^2} \right] \quad (4.17a)
\end{aligned}$$

With the design values of the spindle bearing system (See Table 4.1), the numerical values of the kinetic energy T and potential energy U at the first mode were calculated as follows :

$$T \text{ (graphite spindle)} = 1.473 \cdot 10^{-13} \dot{p}_1^2$$

$$T \text{ (steel spindle)} = 1.864 \cdot 10^{-13} \dot{p}_1^2$$

$$U \text{ (graphite spindle)} = 6.676 \cdot 10^{-7} p_1^2$$

$$U \text{ (steel spindle)} = 6.676 \cdot 10^{-7} p_1^2$$

With the Lagrangian equation, the calculated natural frequencies are as follows :

Table 4.1 Design Values of the Spindle Bearing System

| | Graphite Spindle | Steel Spindle |
|----------------------------|----------------------|----------------------|
| EI (lb·in ²) | $35.0 \cdot 10^6$ | $35.0 \cdot 10^6$ |
| a (in) | 2.5 | 2.5 |
| l (in) | 5.0 | 5.0 |
| k_1 (lb/in) | $1.92 \cdot 10^6$ | $1.92 \cdot 10^6$ |
| k_2 (lb/in) | $1.53 \cdot 10^6$ | $1.53 \cdot 10^6$ |
| ρ (slug/in) | $4.60 \cdot 10^{-3}$ | $1.54 \cdot 10^{-2}$ |
| M_p (slug) | 0.10 | 0.13 |
| M_s (slug) | 0.15 | 0.18 |

$$\begin{aligned}\omega_1 (\text{graphite spindle}) &= \sqrt{\frac{6.676 \cdot 10^{-7} \cdot 12}{1.473 \cdot 10^{-13}}} \\ &= 7.374 \cdot 10^3 \text{ rad/sec} \\ &= 1.17 \text{ kHz}\end{aligned}$$

$$\begin{aligned}\omega_1 (\text{steel spindle}) &= \sqrt{\frac{6.676 \cdot 10^{-7} \cdot 12}{1.864 \cdot 10^{-13}}} \\ &= 6.655 \cdot 10^3 \text{ rad/sec} \\ &= 1.04 \text{ kHz}\end{aligned}$$

The experimentally determined natural frequencies of both spindles at the first mode are as follows (See Fig. 3.3) :

$$\omega_1 (\text{graphite spindle}) = 1.09 \text{ kHz}$$

$$\omega_1 (\text{steel spindle}) = 0.94 \text{ kHz}$$

The numerical factor 12 was multiplied in calculating natural frequencies because the unit of mass is slug, the unit of force is pound and the unit of length is inch. The error in calculating the natural frequencies is about 10 %. This error may come from the inexact estimations of the bearing stiffnesses and the lumped masses.

Since the mass density per unit length of the graphite epoxy spindle is about 1/3 of the steel spindle (See Table

4.1), theoretically the first natural frequency of the graphite epoxy composite spindle bearing system can be increased about 70 % higher ($\sqrt{3} - 1$) than that of the steel spindle bearing system if the spindle nose mass and the power transmission sleeve mass are negligible. Then the maximum width of cut of the graphite spindle bearing system will increase about 70 % if the chatter initiates near the first natural frequencies, because the first mode of the spindle bearing system is rigid body motion between bearing span (See section 4.2). The bearing damping is approximately proportional to the frequency of the lateral vibration (See Section 4.5) and the maximum width of cut of a machine tool that can be taken without expectation of chatter is approximately proportional to damping if the static stiffness is constant (See Appendix E). However, the mass of the spindle nose contributes in lowering the first natural frequency of the spindle bearing system. We cannot eliminate this mass, but we may reduce it greatly if the spindle bearing system is for a milling or a grinding machine because the stiff chuck and spindle nose are not required in these machines as they are with the engine lathes.

4.4.2 The Second Mode

From the Equation (4.15), (4.16) and (4.17), the kinet-

ic energy T and the potential energy U of the spindle bearing system were calculated as follows :

$$T = \frac{\rho}{2} \int_0^{\ell+a} \left[\dot{p}_2 \left(\frac{a}{6\ell} x^3 - \frac{\ell+a}{6\ell} \langle x-\ell \rangle^3 - \frac{a\ell}{6} x \right) + \dot{p}_3 \cos\left(\frac{\pi}{\ell} \cdot x\right) \right]^2 dx$$

$$+ \frac{M_p}{2} \dot{p}_3^2 + \frac{M_s}{2} \left[\frac{a^2 \ell + a^3}{3} \dot{p}_2 + \dot{p}_3 \cos\frac{\pi}{\ell}(\ell+a) \right]^2 \quad (4.18)$$

$$U = \frac{EI}{2} \int_0^{\ell+a} \left[P_2 \left(\frac{a}{\ell} x - \frac{\ell+a}{\ell} \langle x-\ell \rangle \right) - \frac{\pi}{\ell} P_3 \cos\frac{\pi}{\ell} x \right]^2 dx$$

$$+ \frac{k_1}{2} P_3^2 + \frac{k_2}{2} P_3^2 \quad (4.19)$$

With the design values of the spindle bearing systems (See Table 4.1), the kinetic energy T and the potential energy U of the spindle bearing systems were calculated as follows :

$$T(\text{graphite spindle}) = 17.60 \dot{p}_2^2 - 0.0311 \dot{p}_2 \dot{p}_3 + 0.05863 \dot{p}_3^2$$

$$T(\text{steel spindle}) = 23.68 \dot{p}_2^2 - 0.1041 \dot{p}_2 \dot{p}_3 + 0.09387 \dot{p}_3^2$$

$$U(\text{graphite spindle}) = U(\text{steel spindle})$$

$$= 12(2.734 \cdot 10^8 P_2^2 + 7.0 \cdot 10^7 P_2 P_3 + 1.195 \cdot 10^7 P_3^2)$$

$$= 3.280 \cdot 10^9 P_2^2 + 8.40 \cdot 10^8 P_2 P_3 + 1.434 \cdot 10^8 P_3^2$$

By the Lagrange equation, the eigen value problem of the graphite epoxy composite spindle bearing system is expressed as follows :

$$\begin{bmatrix} 17.60 \omega^2 - 3.280 \cdot 10^9 & -0.0156 \omega^2 - 4.20 \cdot 10^8 \\ -0.0156 \omega^2 - 4.20 \cdot 10^8 & 0.0586 \omega^2 - 1.434 \cdot 10^8 \end{bmatrix} \begin{bmatrix} P_2 \\ P_3 \end{bmatrix} = 0$$

(4.20)

From this eigen value problem, the frequency equation of the graphite epoxy composite spindle bearing system becomes as follows :

$$(17.60 \omega^2 - 3.280 \cdot 10^9)(0.0586 \omega^2 - 1.434 \cdot 10^8) - (0.0156 \omega^2 + 4.20 \cdot 10^8)^2 = 0$$

or

$$\omega_2 \text{ (graphite spindle)} = 1.06 \cdot 10^4 \text{ rad/sec} = 1.69 \text{ kHz}$$

$$\omega_3 \text{ (graphite spindle)} = 5.0 \cdot 10^4 \text{ rad/sec} = 8.0 \text{ kHz}$$

ω_2 calculated is the natural frequency of the bending mode and ω_3 has no meaning because the boundary conditions for the third mode were not imposed in the expression of $y(x,t)$. By substituting ω_2 to the eigen value equation, the relation of P_2 and P_3 is obtained as follows :

$$P_3 = -3.08 P_2$$

Therefore, the mode shape of the composite spindle bearing system is expressed as follows :

$$y = \frac{a}{6l}x^3 - \frac{l+a}{6l} \langle x - l \rangle^3 - \frac{al}{6}x - 3.08 \cos \frac{\pi x}{l}$$

By the same method, the natural frequency of the second mode of the steel spindle bearing was calculated as follows :

$$(23.68 \omega^2 - 3.280 \cdot 10^9)(0.09387 \omega^2 - 1.434 \cdot 10^8) - (0.0521 \omega^2 + 4.20 \cdot 10^8)^2 = 0$$

or

$$\omega_2 (\text{steel spindle}) = 1.46 \text{ kHz}$$

and

$$P_3 = -3.10 P_2$$

The experimentally determined natural frequencies of the both spindle bearing systems at the second mode are as follow (See Fig. 3.3) :

$$\omega_2 (\text{graphite spindle}) = 1.50 \text{ kHz}$$

$$\omega_2 (\text{steel spindle}) = 1.61 \text{ kHz}$$

The calculated natural frequency of the steel spindle bearing system is 9 % lower than that which is experimentally determined. On the other hand, the calculated natural frequency of the graphite epoxy composite spindle bearing system is 12 % higher than the experimental value. The positive error of 12 % for the composite is significantly higher than the negative 9 % error for steel. This discrepancy in the calculations stems from the shear effect of the graphite epoxy composite material, which has 1/4 of the shear modulus of steel.

If a conventional beam is subjected both a bending moment and a shear force, the deflection produced is due largely to the bending moment. For the graphite epoxy composite material, the deflection due to shear is considerable because of its small shear modulus.

The governing equation of the deflection of a beam which is under both a bending moment and a shear force, is expressed as [65]

$$EI \frac{d^2 y}{dx^2} = M_b - \kappa \frac{EI}{AG} q \quad (4.21)$$

for which

$$M_b = -k_2 y_0 x - k_1 y_\ell \langle x - \ell \rangle \quad (4.22)$$

$$q = -k_2 y_0 \langle x \rangle_{-1} - k_1 y_\ell \langle x - \ell \rangle_{-1} \quad (4.23)$$

Here M_b is the bending moment, κ the shear coefficient [66],

A the cross sectional area, G the shear modulus of a beam

and q the concentrated load acting in the positive y -direction (See Fig. 4.1).

Integrating Equation (4.21) twice, the deflection equation becomes

$$EI y = -\frac{k_2 y_0}{6} x^3 - \frac{k_1 y_\ell}{6} \langle x - \ell \rangle^3 + \kappa \frac{EI}{AG} (k_2 y_0 x + k_1 y_\ell \langle x - \ell \rangle) + A_3 x + A_4 \quad (4.24)$$

Where A_3 and A_4 are integrating constants.

From the force and moment equilibrium conditions,

$$y_0 = -\frac{a}{k_2 \ell} F_0 \quad (4.25)$$

$$y_\ell = \frac{\ell + a}{k_1 \ell} F_0 \quad (4.26)$$

From the boundary conditions, $y = y_0$ at $x = 0$ and $y = y_\ell$ at $x = \ell$, giving

$$A_3 = \left[\frac{EI}{\ell^2} \left(\frac{\ell + a}{k_1} + \frac{a}{k_2} + \frac{\kappa a \ell}{AG} \right) - \frac{a \ell}{6} \right] F_0 \quad (4.27)$$

$$A_4 = -\frac{EI a}{k_2 \ell} F_0 \quad (4.28)$$

The compliance C' at the spindle nose is expressed as

$$C' = \frac{y_{l+a}}{F_0} = \frac{1}{3EI} (a^2 l + a^3) + \frac{1}{k_1} \left(1 + \frac{a}{l}\right)^2 + \frac{1}{k_2} \left(\frac{a}{l}\right)^2 + \frac{\kappa}{AG} \frac{a}{l} (l + a) \quad (4.29)$$

The last term of Equation (4.29) represents the deflection due to shear. In order to estimate the numerical value of this term, the shear coefficient should be known. From Cowper [66], the shear coefficient for the hollow circle is expressed as

$$\kappa = \frac{(7 + 6\nu)(1 + m^2)^2 + (20 + 12\nu)m^2}{6(1 + \nu)(1 + m^2)^2} \quad (4.30)$$

where $m = r_i / r_o$ and ν = Poisson's ratio

Since m and ν of the graphite epoxy composite are 0.68 and 0.28 respectively,

$$\kappa = 1.79$$

Using the design values given in Table 4.1, the last term of Equation (4.29) becomes

$$\frac{\kappa}{AG} \frac{a}{l} (l + a) = 1.10 \cdot 10^{-6} \text{ in/lb}$$

If we compare the above value with the calculated compliance of $1.79 \times 10^{-6} \text{ in/lb}$ (ignoring shear effects) in Section 4.2, we see that the shear accounts for 61 % of the deflection due to bending. This value of the shear contribution is too large. This discrepancy comes from

Integrating the approximate beam deflection equation rather than the governing differential equation of an orthotropic hollow cylinder [67, 68, 69, 70]. The effect of shear deformation drops if warping is prevented at the boundary. Timoshenko [65] gives two equations for the cantilever beam deflection :

$$y = \frac{P \ell^3}{3EI} \left(1 + 0.98 \frac{h^2}{\ell^2} \right) \quad (4.31)$$

$$y = \frac{P \ell^3}{3EI} \left(1 + 0.71 \frac{h^2}{\ell^2} - 0.10 \frac{h^3}{\ell^3} \right) \quad (4.32)$$

where P is the load acting at the end of the beam, ℓ is the beam length and h is the depth the rectangular beam.

Equation (4.31) is the deflection equation for a cantilever which can warp freely at the boundary, and Equation (4.32) is the deflection equation of a cantilever which cannot warp at the boundary. The first terms of Equation (4.31) and (4.32) represent the deflection due to bending while the other terms represent deflection due to shear. As we can see, the shear effect of Equation (4.32) is less than that of Equation (4.31).

The best way to obtain the deflection shape of the spindle is to integrate the governing differential equation of the orthotropic hollow cylinder with the boundary conditions for the bearings. In addition, if we do not include the clamping effect of the bearing mountings which is

represented as a cosine function in Equation (4.15), the integration of the above equation will result only in correcting the first term in Equation (4.15). The direct integration of the governing equation of the orthotropic hollow cylinder with the inclusion of the clamped condition of the bearing support is not easy.

To avoid this difficulty, the shear effect in the deflection of the graphite epoxy composite spindle is estimated using Equation (4.32). Equation (4.32) was derived for steel whose value for E/G is 2.6. Since the graphite epoxy composite material has an E/G value of 9.7, Equation (4.32) should be corrected as

$$y = \frac{Pl^*2}{3EI} \left[1 + \frac{9.7}{2.6} \left(0.71 \frac{h^2}{l^*2} \right) \right] = \frac{Pl^*2}{3EI} \left(1 + 2.65 \frac{h^2}{l^*2} \right) \quad (4.33)$$

In deriving Equation (4.33), the last term of Equation (4.32) was neglected because the second term is usually much larger than the third term. Also the variation of the shear coefficient was not considered because it does not change much for a rectangle or a circle [66].

In order to obtain the shear effect of the graphite epoxy composite spindle, the equivalent depth h should be estimated first. If we estimate h for a rectangle which has the same area as the composite spindle, h is calculated as

$$h = \sqrt{\pi(1.232^2 - 0.84^2)} = 1.60 \text{ inch}$$

If we estimate h for a rectangle which has the same sectional moment of inertia of the composite spindle, h is calculated as

$$h = [3\pi (1.232^4 - 0.84^4)]^{0.25} = 2.03 \text{ inch}$$

In order to calculate the largest shear effect of the composite spindle, $h = 2.03$ inch is selected. Then the second term of Equation (4.33) is

$$2.65 \frac{h^2}{l^2} = 2.65 \frac{2.03^2}{7.5^2} = 0.20$$

Therefore, we can conclude that the shear deformation accounts for approximately 20 % of the bending deflection.

When there is an additional deflection due to shear deformation, Equation (4.15) should be changed to

$$y = y_b + y_s$$

where y_b is the deflection due to bending (same as in Equation (4.15)) and y_s is the deflection due to shear.

Since y_s / y_b is estimated as 0.2, we obtain

$$y_s(x,t) = 0.2 y_b(x,t)$$

The potential energy relation, Equation (4.17) should contain bending, shear and bearing potential energy effects. The shear energy of the spindle is neglected because of its small shear modulus and small deformation compared to those due to bending. Then the kinetic energy T and the potential energy U are calculated from Equations (4.18) and (4.19) are as follows.

$$T = 25.34 \dot{P}_2^2 - 0.0448 \dot{P}_2 \dot{P}_3 + 0.0844 \dot{P}_3^2$$

$$U = 3.280 \cdot 10^9 P_2^2 + 8.40 \cdot 10^8 P_2 P_3 + 1.732 \cdot 10^8 P_3^2$$

By the Lagrangian equation, the natural frequency of bending is calculated as

$$\omega_2(\text{graphite spindle}) = 1.49 \text{ kHz}$$

The calculated frequency (1.49 kHz) is very close to the experimentally determined one (1.50 kHz). Therefore, this method will be used in calculating the bending natural frequency in the next chapter.

4.5 Damping Estimation

4.5.1 The Source of Damping of the Spindle Bearing System

In this section damping factor or loss factor will be used to represent damping characteristics. Damping factor is selected from other damping parameters (See Appendix A) because it describes the material damping well. The damping factor or loss factor η is defined as

$$\eta = \frac{\Delta U}{2\pi U_{\max}} \quad (4.34)$$

where ΔU is the energy dissipated per cycle and U_{\max} is the maximum potential energy stored in the system.

The damping factor of the steel is less than 0.001 for vibration frequencies higher than 100 Hz [46]. Crawley [49] shows that the damping factor of the graphite epoxy composite at 200 Hz vibrational frequency is about 0.015 (See Fig. 4.2). Moreover, the damping factor of the graphite epoxy composite has the tendency to increase slightly with frequency, while the damping of the metal has the tendency to decrease with frequency for vibration frequencies higher than 100 Hz. High damping property of the graphite epoxy composite comes from the damping of the epoxy material. Usually polymeric materials have high damping for a wide

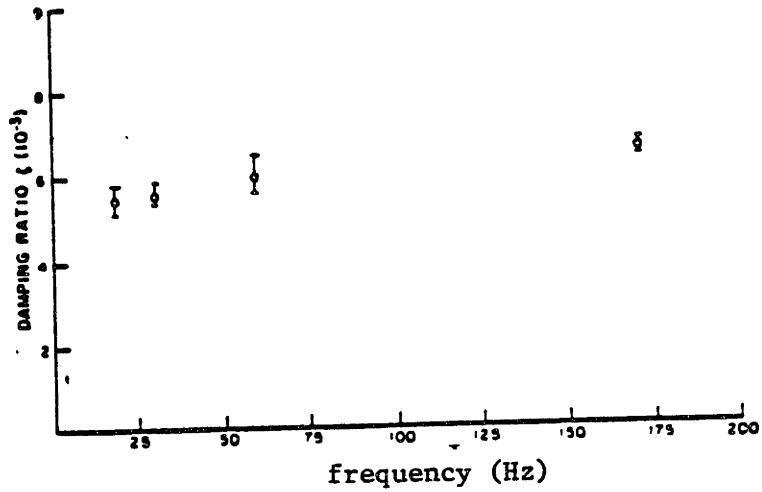


Fig. 4.2 Damping Ratio vs. Frequency in Graphite/Epoxy $[+45]_{2s}$

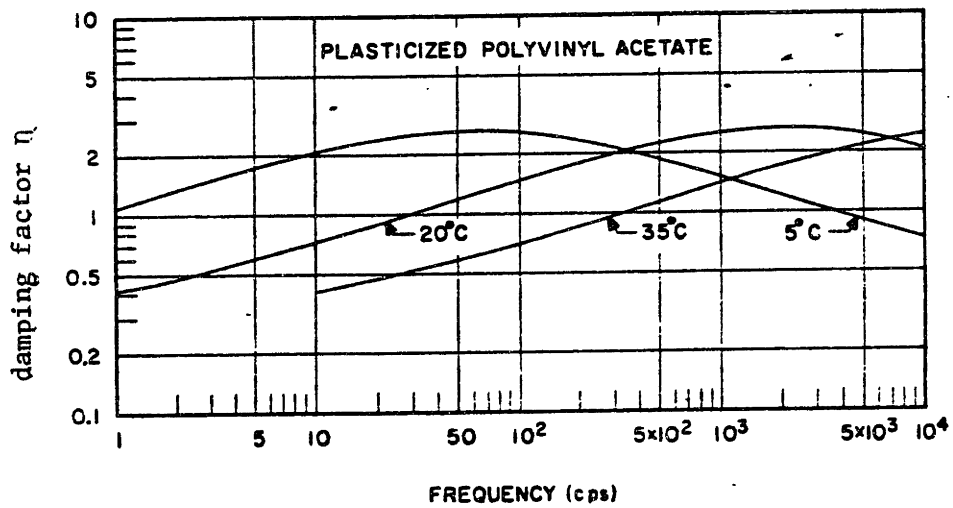


Fig. 4.3 Damping Factor Possessed by Unfilled Plasticized Polyvinyl Acetate

range of frequency. Snowdon [55] gives the damping factors of several polymeric materials. He shows that the damping factor of plasticized polyvinyl acetate has almost constant damping factor up to 10 kHz (See Fig. 4.3). Also, Ferry [71] gives a similar trend of the damping factors for several polymeric materials. Since the natural frequency of the bending vibration is about 1.5 kHz, the material damping factor of the graphite epoxy composite material is chosen as 0.02. The reason why 0.02 damping factor is chosen is further explained when the experimental data of Fig. 4.8 is discussed in the later part of this section.

The data of bearing damping is rare. Stone [14] gave some damping properties of the spindle bearings. The viscous damping coefficient of the lightly preloaded ball bearings for the machine tools was given about 1000 N·s/m or 5.7 lb·s/in in Stone's paper. The viscous damping coefficient of the unpreloaded ball bearing was given almost the same value of the preloaded ball bearing in this paper. This value of the viscous damping coefficient was used in this thesis to estimate the overall damping factor of the spindle bearing systems because it is too difficult to measure the damping of the bearing with some preload. Then the total damping coefficients of the front and rear bearings will be about 17.1 lb·s/in and 11.4 lb·s/in respectively.

The epoxy adhesive bonded area between the graphite shaft and the two steel sleeves of the graphite epoxy compo-

site spindle bearing system may produce some damping. In order to investigate the damping property of the bonded area, three shafts were made and tested : a steel shaft (See Fig. 4.4a), a steel shaft with the bonded steel sleeves (See Fig. 4.4b) and a graphite shaft with the bonded steel sleeves (See Fig. 4.5). The Hysol EA 9309.2 epoxy adhesive (See Appendix D), which is the same epoxy adhesive used in the graphite epoxy composite spindle, was used in bonding operation. The graphite epoxy composite shaft has almost same dimensions of the spindle of the graphite epoxy composite spindle bearing system. The steel shaft was made from a thick pipe (AISI 1018) because of the boring difficulty of a solid bar. The inside diameter of the steel shaft is 2.0 inch which is a little larger than the spindle of the steel spindle bearing system. Since the outside diameter of the steel shaft is the same size as the spindle of the steel spindle bearing system, the bending stiffness was lowered 2 %.

The frequency and damping data (Table 4.2, Table 4.3 and Table 4.4) and the transfer functions (Fig. 4.6, Fig. 4.7 and Fig. 4.8) of these shafts were obtained by giving an impulse at the upper center of the shaft and picking up an acceleration signal at the lower center of the shaft. The acceleration signal was processed by the HP 5423A Structural Dynamic Analyzer.

Fig. 4.6 shows the transfer function of the steel

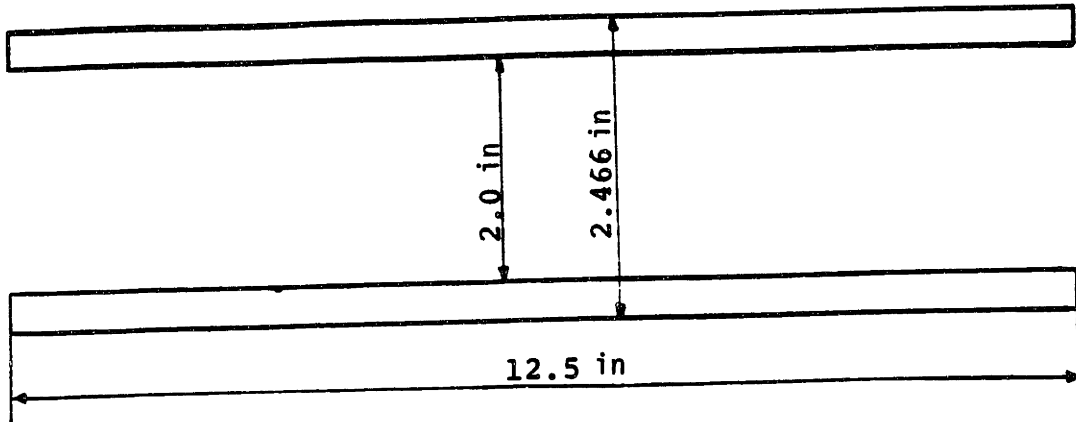


Fig. 4.4a Steel Shaft Used in the Vibration Test

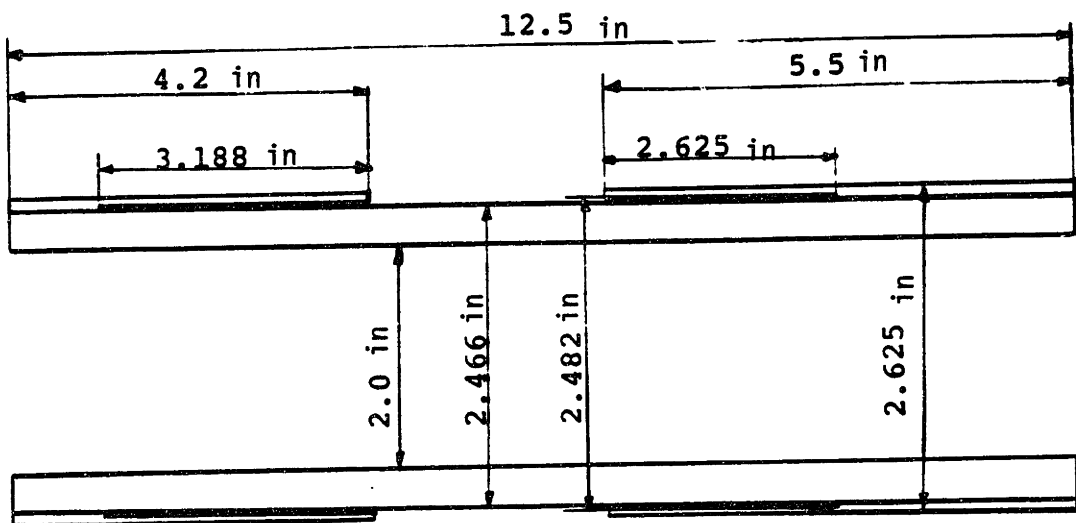


Fig. 4.4b Steel Shaft with the Epoxy Bonded Steel Sleeves Used in the Vibration Test

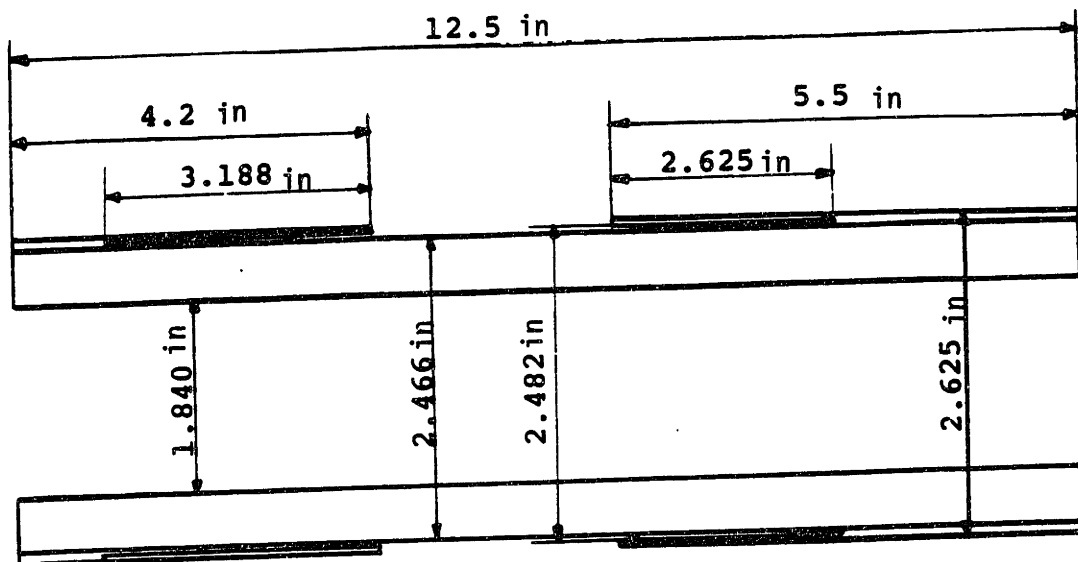


Fig. 4.5 Graphite Epoxy Composite Shaft with the Epoxy Bonded Steel Sleeves Used in the Vibration Test

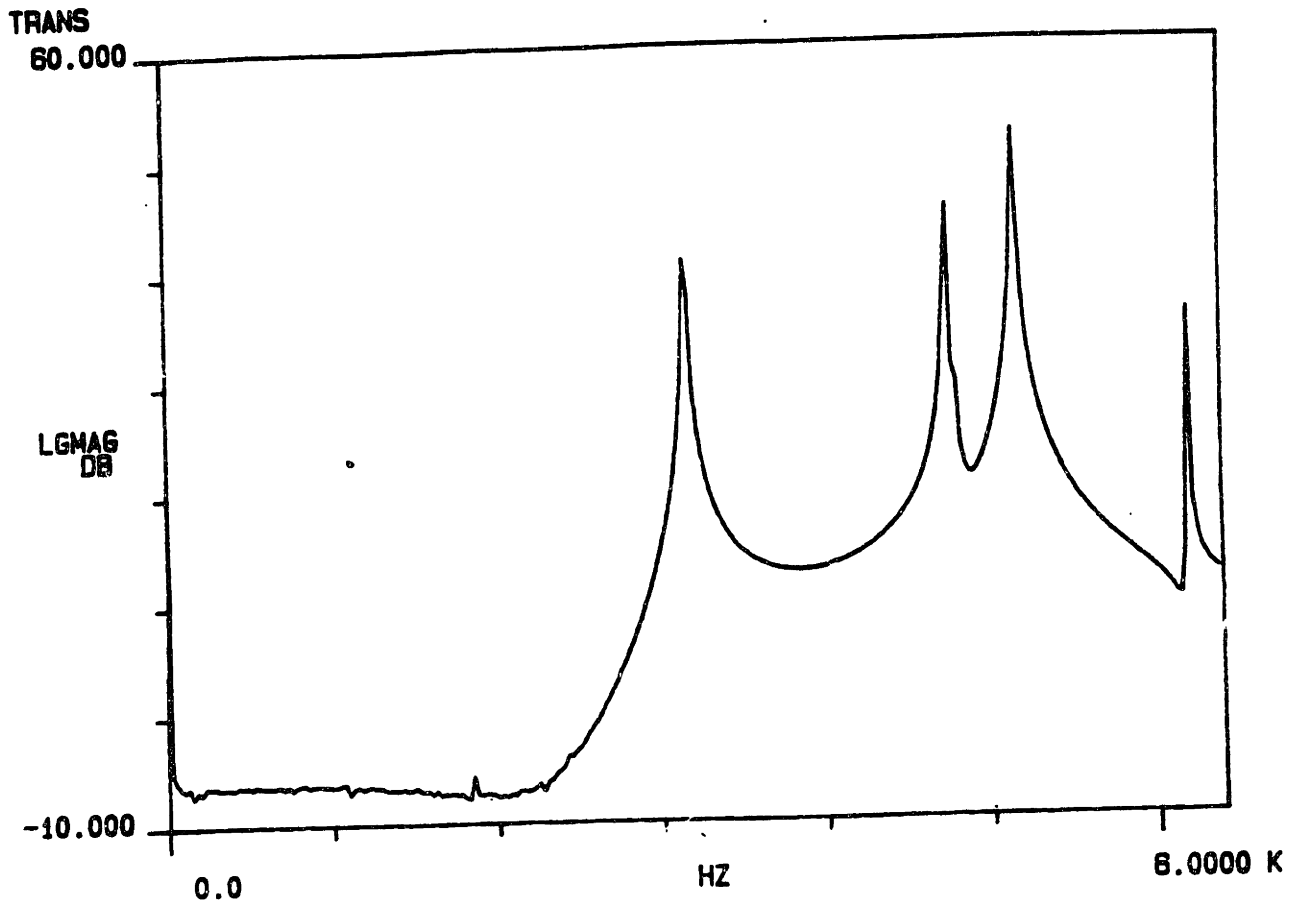


Fig. 4.6 Transfer Function of the Steel Shaft

Table 4.2 Frequency and Damping Data of Fig. 4.4

| MODE NO. | FREQUENCY | | DAMPING | | |
|----------|-----------|----------|---------|---------|--------|
| | HZ | R/S | % | HZ | R/S |
| 1 | 3.150 K | 19.792 K | 15.732 | 495.549 | 3.114 |
| 2 | 4.750 K | 29.845 K | 87.838 | 3.213 | 20.188 |
| 3 | 5.150 K | 32.358 K | 20.841 | 1.083 | 8.879 |
| 4 | 6.200 K | 38.958 K | 131.087 | 8.128 | 51.058 |

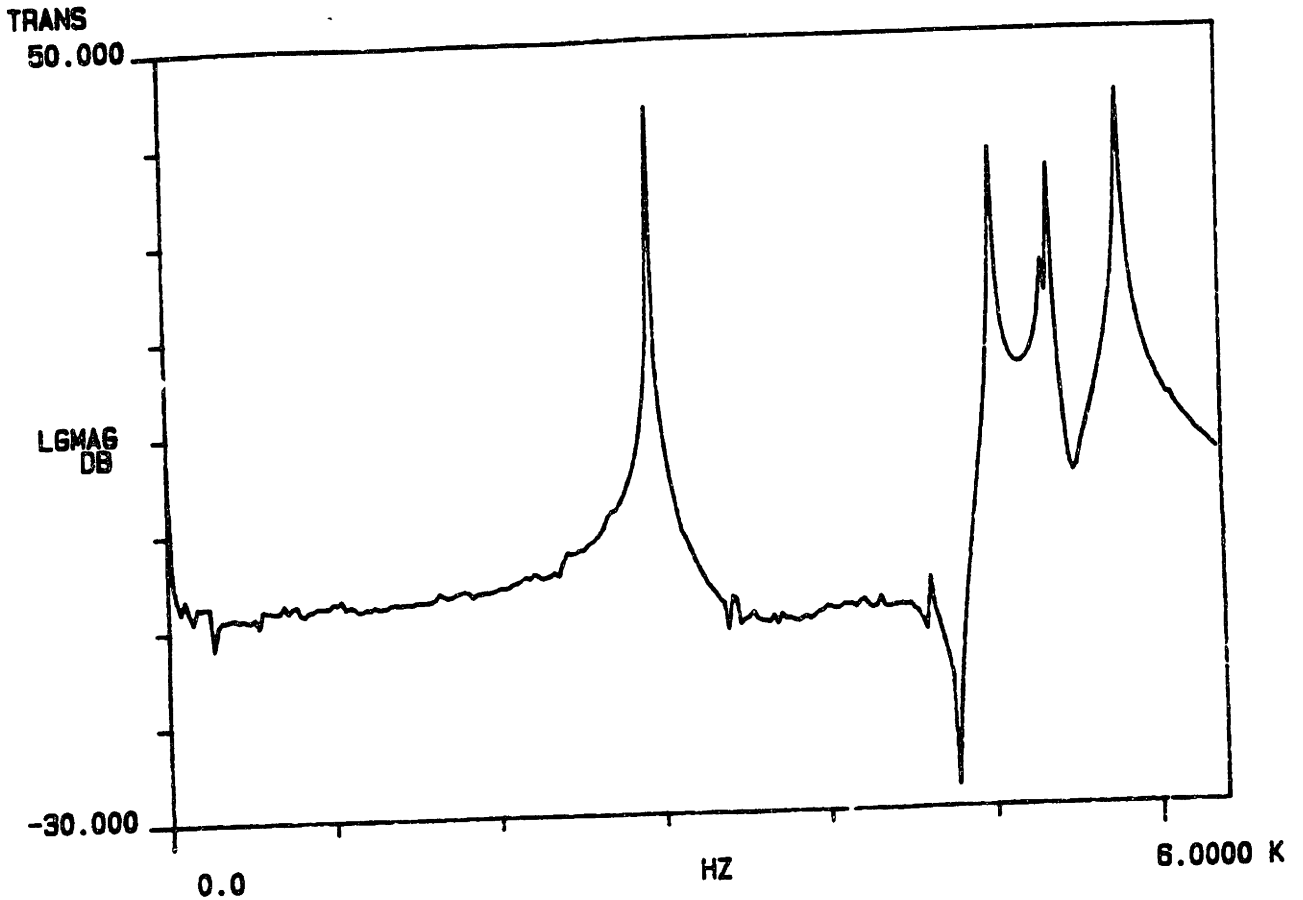


Fig. 4.7 Transfer Function of the Steel Shaft with the Epoxy Bonded Steel Sleeves

Table 4.3 Frequency and Damping Data of Fig. 4.5

| MODE NO. | F R E Q U E N C Y | | D A M P I N G | | |
|----------|-------------------|----------|---------------|-------|--------|
| | H Z | R/S | % | H Z | R/S |
| 1 | 2.950 K | 18.535 K | 52.890 | 1.554 | 9.768 |
| 2 | 5.025 K | 31.573 K | 39.288 | 1.973 | 12.397 |
| 3 | 5.375 K | 33.772 K | 137.104 | 7.369 | 46.303 |
| 4 | 5.800 K | 38.442 K | 83.145 | 3.882 | 23.012 |

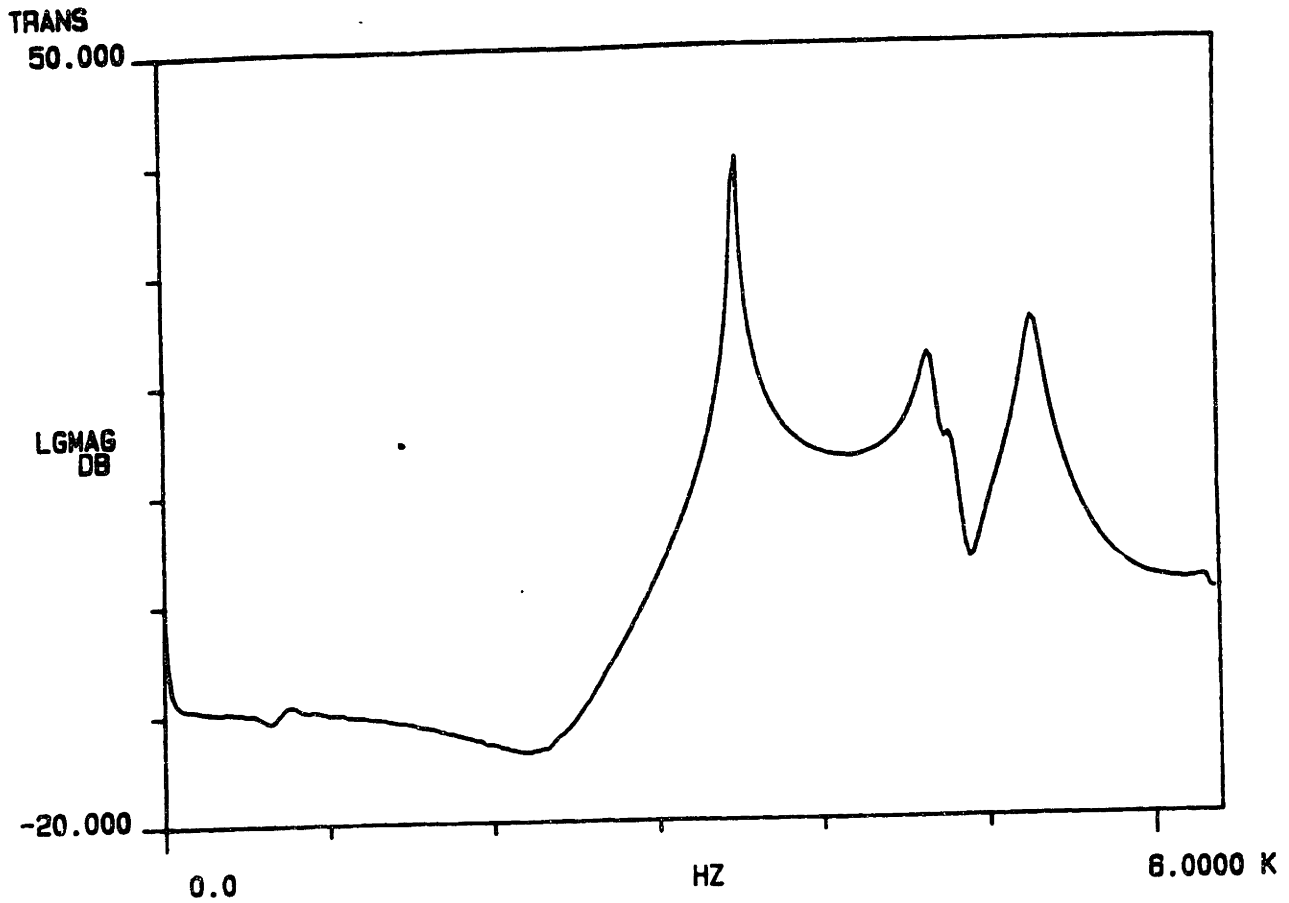


Fig. 4.8 Transfer Function of the Graphite Epoxy Composite Shaft with the Epoxy Bonded Steel Sleeves

Table 4.4 Frequency and Damping Data of Fig. 4.6

| MODE NO. | F R E Q U E N C Y | | D A M P I N G | | |
|----------|-------------------|----------|---------------|--------|---------|
| | H Z | R/S | % | H Z | R/S |
| 1 | 3.500 K | 21.991 K | 199.434 m | 6.980 | 43.858 |
| 2 | 4.675 K | 29.374 K | 1.004 | 46.928 | 294.855 |
| 3 | 5.275 K | 33.144 K | 887.519 m | 46.818 | 294.169 |

shaft and Table 4.2 shows the damping ratio (which is one half the damping factor, See Appendix A) of the same shaft. As already mentioned, the damping ratio of the steel shaft is negligible (order of 0.001) if the frequency is higher than 3 kHz.

Fig. 4.7 shows the transfer function of the steel shaft with the bonded steel sleeves and Table 4.3 shows the damping ratio of the same shaft. The damping ratio of the steel shaft with the bonded steel sleeves was more than 300 % higher than the damping ratio of the steel shaft at the first mode. However, the absolute increase of the damping ratio owing to the bonded area is less than 0.001, which is negligible. This result verifies the fact that the damping of a stiff structure can not be increased much with only one layer visco-elastic constrained damping [16,22].

Fig. 4.8 shows the transfer function of the graphite epoxy composite shaft with the bonded steel sleeves. The first natural frequency comes from the property of the steel sleeves and the second and the third natural frequencies comes from the property of the graphite epoxy composite shaft. Table 4.4 shows the damping ratios and the natural frequencies of the graphite epoxy composite shaft with the bonded steel sleeves. The damping factor (twice of damping ratio) of the first natural frequency is order of 0.001. The damping factors of the second and third natural frequencies are about 0.02. As already mentioned, this value of

damping factor is used in future calculation because the damping factor of the graphite epoxy material is not sensitive with frequency variation.

From these experimental results, we can see that the viscous damping of the bearings and the material damping of the spindle are the two main sources of the damping of the spindle bearing system.

The energy loss per cycle ΔU_b from the bearing is expressed, when the lateral vibration is sinusoidal with respect to time, as follows :

$$\Delta U_b = \int_0^{2\pi} f_d \frac{dy}{dt} dt = \pi b \omega A^2 \quad (4.35)$$

where

f_d = viscous damping force of the bearing

b = viscous damping coefficient of the bearing

ω = frequency of the lateral vibration

A = amplitude of the lateral vibration

The energy loss per cycle ΔU_m from the material damping of the spindle is calculated by the definition of the damping factor as follows (See Equation 4.34) :

$$\Delta U_m = 2\pi \eta_m U_m \quad (4.36)$$

where

U_m = bending potential energy of the spindle

η_m = damping factor of the spindle material

From Equation (4.35) and Equation (4.36), the total energy loss factor per cycle U of the spindle bearing system can be calculated as follows :

$$\Delta U = \pi\omega (b_1 y_l^2 + b_2 y_o^2) + 2\pi \eta_m U_m \quad (4.37)$$

The overall damping factor of the spindle bearing system is expressed as

$$\eta = \frac{\Delta U}{2\pi U} = \frac{\omega(b_1 y_l^2 + b_2 y_o^2)}{2U} + \eta_m \frac{U_m}{U} \quad (4.38)$$

where

U is given by Equation (4.17).

4.5.2 The Calculation of the Damping Factor

(a) The First Mode

The bending potential energy U of the spindle at the first mode is zero because the first mode was assumed as a rigid body motion. Then the total potential energy U is

$$U = U_b = \frac{k_2}{2} y_0^2 + \frac{k_1}{2} y_\ell^2$$

From Equation (4.13), y_0 and y_ℓ were calculated as follows :

$$y_0 = P_1(t) \left(-\frac{a}{k_2 \ell} \right)$$

$$y_\ell = P_1(t) \left(1 + \frac{a}{\ell} \right) \frac{1}{k_1}$$

Then from Equation (4.38), the overall damping factor of the spindle bearing system is expressed as follows :

$$\eta = \frac{\omega \left[\frac{b_1}{k_1^2} \left(1 + \frac{a}{\ell} \right)^2 + \frac{b_2}{k_2^2} \frac{a^2}{\ell^2} \right]}{\frac{1}{k_2} \left(\frac{a}{\ell} \right)^2 + \frac{1}{k_1} \left(1 + \frac{a}{\ell} \right)^2} \quad (4.38a)$$

In order to calculate the overall damping factor, the experimentally determined natural frequencies are used which are

$$\omega_1 (\text{graphite spindle}) = 1.09 \text{ kHz} = 6.85 \cdot 10^3 \text{ rad/sec}$$

$$\omega_1 (\text{steel spindle}) = 0.94 \text{ kHz} = 5.91 \cdot 10^3 \text{ rad/sec}$$

Since the viscous damping coefficients of the bearing were assumed as

$$b_1 = 17.1 \text{ lb}\cdot\text{s/in}$$

$$b_2 = 11.4 \text{ lb}\cdot\text{s/in}$$

and other parameters are

$$a/\ell = 0.5$$

$$k_1 = 1.92 \cdot 10^6 \text{ lb/in}$$

$$k_2 = 1.53 \cdot 10^6 \text{ lb/in}$$

Then the calculated overall damping factors are as follows :

$$\eta_1(\text{graphite spindle}) = 0.060$$

$$\eta_1(\text{steel spindle}) = 0.051$$

The calculated damping factors are close to the experimentally determined damping factors both of which are about 0.05.

(b) The Second Mode

With the result of Section 4.4.2, the total potential energy U and the bending potential energy U_m are calculated as follows :

$$\begin{aligned} U &= \frac{EI}{2} \int_0^{\ell+a} \left(\frac{a}{\ell} x - \frac{\ell+a}{\ell} \langle x - \ell \rangle + 3.08 \frac{\pi^2}{\ell^2} \cos \frac{\pi x}{\ell} \right)^2 dx \\ &\quad + \frac{k_1}{2} \cdot 3.08^2 + \frac{k_2}{2} \cdot 3.08^2 \\ &= 2.053 \cdot 10^9 \end{aligned}$$

$$U_m = \frac{EI}{2} \int_0^{l+a} \left(\frac{a}{l} x - \frac{l+a}{l} \langle x - l \rangle + 3.08 \frac{\pi^2}{l^2} \cos \frac{\pi}{l} x \right)^2 dx$$

$$= 2.037 \cdot 10^9$$

If the damping factor of the graphite epoxy composite is assumed 0.02 from the experimental result of Table 4.4, the overall damping factor of the graphite epoxy composite spindle bearing system can be calculated as follows :

$$\eta_2 (\text{graphite spindle}) = \frac{1.5 \cdot 10^3 \cdot 6.28 (17.1 \cdot 3.08^2 + 11.4 \cdot 3.08^2)}{2 \cdot 2.053 \cdot 10^9}$$

$$+ 0.02 \frac{2.037 \cdot 10^9}{2.053 \cdot 10^9}$$

$$= 2.05 \cdot 10^{-2}$$

By the same method, the overall damping factor of the steel spindle bearing system was calculated as follows :

$$\eta_2 (\text{steel spindle}) = 1.70 \cdot 10^{-3}$$

In calculating the overall damping factor of the steel spindle bearing system, the material damping factor of steel was assumed to be 0.001.

However, the experimentally determined damping factors of the graphite epoxy composite spindle bearing and the steel spindle bearing system are 0.114 and 0.074 respectively.

Therefore, the larger part of the damping at the second

mode may come from other sources rather than material damping and bearing damping. The damping source may be the joints between the bearings and the spindle. The difference between the damping factors of the two spindle bearing systems are 0.02 in calculated values and 0.03 in experimentally determined values. Therefore, damping factor of about 0.07 at the second mode may come from joints.

The 16 % increase of the natural frequency of the graphite epoxy composite spindle bearing system at the first mode compared to that of the steel spindle may explain the 23 % increase of the width of cut of the graphite epoxy composite spindle bearing system. The chatter of the machine tool usually occurs near the first natural frequency if the cutting speed is low. The damping of a spindle bearing system at the first mode is proportional to the natural frequency of the lateral vibration of the spindle because the damping of the spindle bearing system at the first mode comes largely from the damping of bearings. If the cutting force is increased in the metal cutting operation, the oil gap of the bearing will be decreased. This will increase the damping of the bearing because the damping of the bearing is inversely proportional to the oil gap of the bearing [76]. As a result, the spindle bearing system which has a high natural frequency will have a high cutting force and high bearing damping. The increase of damping also increases the cutting ability of a machine tool (See Appendix E)

5. THE OPTIMAL DESIGN OF A SPINDLE BEARING SYSTEM

5.1 Introduction

The performance results of the manufactured graphite epoxy composite spindle bearing system, as described in Chapter 3, are as follows :

(a) The damping of the graphite epoxy composite spindle bearing system at the second mode was increased about 50 % compared to that of the steel spindle bearing system

(b) The width of cut for the metal cutting test of the graphite epoxy composite spindle bearing system was increased by 23 % compared to that of the steel spindle bearing system.

(c) The natural frequency of the graphite epoxy composite spindle bearing system at the first mode was increased by 16 % compared to that of the steel spindle bearing system.

In order to further improve the performance of the spindle bearing system, in this chapter the performance of a spindle bearing system is optimized and the relationships among the parameters of the optimal spindle bearing system are formulated for use in the design stage.

In Section 5.2 the general description of the optimal design procedure for a spindle bearing system is presented. In section 5.3 the procedure developed in Section 5.2 is

illustrated through its application to the design of a milling machine.

5.2 Optimal Design Procedure for a Spindle Bearing System

5.2.1 Preliminary Specifications

In order to design a spindle bearing system, several preliminary specifications of the spindle bearing systems should first be given. These specifications are

- (a) Type of Machine (Lathe, Milling Machine, Boring Machine or Grinding Machine)
- (b) Maximum RPM
- (c) Static Stiffness at the Spindle Nose
- (d) Minimum Fundamental Natural Frequency

If the type of machine is determined, we can select the minimum values of a , M_p and M_s (See Fig. 4.1). The value of a cannot be reduced significantly to increase the static stiffness and the natural frequency of the spindle bearing system, because the labyrinth seal and the spindle case must be mounted between the spindle nose and the front bearings. The values of M_p and M_s also cannot be reduced much in a lathe. However, for a grinding machine and a milling machine, the values of M_p and M_s can be reduced significant-

ly. For the grinding machine and the milling machine, the spindle mass constitutes the largest fraction of the total mass of the spindle bearing system. In order to reduce this fraction, we will consider the use of graphite epoxy composites.

Specification (d) given above is usually not required by customers, but is included in this thesis because dynamic performance is dominated by the fundamental natural frequency. The damping of a spindle bearing system in the fundamental natural mode of vibration is proportional to the natural frequency (See Chapter 4), while the width of cut for a machine tool without chatter is proportional to the damping (See Appendix E).

5.2.2 The Selection of a Lubrication Method

The first step in the design of a spindle bearing system is to select a lubrication method. There are two main lubrication methods : grease lubrication and oil lubrication.

The maximum RPM for oil lubrication in roller bearings is about two times higher than that for grease lubrication (See Table 5.1). However, the use of grease lubrication for roller bearings has been steadily increasing [73]. The simplicity of housing designs and decreased sealing and

Table 5.1 Maximum Speed for Oil Lubrication and Grease Lubrication [72]

APPROXIMATE MAXIMUM SPEED (REV/MIN) OF GREASE-LUBRICATED RADIAL BEARINGS

| Bearing diameter (mm) | Bearing series number | | |
|-----------------------|-----------------------|--------------------------------|------------|
| | 02 (light) | 03 (medium) Speed (rev/min) | 04 (heavy) |
| 20 | 15 000 | 12 000 | 9 000 |
| 30 | 10 000 | 8 500 | 7 000 |
| 40 | 8 000 | 6 700 | 5 700 |
| 50 | 6 800 | 5 500 | 4 800 |
| 60 | 5 500 | 4 500 | 4 000 |
| 70 | 4 700 | 3 900 | 3 500 |
| 80 | 4 000 | 3 300 | 3 000 |
| 90 | 3 600 | 3 000 | 2 600 |
| 100 | 3 000 | 2 500 | 2 300 |
| 110 | 2 800 | 2 200 | — |
| 120 | 2 500 | — | — |
| 130 | 2 300 | — | — |

| Bearing type factor | Pressed metal cage retaining elements | Land-riding cages | Mounting factor |
|---------------------------------------------|---------------------------------------|-------------------|-----------------|
| Radial bearing with ball or roller elements | 1.00 | 0.7 | — |
| Radial bearings with taper rollers | 0.60 | — | — |
| Spherical roller bearings | 0.40 | — | — |
| Adjacent pairs or vertical shaft bearings | — | — | 0.75 |
| Housing and outer race rotating | — | — | 0.50 |

MAXIMUM SPEED FOR OIL LUBRICATION

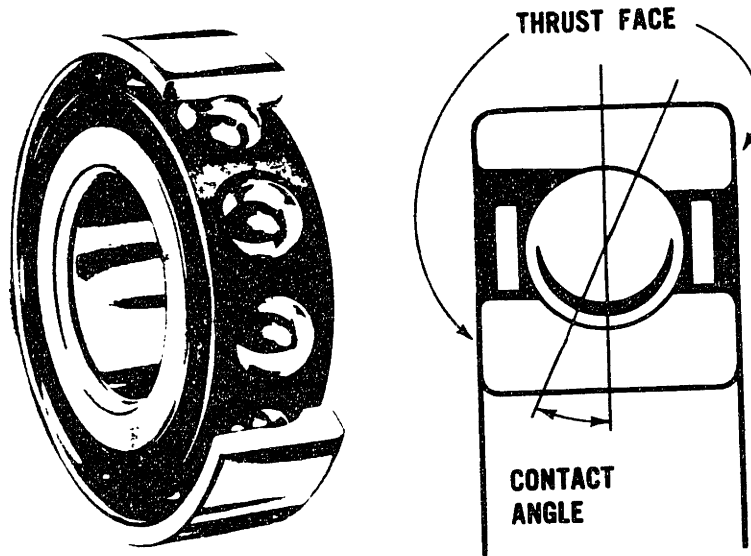
| Type of bearing | Maximum speed $N_1 D_p$ |
|---------------------------------------------------|-------------------------|
| Ball bearings: | |
| Radial, pressed-steel cages | 550 000 |
| Radial machined cages | 800 000 |
| Radial special cages and precision components | 2 000 000 |
| Roller bearings: | |
| Cylindrical elements, solid machined cages | 550 000 |
| Taper elements and double-row self-aligning units | 375 000 |

maintenance requirements have led to almost universal use of grease lubrication for ball and roller bearings in electric motors, household appliances, automotive wheel bearings, machine tools, aircraft, and railroad apparatus. Oil lubrication is still used where the oil is also needed for related mechanical devices (e.g. gears, in which the bearings must operate at very high temperatures or high speeds), or to permit lower starting torque, or to provide more cooling than is possible with grease.

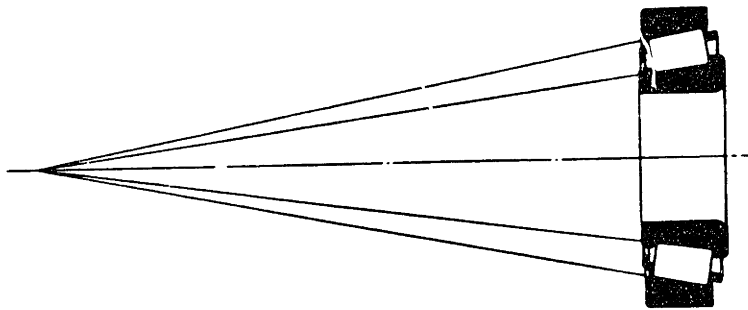
When grease is used, it takes up $1/3$ of the non-solid volume of a spindle bearing system ; sealing the grease ensures that it lasts for the lifetime of the spindle bearing system. In most cases, sealed grease lubrication should be the first choice in the optimal design procedure unless other conditions prohibit its use.

5.2.3 The Selection of Bearings

The two most widely used bearings for machine tools are angular contact ball bearings and tapered roller bearings (See Fig. 5.1). The characteristics of the angular contact ball bearing are high accuracy, high speed and low friction while the characteristics of the tapered roller bearing are high stiffness, low speed and high friction. The maximum speed of the tapered roller bearing is about 60 % of that of



(a)



(b)

Fig. 5.1 Basic Principles of Bearings [56] : (a) Angular Contact Bearing ; (b) Tapered Roller Bearing

the angular contact ball bearing (See Table 5.1).

The angular contact ball bearing has self aligning characteristics even if the inner and outer races of the bearing are not perfectly parallel. However, the tapered roller bearing requires accurate alignment between the inner and outer races of the bearing ; otherwise the line contact of the rollers and the race of the bearing will turn into a point contact.

For this reason, the angular contact ball bearing is the first choice for the bearing mounting and the spindle machining.

In addition, the development of new cutting tool materials elevates the importance of the high speed characteristics of a spindle bearing system.

However, the tapered roller bearing may be the only choice when very high static stiffness is required for the spindle bearing system.

After the selection of the type of bearings, we should determine how many bearings are required to satisfy the given specifications. If we increase the diameter of a angular contact ball bearing by a factor of two to increase the radial static stiffness, the radial static stiffness increases about two times (for example, the SEB 140 angular contact ball bearing has 1.9 times the stiffness of the SEB 70 bearing). However, the maximum speed decreases almost linearly with an increase of the diameter of the bearing

(See Table 5.1). In this case the lubrication method should be changed to prevent the maximum speed from decreasing. As a result the size of the spindle bearing system will increase dramatically.

One feasible method of increasing the bearing stiffness is to use more bearings. If the mounting of many bearings is difficult, tapered roller bearings represent the next choice for increasing the static stiffness.

From these considerations, one of the goals of the optimization of the spindle bearing system is to select the minimum number of bearings which satisfy the given specifications.

5.2.4 The Relationships Among the Properties of an Optimal Spindle Bearing System

From Equation (4.7) and Fig. 4.1, the compliance of the spindle nose was expressed as follows :

$$C = 1/K = \frac{a^2 (\ell + a)}{3 EI} + \frac{1}{k_1} \left(1 + \frac{a}{\ell}\right)^2 + \frac{1}{k_2} \left(\frac{a}{\ell}\right)^2 \quad (5.1)$$

where a is the fixed length between the front bearing and the spindle nose.

If we increase any of the values of k_1 , k_2 and EI of Equation (5.1), the compliance decreases. However, the com-

pliance decreases first and increases after some length ℓ_0 , if we increase ℓ (See Fig. 5.2). Therefore, there is an optimal bearing span length which gives the maximum static stiffness.

If we differentiate Equation (5.1) w.r.t. ℓ and equate zero, we can get the following relationship between ℓ_0 and other properties of the spindle bearing system :

$$EI = \frac{a \ell_0^2}{6 \left[\frac{a}{\ell_0} \left(\frac{1}{k_1} + \frac{1}{k_2} \right) + \frac{1}{k_1} \right]} \quad (5.2)$$

Equation (5.2) increases monotonically with an increase of ℓ_0 . Therefore, the large optimal bearing span length requires a large value for EI.

If we substitute EI of Equation (5.2) in Equation (5.1), the minimum compliance C_{min} is expressed as follows :

$$C_{min} = 2 \left(\frac{a}{\ell_0} \right) \left(1 + \frac{a}{\ell_0} \right) \left[\frac{a}{\ell_0} \left(\frac{1}{k_1} + \frac{1}{k_2} \right) + \frac{1}{k_1} \right] + \frac{1}{k_1} \left(1 + \frac{a}{\ell_0} \right)^2 + \frac{1}{k_2} \left(\frac{a}{\ell_0} \right)^2 \quad (5.3)$$

Fig. 5.3 shows the characteristics of Equation (5.3). The dominant factors of Equation (5.3) are a/ℓ_0 and k_1 . The rear bearing stiffness k_2 has little effect on the static stiffness characteristics of a spindle bearing system. If we increase the optimal bearing span length ℓ_0 , the static compliance decreases but never becomes smaller than $1/k_1$. Therefore, we should increase the number of bearings

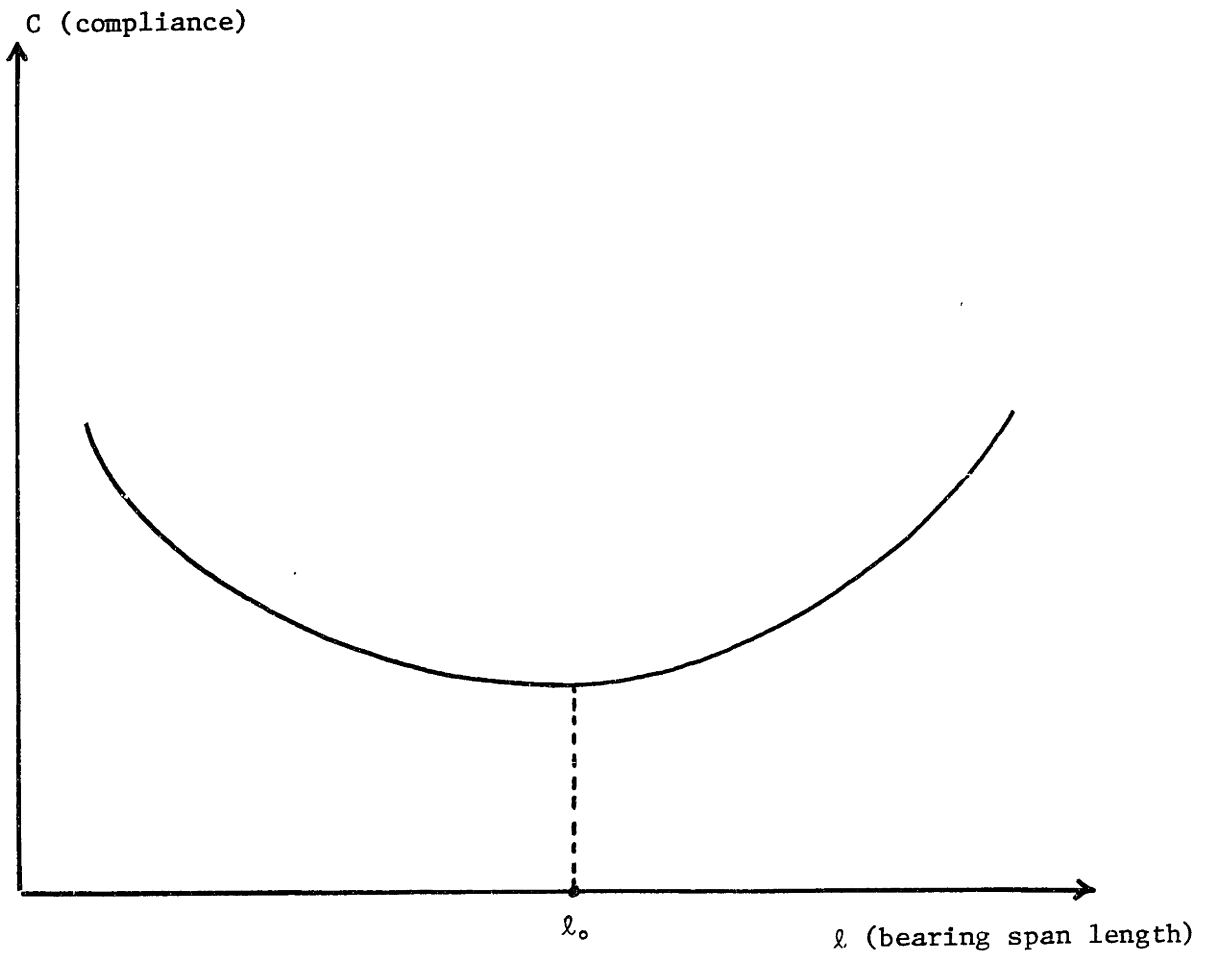


Fig. 5.2 Relationships Between the Compliance C and the Bearing Span Length l

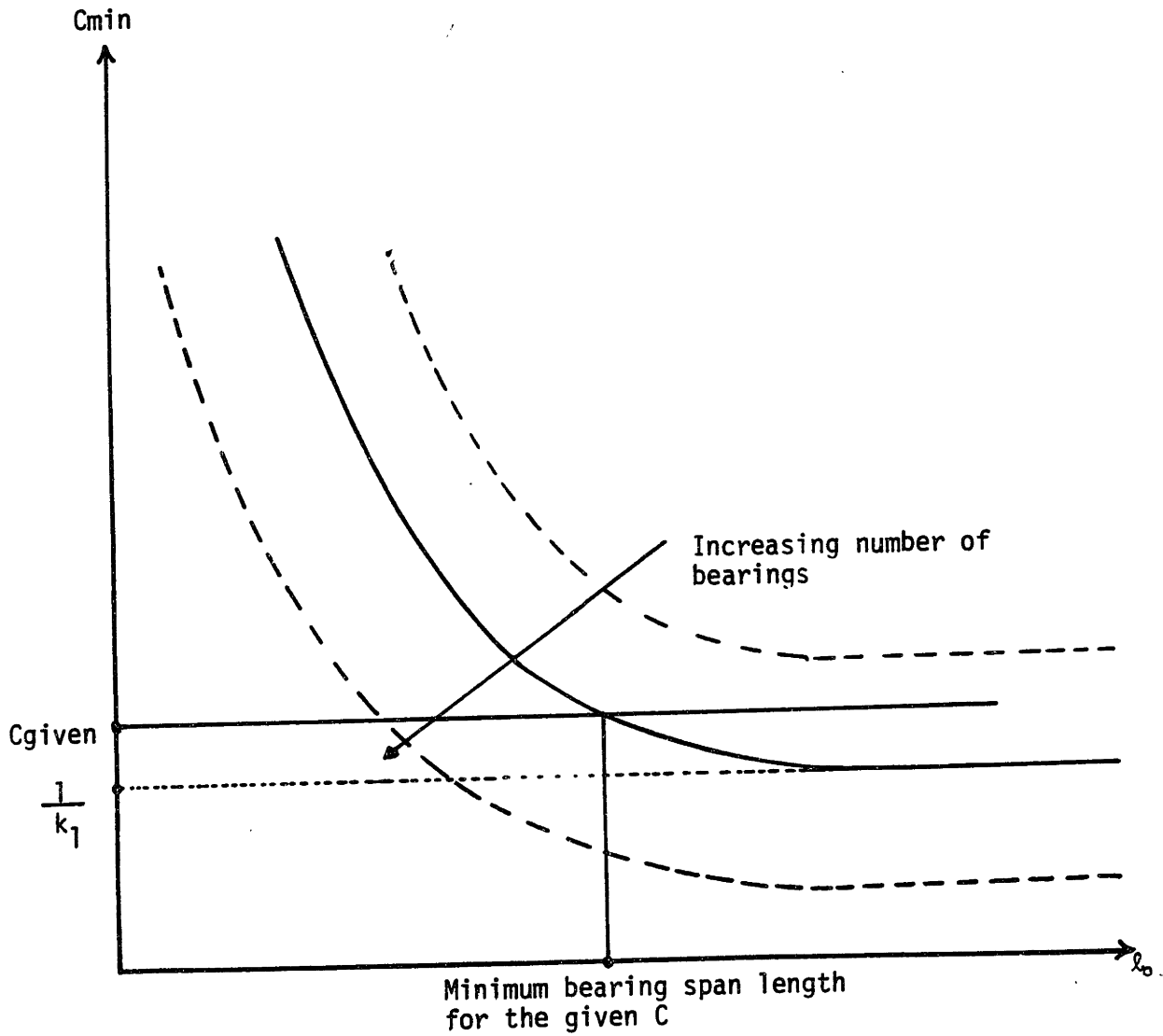


Fig. 5.3 Relationships Between the Minimum Compliance C_{min} and the Optimal Bearing Span Length l_o

(or change the bearing type) rather than increase the optimal bearing span l_o . If the required compliance is less than $1/k_1$. Moreover, the sectional moment of inertia I with the given bearing diameter, which satisfies the maximum RPM condition and Equation (5.2), cannot be achieved even if we use a solid bar as a spindle, if the optimal bearing span length is too long.

However, the optimal bearing span length cannot be too small. If the optimal bearing span length is too small, we should use many bearings to satisfy the given compliance conditions (See Fig. 5.3). Since the bearing has some length, many bearings cannot be mounted in a short bearing span.

The optimal bearing span length of the spindle bearing system is also constrained by the bearing preloading characteristics. If the temperature difference between the spindle and the spindle case is 20°F , the maximum values of l_o/D of the angular contact ball bearings are as follows :

$$l_o/D = 2.5 \text{ for the SEB 220 with heavy preload (D = 220 mm)}$$

$$l_o/D = 8.0 \text{ for the SEB 10 with heavy preload (D = 10 mm)}$$

where D is the bearing inner diameter.

The wall thickness of the spindle of a lathe (hence the optimal bearing span length as given by Equation (5.2)) cannot be increased significantly in order to increase the

sectional modulus I , because the bar work of a lathe requires a large inner diameter for the spindle.

The difficulty of boring a spindle is another constraint on the optimal bearing span length.

Fig 5.4 shows these constraints. From this figure we can see that a temperature compensation mechanism is necessary if we want to use n_1 number of bearings. However, if we use n_2 number of bearings with same compliance condition, the temperature compensation mechanism is not necessary.

The preloading constraint is usually the first encountered constraint and the temperature compensation mechanism is usually required to give a moderate value of the optimal bearing span length l_0 in a high speed, high accuracy machine tool spindle bearing system. This is a major constraint in the machine tool spindle bearing design. However, the graphite epoxy composite spindle bearing system bypasses this constraint because of its near-zero thermal expansion coefficient.

5.2.5 The Calculation of the Natural Frequency of the Spindle Bearing System

The next step of the design procedure of the spindle bearing system is to calculate the natural frequencies. The mathematical model of the spindle bearing system developed

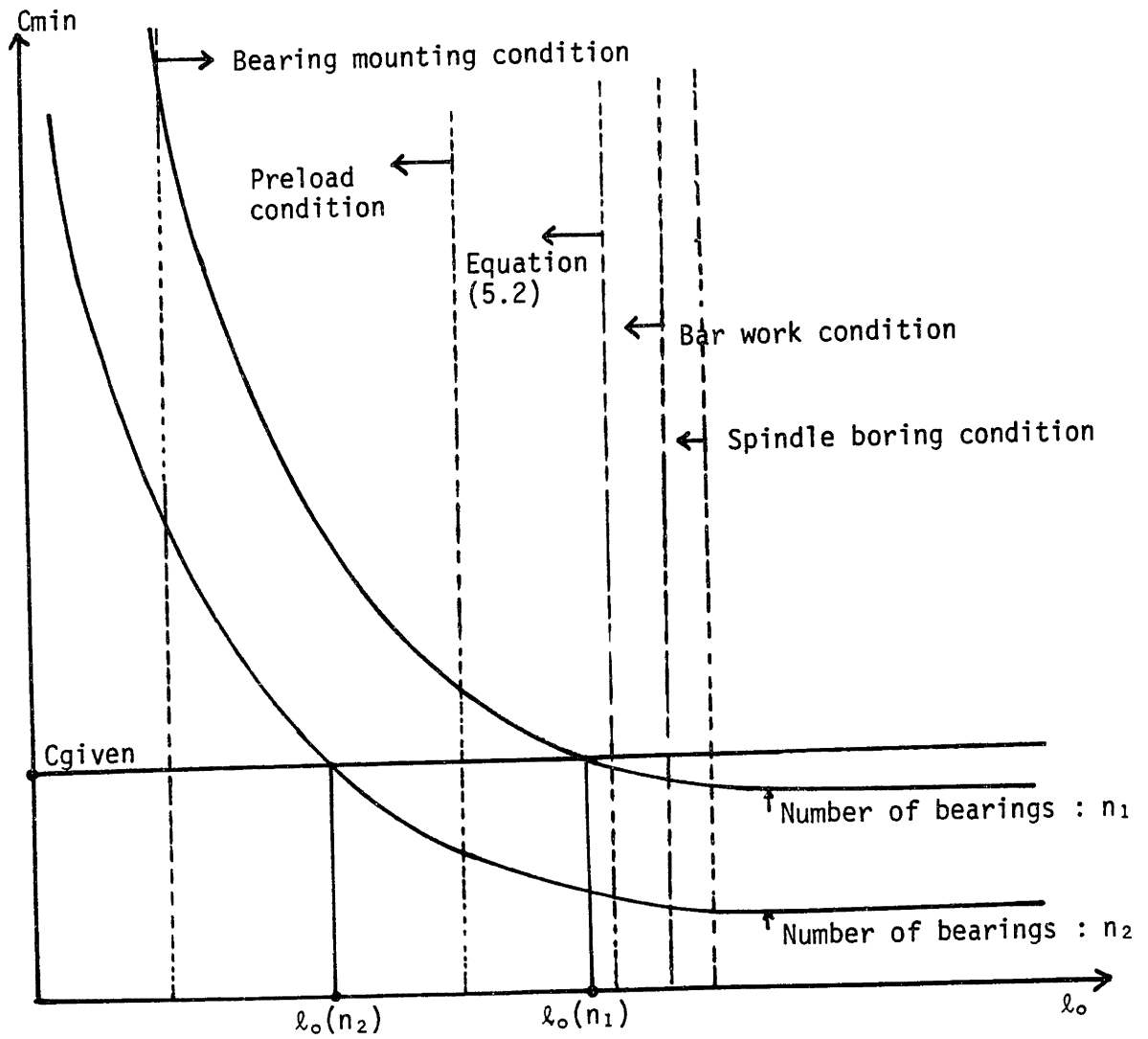


Fig. 5.4 Several Limitations on the Optimal Bearing Span Length l_o .

in Chapter 4 predicts the natural frequencies well. Also, the model predicts the damping of the rigid body mode well but does not predict the damping of the bending mode. However, the damping for the bending mode is large compared to that of the rigid body mode (See Fig. 3.3). Moreover, if the spindle material is made of a graphite epoxy composite material, the damping of the bending mode is larger than 10 %. Therefore, the primary concern is to increase the natural frequency of the rigid body mode in order to increase the damping of the spindle bearing system at this mode.

In order to increase the natural frequency of a spindle bearing system, the spindle bearing system should have high static stiffness. It should also have small spindle mass and spindle nose mass. The spindle nose mass of a milling machine can be reduced greatly compared to that for a lathe. Hence, the optimal design procedure for the spindle bearing system of a milling machine is presented in the next section using both steel and graphite epoxy composite materials.

5.3 The Example of the Optimal Design Procedure of a Milling Machine

In this section the optimal design procedure of a milling machine is presented using the principles developed in the previous sections. The objectives of the optimal design of the milling machine are selected as follows :

- (a) Minimal Maintenance Requirements
- (b) Ease of Manufacture
- (c) Small Number of Bearings and Small Size
for a Given Set of Specifications.

Let us design a milling machine which has the following specifications :

$$a = 2.0 \text{ in}$$

$$M_s = 0.03 \text{ slug}$$

$$M_p = 0.03 \text{ slug}$$

$$C = 1.50 \cdot 10^{-6} \text{ in/lb}$$

$$\text{Maximum RPM} = 4,000 \text{ RPM}$$

$$\text{Minimum Natural Frequency} = 1.50 \text{ kHz}$$

Then the design steps are as follows.

Step 1 :

The first step in the optimal design of a spindle bearing system is to select the lubrication method. From objective (a), the first choice of lubrication method is sealed grease lubrication. If other conditions preclude the use of this method, oil lubrication will be the next choice.

Step 2 :

After the selection of the lubrication method, the type of bearings should be determined. From objective (b), the first choice for the type of bearings is angular contact ball bearings. If other conditions preclude the use this type of bearings, then the tapered roller bearing will be the next choice.

Step 3 :

After the selection of the lubrication method and the type of bearings, the bearing diameter, the number of bearings, the optimal bearing span length l_0 and the sectional moment

of inertia I of the spindle should be determined.

Sometimes there is no solution in this step which is compatible with the lubrication method and the bearing type selected in steps 1 and 2. In this case we should go back and change the lubrication method or the type of bearings.

In order to have high bearing stiffness, we should select the largest bearing diameter which satisfies the maximum RPM condition (See Table 5.1). If we select the medium preload condition, the maximum diameter of the angular contact ball bearing, which allows 4,000 RPM (actually 3,900 RPM), is 70 mm (from Table 5.1).

Therefore, let us select the SEB 70 bearing with a contact angle of 15 degrees, and a preload of 180 lb (maximum preload of 230 lb). Then from Equation (4.9), the static stiffness of the bearing is $7.66 \cdot 10^5$ lb/in.

If we can use separate preloading mechanisms for the front and rear bearings, the number of front bearings and the number of rear bearings need not be the same. We can use more bearings in the front of the spindle because the front bearings greatly affect the static stiffness of the spindle bearing system (See equation 5.3).

However, in this design, the same number of bearings for the front and rear of the spindle are assumed in order to simplify the preloading mechanism.

For the first trial, let us use one bearing at the front of the spindle and one bearing at the rear of the spindle. Then

$$k_1 = k_2 = 7.66 \cdot 10^5 \text{ lb/in}$$

From Equation (5.3) and the compliance condition ($C = 1.50 \cdot 10^{-6}$ in/lb), the optimal bearing span length ℓ_o is calculated as follows :

$$1.50 \cdot 10^{-6} = 2 \left(\frac{a}{\ell_o} \right) \left(1 + \frac{a}{\ell_o} \right) \left(2.62 \cdot 10^{-6} \frac{a}{\ell_o} + 1.31 \cdot 10^{-6} \right) + 1.31 \cdot 10^{-6} \left(1 + \frac{a}{\ell_o} \right)^2 + 1.31 \cdot 10^{-6} \left(\frac{a}{\ell_o} \right)^2$$

or

$$\ell_o / a = 33.3$$

Since $a = 2.0$ inch was given in the preliminary specifications, we obtain

$$\ell_o = 66.6 \text{ inch}$$

With these values, EI is calculated from Equation (5.2) as :

$$EI = \frac{2 \cdot 66.6^2}{6 \left[\frac{2.0}{66.6} 2.62 \cdot 10^{-6} + 1.31 \cdot 10^{-6} \right]} = 1.06 \cdot 10^9 \text{ lb} \cdot \text{in}^2$$

Since a 70 mm diameter solid graphite epoxy composite bar with winding angle $[\pm 15]_s$ has $EI = 65.7 \cdot 10^6$ lb.in, there is no solution in this case (See Fig. 5.4). The largest optimal bearing span of the 70 mm spindle using graphite epoxy composite, which has a winding angle $[\pm 15]_s$, is calculated from Equation (5.2) as follows :

$$65.7 \cdot 10^6 \text{ lb.in}^2 = \frac{a \ell_o^2}{6 \left[\frac{a}{\ell_o} \left(\frac{1}{k_1} + \frac{1}{k_2} \right) + \frac{1}{k_1} \right]}$$

or

$$\ell_o/a \leq 9.5$$

For the second trial, let us use two bearings at the front of the spindle and two bearings at the rear of the spindle. Then

$$k_1 = k_2 = 2k_o = 1.532 \cdot 10^6 \text{ lb/in}$$

From Equation (5.3) and the given compliance condition, the optimal bearing span length is

$$1.50 \cdot 10^{-6} = 2 \left(\frac{a}{\ell_o} \right) \left(1 + \frac{a}{\ell_o} \right) \left(1.251 \cdot 10^{-6} \frac{a}{\ell_o} + 6.527 \cdot 10^{-7} \right) \\ + 6.527 \cdot 10^{-7} \left(1 + \frac{a}{\ell_o} \right)^2 + 6.527 \cdot 10^{-7} \left(\frac{a}{\ell_o} \right)^2$$

or

$$\ell_o/a = 10.0$$

With the given bearing stiffnesses and the maximum $EI = 65.7 \cdot 10^6$ lb.in² of the 70 mm spindle, the largest optimal bearing

span length is

$$65.7 \cdot 10^6 \text{ lb} \cdot \text{in}^2 = \frac{a \ell_o^2}{6 \left[\frac{a}{\ell_o} 1.251 \cdot 10^{-6} + 6.527 \cdot 10^{-7} \right]}$$

or

$$\ell_o / a \leq 6.5$$

Therefore, there is no solution in this case either.

For the third trial, let us use three bearings at the front of the spindle and three bearings at the rear of the spindle. Then

$$k_1 = k_2 = 3k_o = 2.30 \cdot 10^6 \text{ lb/in}$$

From Equation (5.3) and the given compliance condition, the optimal bearing span length is

$$1.50 \cdot 10^{-6} = 2 \left(\frac{a}{\ell_o} \right) \left(1 + \frac{a}{\ell_o} \right) \left(\frac{a}{\ell_o} 8.696 \cdot 10^{-7} + 4.348 \cdot 10^{-7} \right)$$

or

$$\ell_o / a = 1.9$$

With these values and Equation (5.2), EI is

$$EI = \frac{2 \cdot 3.8^2}{6 \left(1/1.9 \cdot 8.696 \cdot 10^{-7} + 4.348 \cdot 10^{-7} \right)} = 5.393 \cdot 10^6 \text{ lb} \cdot \text{in}^2$$

In this case there is an optimal solution because the calculated EI is less than $65.7 \cdot 10^6 \text{ lb} \cdot \text{in}^2$.

If we use [± 15]s graphite epoxy composite as the spindle material, the inner diameter of the spindle (DI) is 68.5 mm, or 2.70 inch. The wall thickness of the spindle is only 0.03 inch in this case. If we use steel as a spindle material, the wall thickness is thinner than 0.03 inch. Therefore, it is not the optimal solution from the point of view of spindle boring operation or of manufacturing the graphite epoxy composite shaft.

We now have two options :

- (1) Increasing the wall thickness (hence increasing the optimal bearing span length from Equation (5.2)) to increase the static stiffness (See Equation (5.3)).
- (2) Decreasing the bearing diameter to increase the maximum RPM.

Let us consider the second case : decreasing the bearing diameter to increase the maximum rotational speed. If we select the SEB 60 bearing with a 15 degree contact angle, the maximum rotational speed is 4,500 RPM with medium pre-load (from Table 5.1). The bearing data of SEB 60 are as follows :

$$Z = 22$$

$$d = 7.94 \text{ mm}$$

If we give 130 lb preload to the bearing, the radial stiffness of the bearing from Equation (4.8) is

$$\begin{aligned} k_o &= 2.2 \cdot 10^6 \cdot \cot(15^\circ) \cdot (\sin(15^\circ))^{5/3} \left(\frac{130}{0.22} \right)^{1/3} \cdot 22^{2/3} \cdot 7.94^{1/3} \\ &= 6.35 \cdot 10^5 \text{ (lb/in)} \end{aligned}$$

Hence

$$k_1 = k_2 = 3k_o = 1.91 \cdot 10^6 \text{ lb/in}$$

With these bearing stiffnesses and the given compliance condition, the optimal bearing span length from Equation (5.3) is

$$\begin{aligned} 1.5 \cdot 10^{-6} &= 2 \left(\frac{a}{l_o} \right) \left(1 + \frac{a}{l_o} \right) \left(1.05 \cdot 10^{-6} \frac{a}{l_o} + 5.25 \cdot 10^{-7} \right) \\ &\quad + 5.25 \cdot 10^{-7} \left(1 + \frac{a}{l_o} \right)^2 + 5.25 \cdot 10^{-7} \left(\frac{a}{l_o} \right)^2 \end{aligned}$$

$$\text{or } l_o/a = 3.57$$

With these values, EI from Equation (5.2) is calculated as follows :

$$EI = \frac{a l_o^2}{6 \left[\frac{a}{l_o} \left(\frac{1}{k_1} + \frac{1}{k_2} \right) + \frac{1}{k_1} \right]} = 20.52 \text{ lb} \cdot \text{in}^2$$

If we use [± 15]s graphite epoxy composite as the spindle material, the inner and outer diameter of the spindle in

this case are 1.90 inch and 2.36 inch respectively (mass density per length = $2.77 \cdot 10^{-3}$ slug/in). If we use steel as the spindle material, the inner and outer diameters of the spindle are 2.03 inch and 2.36 inch respectively (mass density per length = $1.0 \cdot 10^{-2}$ slug/in).

The maximum length of the steel spindle for SEB 60 with 130 lb preload without temperature compensation, when the temperature difference between the spindle and spindle case is 20°F, $\lambda_0 = 5.1$ inch from Equation (3.1). Therefore, temperature compensation is necessary for the steel spindle in this optimal solution. If static stiffness were to be increased rather than the maximum speed, then the optimal solution of the steel spindle without temperature compensation would be possible.

Step 4 :

Since all the properties of the spindle bearing system were determined in the last three steps, the natural frequencies of the spindle bearing systems can be calculated.

If we use [± 15]s graphite epoxy composite as the spindle material of the milling machine, we have the following properties :

$$k_1 = k_2 = 1.91 \cdot 10^6 \text{ lb/in}$$

$$a = 2 \text{ in}$$

$$l_o = 7.1 \text{ in}$$

$$EI = 20.52 \text{ lb}\cdot\text{in}^2$$

$$M_s = 0.03 \text{ slug}$$

$$M_p = 0.03 \text{ slug}$$

$$\rho = 2.77 \cdot 10^{-3} \text{ slug/in}$$

If we use steel as the spindle material of a milling machine, all the properties are same except for ρ , M_s and M_p . Since the steel spindle has the larger mass density (0.01 slug/in) than graphite composite spindle, the lumped mass M_s and M_p are increased by the following amount :

$$(0.01 \text{ slug/in} - 0.00277 \text{ slug/in}) \cdot 2 \text{ in} = 0.0144 \text{ slug}$$

Therefore, the properties of the steel spindle for the milling machine are as follows :

$$k_1 = k_2 = 1.91 \cdot 10^6 \text{ lb/in}$$

$$a = 2 \text{ in}$$

$$l_o = 7.1 \text{ in}$$

$$EI = 20.52 \text{ lb}\cdot\text{in}^2$$

$$M_s = 0.0444 \text{ slug}$$

$$M_p = 0.0444 \text{ slug}$$

$$\rho = 0.01 \text{ slug/in}$$

(a) The Fundamental Mode

From Equations (4.16a) and (4.17a), the kinetic energy T and potential energy U are calculated with the above spindle properties as follows :

$$T(\text{graphite spindle}) = 1.852 \cdot 10^{-14} \dot{P}_1^2$$

$$T(\text{steel spindle}) = 3.997 \cdot 10^{-14} \dot{P}_1^2$$

$$U(\text{graphite spindle}) = U(\text{steel spindle}) = 4.520 \cdot 10^{-7} P_1^2$$

Therefore, the natural frequency of the graphite spindle is

$$\begin{aligned} \omega_1(\text{graphite spindle}) &= \sqrt{\frac{4.520 \cdot 10^{-7} \cdot 12}{1.852 \cdot 10^{-14}}} \\ &= 1.71 \cdot 10^4 \text{ rad/sec} \\ &= 2.72 \text{ kHz} \end{aligned}$$

By the same method the natural frequency of the steel spindle is calculated as

$$\omega_1(\text{steel spindle}) = 1.85 \text{ kHz}$$

The natural frequency of the graphite spindle in this case is about 50 % higher than that of the steel spindle.

The damping factor of the graphite spindle from Equation (4.26a) is calculated as follows :

$$\eta_1 (\text{graphite spindle}) = \frac{1.71 \cdot 10^4 \left\{ \frac{17.1}{(1.91 \cdot 10^6)^2} \cdot (1+0.28)^2 + \frac{17.1}{(1.91 \cdot 10^6)^2} \cdot 0.28^2 \right\}}{\frac{1}{1.91 \cdot 10^6} \cdot 0.28^2 + \frac{1}{1.91 \cdot 10^6} \cdot 1.28^2}$$

$$= 0.153$$

In this calculation, the following viscous damping coefficients were assumed :

$$b_1 = b_2 = 17.1 \text{ lb}\cdot\text{s/in}$$

By the same method the damping factor of the steel spindle is calculated as follows :

$$\eta_1 (\text{steel spindle}) = 0.102$$

(b) The Bending Mode

The shear effect term in Equation (4.33) for the optimally designed graphite epoxy composite spindle is

$$2.65 \frac{h^2}{l^2} = 0.05$$

From this result and using Equations (4.18) and (4.19), the kinetic energy T and the potential energy U are calculated as follows :

$$T(\text{graphite spindle}) = 2.815 \dot{P}_2^2 - 0.273 \dot{P}_2 \dot{P}_3 + 0.0310 \dot{P}_3^2$$

$$T(\text{steel spindle}) = 4.466 \dot{P}_2^2 - 0.406 \dot{P}_2 \dot{P}_3 + 0.0566 \dot{P}_3^2$$

$$U(\text{graphite spindle}) = 12(1.242 \cdot 10^8 P_2^2 + 1.906 \cdot 10^7 P_2 P_3$$

$$+ 3.916 \cdot 10^6 P_3^2)$$

$$= 1.490 \cdot 10^9 P_2^2 + 2.287 \cdot 10^8 P_2 P_3 + 4.70 \cdot 10^7 P_3^2$$

$$U(\text{graphite spindle}) = U(\text{steel spindle})$$

By the Lagrange equation, we have the following eigen value problem for the graphite epoxy composite spindle bearing system :

$$\begin{bmatrix} 2.815 \omega^2 - 1.490 \cdot 10^9 & -0.137 \omega^2 - 1.144 \cdot 10^8 \\ -0.137 \omega^2 - 1.144 \cdot 10^8 & 0.0310 \omega^2 - 4.70 \cdot 10^7 \end{bmatrix} \begin{bmatrix} P_2 \\ P_3 \end{bmatrix} = 0$$

From the eigen value problem, we can obtain following frequency equation :

$$\omega^4 - 3.063 \cdot 10^9 \omega^2 + 8.313 \cdot 10^{17} = 0$$

or

$$\omega_2(\text{graphite spindle}) = 1.735 \cdot 10^4 \text{ rad/sec} = 2.76 \text{ kHz}$$

If we substitute the frequency obtained in the eigenvalue equation, the following relation is obtained.

$$P_3 = -4.1 P_2$$

By the same method, the natural frequency of the steel spin-

die is obtained as follows :

$$\omega_2 \text{ (steel spindle) } = 2.2 \text{ kHz}$$

$$P_3 = -4.5 P_2$$

Table 5.2 compares several characteristics of the manufactured graphite epoxy composite spindle bearing system and the optimally designed graphite epoxy composite spindle bearing system.

Table 5.3 compares the several characteristics of the optimally designed graphite epoxy composite spindle bearing system and the optimally designed steel spindle bearing system. Figure 5.5 shows the proposed spindle bearing system for the milling machine.

In summary, the graphite epoxy composite spindle bearing system is better than the steel spindle bearing system in maintaining the bearing preload at higher bearing temperatures. The graphite epoxy composite spindle bearing system is suitable for a high speed machine tool which has a small spindle nose mass, because the natural frequency of a spindle bearing system is dependent on the spindle nose mass as well as the spindle mass. Since the graphite epoxy composite spindle is very light and has high material damping, this spindle is suitable for both high speed air bearing and magnet bearing because these two bearings have little damping and require the highly damped spindle material. The

Table 5.2 Comparison of the Properties of the Manufactured and the Optimally Designed Graphite Epoxy Composite Spindle Bearing Systems

| | Manufactured spindle | Optimally designed Spindle |
|--------------------------------|----------------------|----------------------------|
| C (in/lb) | $1.79 \cdot 10^{-6}$ | $1.50 \cdot 10^{-6}$ |
| a (in) | 2.5 | 2.0 |
| ℓ (in) | 5.0 | 7.1 |
| EI (lb·in ²) | $35 \cdot 10^6$ | $20.52 \cdot 10^6$ |
| Frequency of rigid body motion | 1.09 kHz | 2.72 kHz |
| Frequency of bending motion | 1.50 kHz | 2.76 kHz |
| Maximum RPM | 4,000 | 4,500 |
| Number of bearings | 5 (SEB 70) | 6 (SEB 60) |

Table 5.3 Comparison of the Properties of the Optimally Designed Graphite Epoxy Composite Spindle Bearing System and the Optimally Designed Steel Spindle Bearing System

| | Graphite spindle | Steel spindle |
|--------------------------------|----------------------|---------------------|
| Temperature Compensation | not necessary | necessary |
| ρ (slug/in) | $2.77 \cdot 10^{-3}$ | $1.0 \cdot 10^{-2}$ |
| Frequency of rigid body motion | 2.72 kHz | 1.85 kHz |
| Frequency of bending motion | 2.76 kHz | 2.2 kHz |

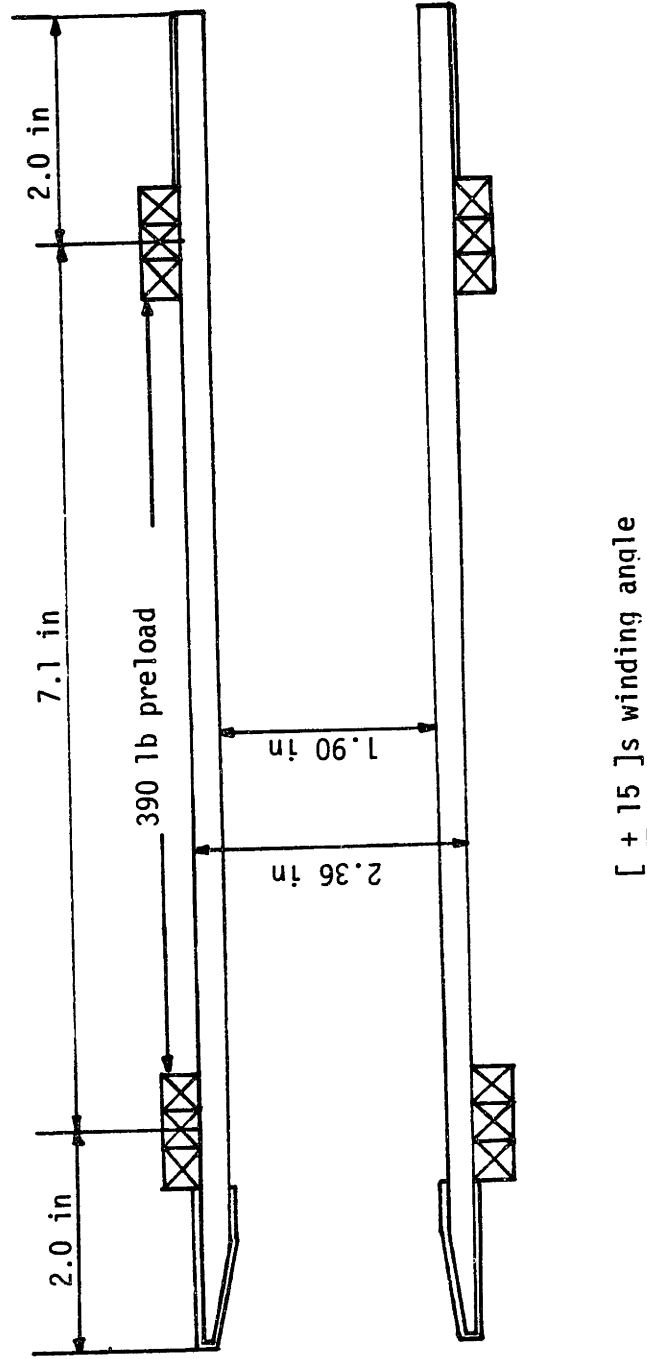


Fig. 5.5 Schematic Drawing of the Optimally Designed Graphite Epoxy Composite Spindle Bearing System

acceleration and deceleration time of the graphite epoxy composite spindle can be reduced significantly in high speed machining because of its light weight and low rotational moment of inertia. The decrease of the acceleration and deceleration time will increase the productivity in automated factories.

The disadvantages in the use of the graphite epoxy composite spindle over the conventional spindle are that the raw material for the composite spindle is expensive and also difficult to be machined. It usually requires grinding machines or diamond grit tools to machine the graphite epoxy composite. As for the cost of the material, the price of high strength graphite fiber pre-preg tape is about \$ 30 per pound and the price of high modulus graphite fiber pre-preg tape is about 80 \$ per pound. The future prices of graphite epoxy composites will be cheaper than these values.

However, these two disadvantages can be minimized by designing the spindle such that the machining requirements will be reduced. During the process of manufacturing the steel spindle about 90 % of the raw material should be machined out. However in the case of the composite spindle, the shape of the graphite epoxy material can be made to resemble the final design of the spindle. Thus, minimal machining is needed and the expensive raw material is conserved.

6. THE MANUFACTURING OF THE COMPOSITE BED

6.1 Introduction

It has been established that some damping materials, such as visco-elastic materials [16-27] or sands [6], can increase the damping of the machine tool structure. Polymer concrete is another high damping material which has been used in machine tool structures in Europe [9].

In this chapter the composite bed structure is designed and manufactured using these high damping materials simultaneously. In section 6.2 the manufacturing method of the composite bed structures is presented. In section 6.3 the dynamic performance of the composite bed is compared to that of the existing, similar size cast iron bed.

6.2 The Manufacturing Method of the Composite Bed Structure

From the several polymer concrete materials available [10], the epoxy resin concrete was used in manufacturing the composite bed. It has a modulus of elasticity about 5.3 Mpsi and a coefficient of thermal expansion about $5.3 \cdot 10^{-6} / ^\circ\text{F}$ (See Table 6.1). Its modulus of elasticity and density are about 0.2 and about 0.3 times that of the cast iron. The

Table 6.1 Properties of Polymer Concrete [10]

Table 1. Properties of Polymer/Concrete Composites in Comparison with Ordinary Concrete (1)

| Property | PC | PIC | PPCC | Concrete |
|----------------------------------------------------------|--------|--------|--------|----------|
| Compressive strength, psi | 20,000 | 21,000 | 6,000 | 5,000 |
| Tensile strength, psi | 1,400 | 1,500 | 600 | 250 |
| Modulus of elasticity, 10 ⁶ psi | 5.3 | 6.1 | 3.8 | 3.6 |
| Shear strength, 10 ³ psi | 3.7 | 3.8 | 2.0 | 1.1 |
| Modulus of rupture, 10 ³ psi | 2.2 | 3.0 | 2.4 | 0.7 |
| Coefficient of expansion, 10 ⁻⁶ in./in.-°F | 5.3 | 5.1 | 4.3 | 4 |
| Water permeability, 10 ⁻⁴ ft/yr | 0 | 1.2 | 3.8 | 5.3 |
| Water absorption, %w | 0.3 | 2.2 | 3.6 | 5.3 |
| Freeze/thaw resistance, # of cycles | 3,300 | 4,600 | 1,600 | 590 |
| % weight lost | 0 | 0 | 12 | 25 |
| Hardness, impact hammer | 55 | 52 | 41 | 32 |
| Acid resistance | | | | |
| % weight lost after 3 months of immersion: | | | | |
| 5% HCl | 0.3 | 5 | 13 | 24 |
| 15% HCl | 3 | 9 | 19 | 27 |
| 10% H ₂ SO ₄ | 1.2 | 26 | 30 | 39 |
| Sulphate attack | | | | |
| % expansion after 2 years of exposure | 0.003 | 0.006 | 0.25 | 0.5 |
| Corrosion by distilled water | None | None | Slight | Severe |
| Thermal conductivity BTU/ft ² -h-°F | 1.206 | 1.265 | 1.306 | 1.332 |

Table 2. Comparison of PC with Other Structural Materials (1)

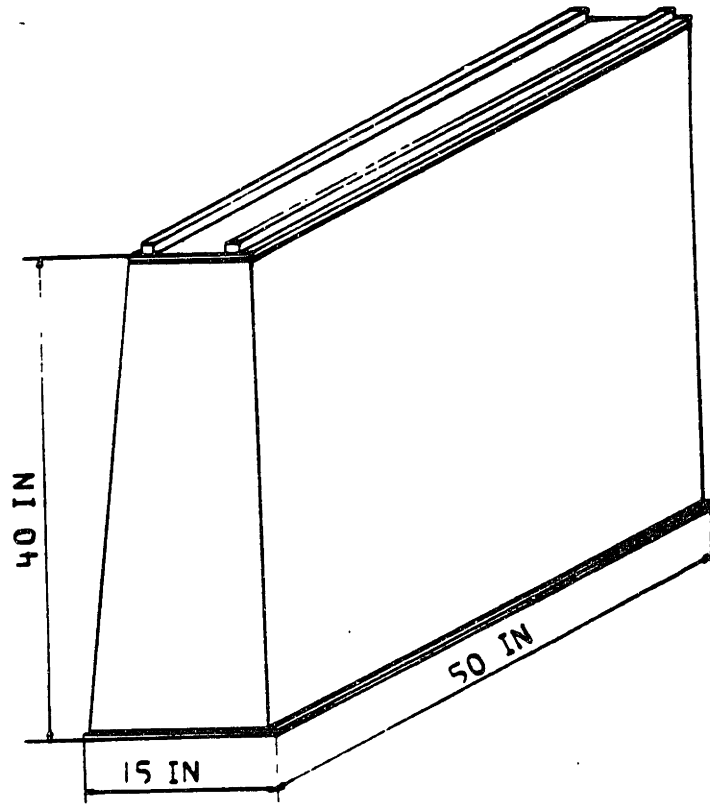
| Material | Strength property (S), psi | Density (W) lb/ft ³ | Strength to weight ratio (S/W), psi-ft ³ /lb |
|---------------------------------|----------------------------------|-----------------------------------|---------------------------------------------------------------|
| Tensile | | | |
| Concrete | 250 | 156 | 1.6 |
| PC | 1,400 | 140 | 10 |
| Polymer | 7,000 | 62 | 113 |
| Steel | 70,000 | 490 | 143 |
| Aluminium | 30,000 | 165 | 182 |
| Glass | 7,000 | 137 | 51 |
| Compressive | | | |
| Concrete | 5,000 | 156 | 32 |
| PC | 20,000 | 140 | 143 |
| Polymer | 15,000 | 62 | 242 |
| Steel | 42,000 | 490 | 86 |
| Aluminium | 25,000 | 165 | 152 |
| Glass | 300,000 | 137 | 2,190 |
| Modulus of elasticity, E | | | |
| Concrete | 3.6 × 10 ⁶ | 156 | 2.3 × 10 ⁶ |
| PC | 5.3 × 10 ⁶ | 140 | 3.8 × 10 ⁶ |
| Polymer | 0.4 × 10 ⁶ | 62 | 0.6 × 10 ⁶ |
| Steel | 30 × 10 ⁶ | 490 | 6.1 × 10 ⁶ |
| Aluminium | 10 × 10 ⁶ | 165 | 6.1 × 10 ⁶ |
| Glass | 10 × 10 ⁶ | 137 | 7.4 × 10 ⁶ |

damping factor of the epoxy resin concrete is about 0.02 at about 1,000 Hz vibration frequency. This value of damping factor is very large compared to the damping factors of steel and cast iron. The damping factor of the metallic materials is usually less than 0.001 at about 1,000 Hz vibrational frequency.

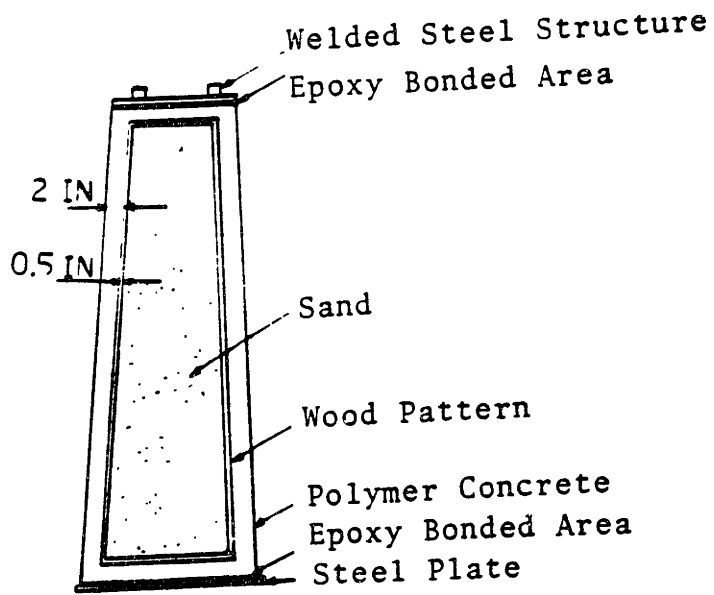
The dynamic performance of the machine tool structure is determined by the product of the stiffness and damping of the structure (See Appendix E). Therefore, the epoxy resin concrete machine tool bed can perform statically and dynamically better than the steel or cast iron bed structure if we design an epoxy concrete bed which has more sectional moment inertia (I) than that of the steel or cast iron bed. The method to increase the stiffness of a structure which is composed of high damping material costs less than the method to increase the damping of a structure which is composed of high stiffness material [6].

Koenigsberger [74] has suggested the closed box cross-section as a bed shape to increase both the bending and torsional stiffness. Other researchers [6] pointed out the possibility of increasing stiffness by using welded steel structure instead of cast iron.

With these concepts in mind, the model of the composite bed in this research was made as a box type cross-section structure (See Fig. 6.1). The model of the slide was made with a welded steel structure (ASTM A36 steel plate) and the



(a)



(b)

Fig. 6.1 Composite Bed Structure : (a) Overview ;
(b) Cross section.

bottom plate was made with 0.5 inch thick ASTM A36 steel plate. These two steel plates were bonded to the epoxy concrete structure by epoxy adhesives to give constrained damping to the bed structure. The epoxy adhesive used in the bonding operation is the same epoxy used in making epoxy concrete.

The polymer concrete is composed of epoxy, epoxy hardener, portland cement, sand and pebble.

The epoxy resin used is EPON 828 made by the Shell Chemical Company and the hardener used is Ancamide 506 made by the Pacific Anchor Chemical Corporation. Ancamide 506 hardener is the Amine based hardener which can be cured at room temperature and has long pot life (6 hours).

The size of the sand used is 50 sieve number and the diameter of pebble used is from 1.0 in to 1.5 in.

The weight percentages of the resin, portland cement, sand and pebble are 10 %, 10 %, 40 % and 40 % respectively.

The inside of the polymer concrete is composed of the plywood pattern and the sand. The inside wood pattern is not eliminated from the composite bed to increase damping. Several sizes of sand (1, 25, 50 and 100 sieve numbers) were poured into the wood pattern because sand has good damping properties if the amplitude of vibration exceeds 0.001 in [6].

Fig. 6.2 shows the prototype composite bed on which the graphite epoxy composite spindle bearing system was

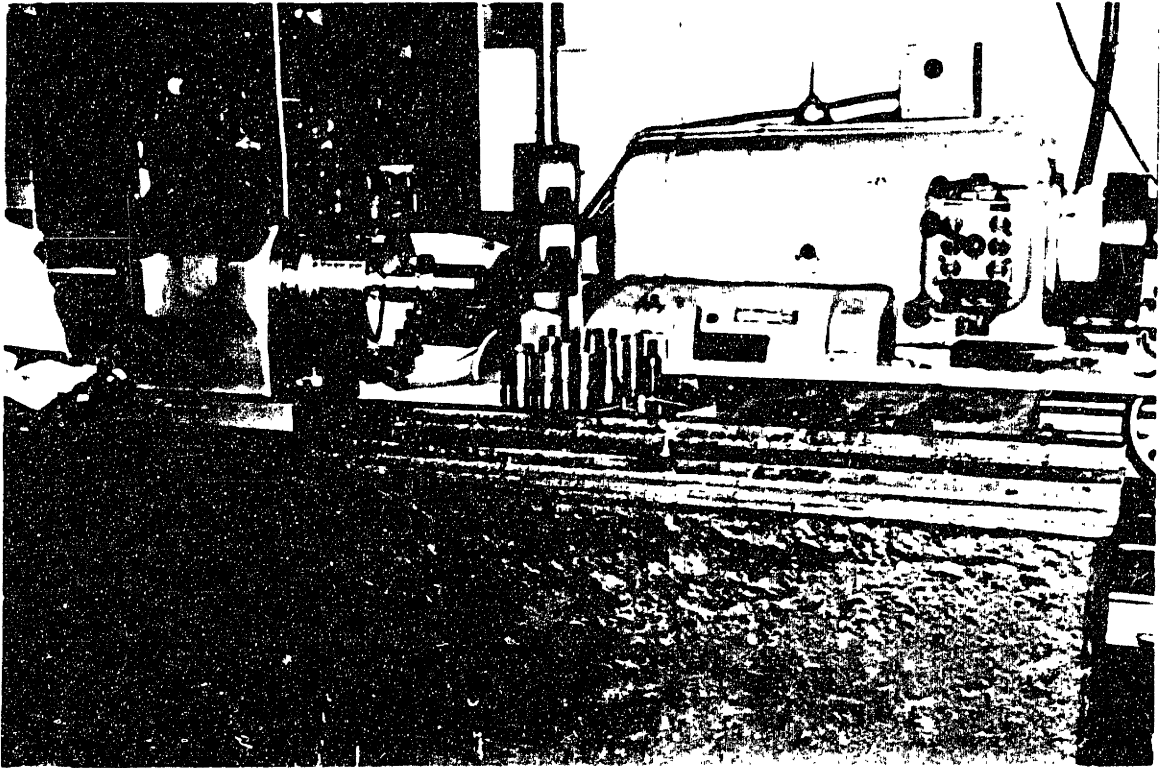


Fig. 6.2 Composite Bed Model on Which the Graphite Epoxy Composite Spindle Bearing System is Mounted

mounted.

6.3 The Dynamic Test Results of the Composite Bed

The vibration characteristics of the composite bed were measured by an accelerometer and a data acquisition system. The accelerometer used is BBN Instruments Company 507 LF/HS having a sensitivity of 100 mv/g. The data acquisition system is composed of IBM personal computer and Tektronix 7603 digital oscilloscope (See Fig. 6.3). The vibration characteristics of the cast iron bed, which was manufactured by Delta Rockwell Company, was measured to be compared to that of the composite bed.

The outside dimensions of the composite bed are identical to those of the cast iron bed. The inside shape of the composite bed is different from that of the cast iron bed because the box type cross section was employed in manufacturing the composite bed. Fig. 6.4 shows the detailed cross-sections of the composite bed and the cast iron bed.

The vibrations of the beds were induced by dropping a steel ball at the center of the slides of the beds (See Fig. 6.5). The impulse kinetic energy of the steel ball which was given to the cast iron bed was reduced to half of the impulse kinetic energy which was given to the composite bed because the stiffness of the cast iron was so low that the

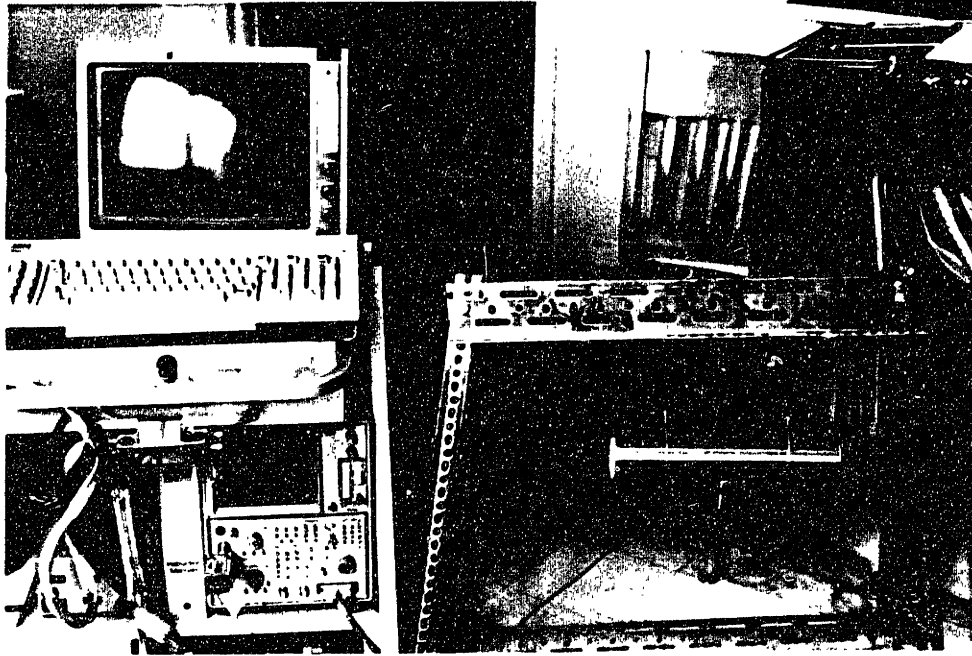
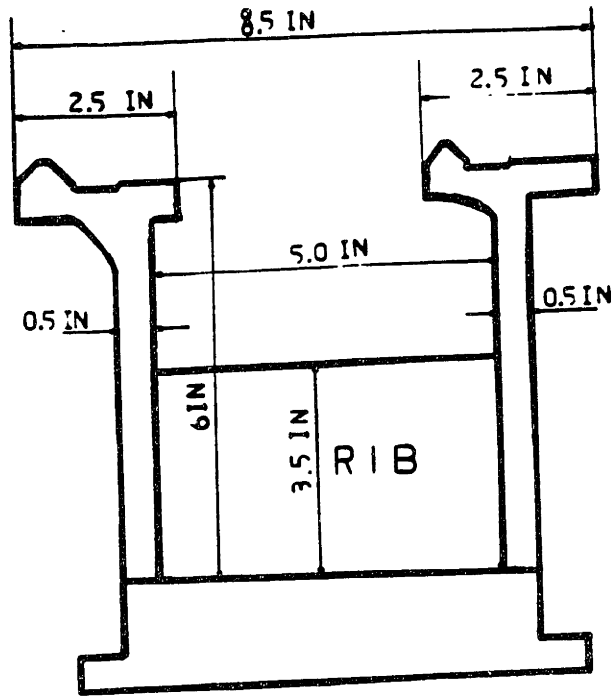
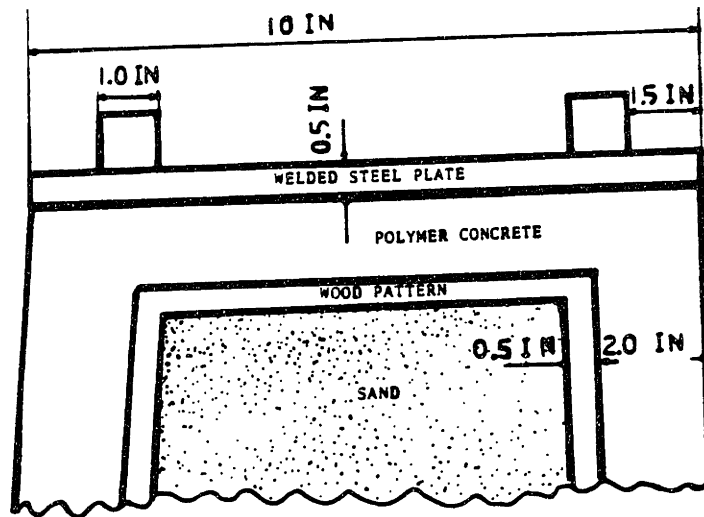


Fig. 6.3 Data Acquisition System Used in Measuring the Vibration of the Composite Bed



(a)



(b)

Fig. 6.4 Cross Sections of the Beds : (a) Cast Iron Bed ;
(b) Composite Bed

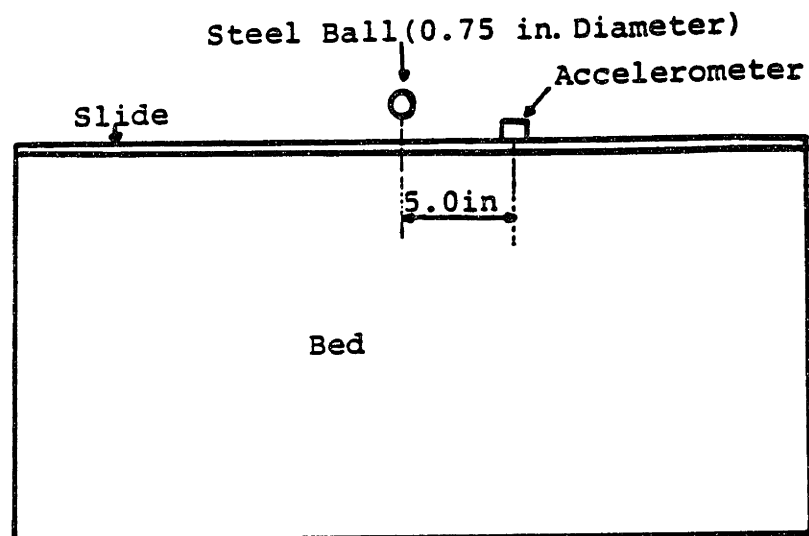


Fig. 6.5 Vibration Test Method of the Composite Bed

accelerometer output from the cast iron bed was saturated.

Fig. 6.6 shows the vibration characteristics of the composite bed and the cast iron bed. The vibration of the composite bed disappears after 2.5 millisecond. However, the vibration of the cast iron bed continues until 5.0 millisecond. Also Fig. 6.7 shows the high frequency characteristics of the composite bed.

In order to calculate the approximate damping factor of the beds from the vibration curve of Fig. 6.6, logarithmic decrement method was used (See Appendix A). The approximate damping factor of the composite bed is 0.055 and that of the cast iron bed is 0.035. Therefore, the damping of the composite bed is about 60 % higher than that of the cast iron bed. The cast iron bed was equipped with saddle, head stock, power transmitting gears and several screws when the vibration test was conducted. The composite bed had no such components when the vibration test was conducted. Therefore, 60 % higher damping of the composite bed is remarkable because the natural frequency of the composite bed is higher than that of the cast iron bed. The damping of the conventional material usually decreases with the increase of the frequency [46, 75].

The vibration amplitudes of the two beds from Fig. 6.6 are almost the same even though the impulse which was given to the composite bed was 50 % larger than that which was given to the cast iron bed. Therefore, we can estimate that

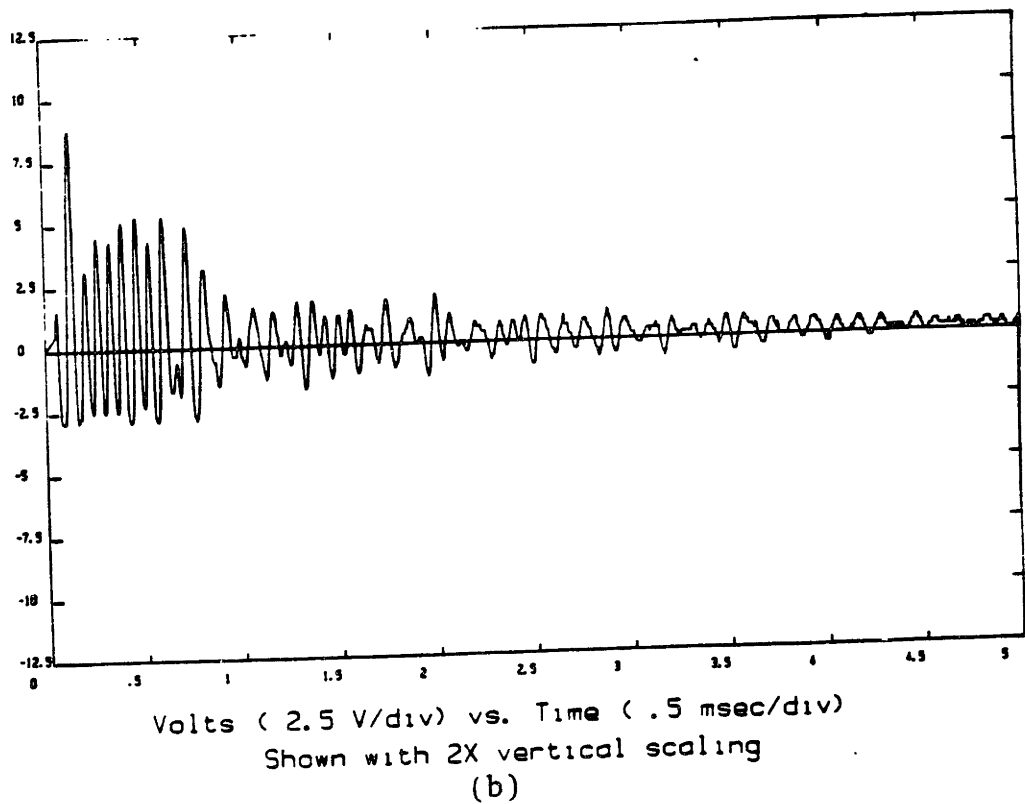
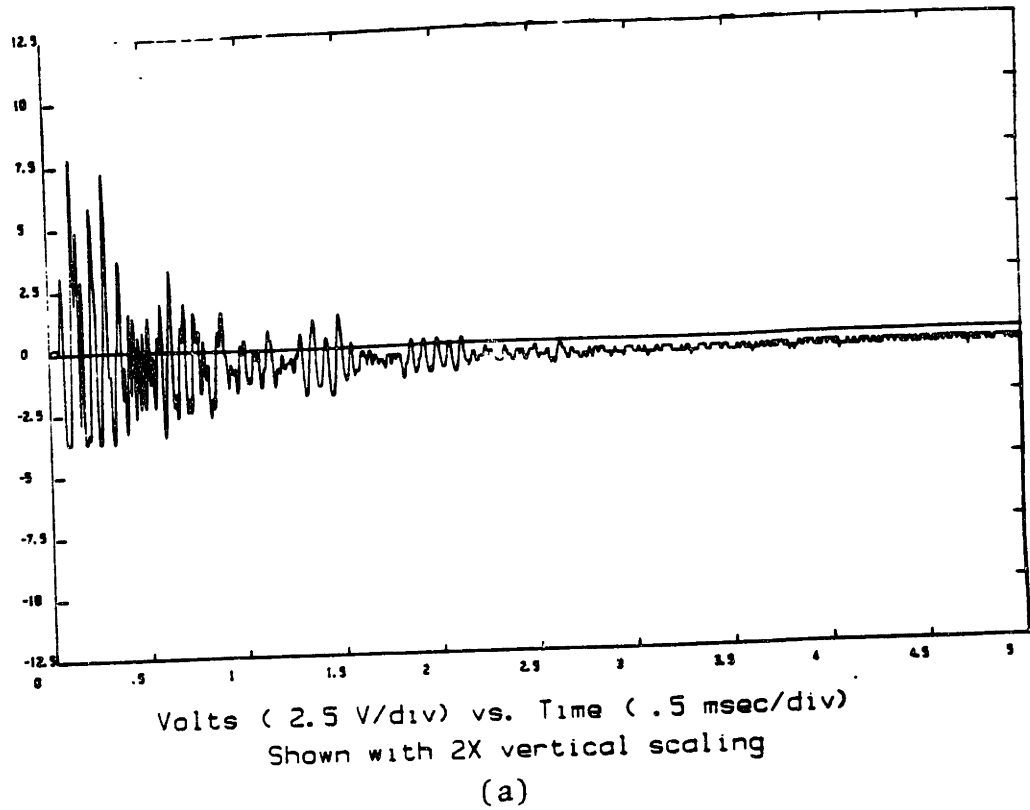


Fig. 6.6 Vibration of the Beds : (a) Composite Bed (0.2 lb-in Kinetic Energy) ; (b) Cast Iron Bed (0.1 lb-in Kinetic Energy)

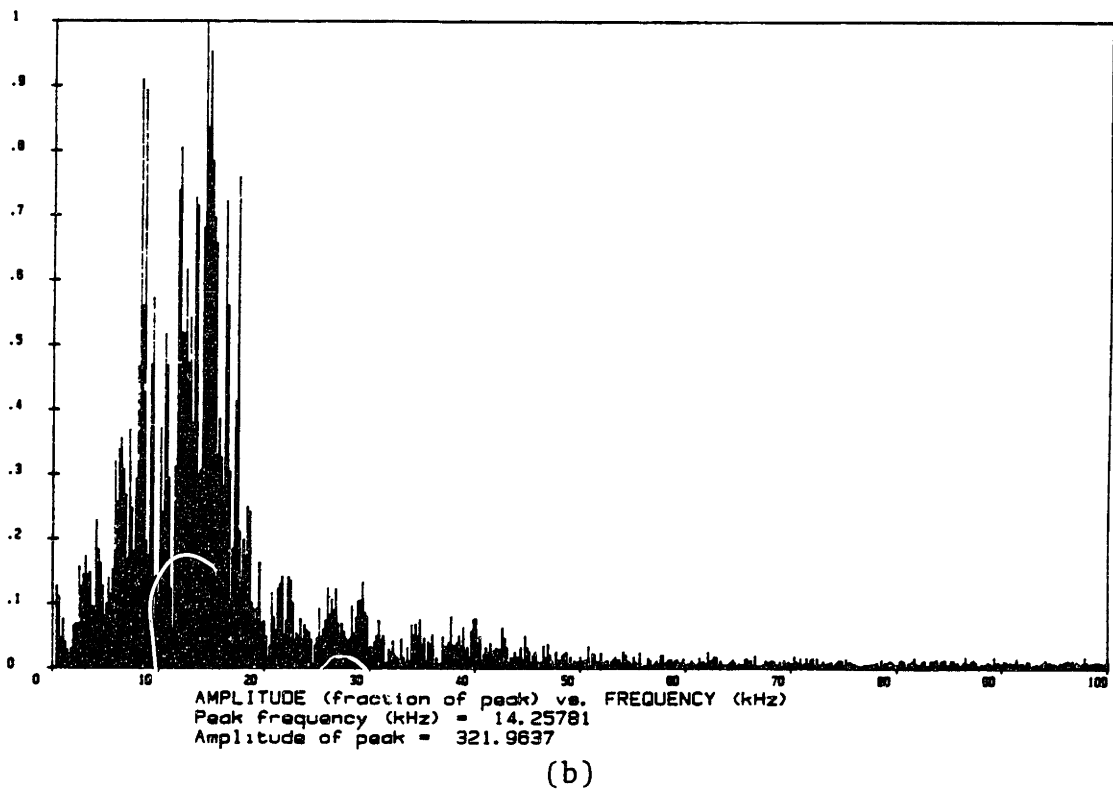
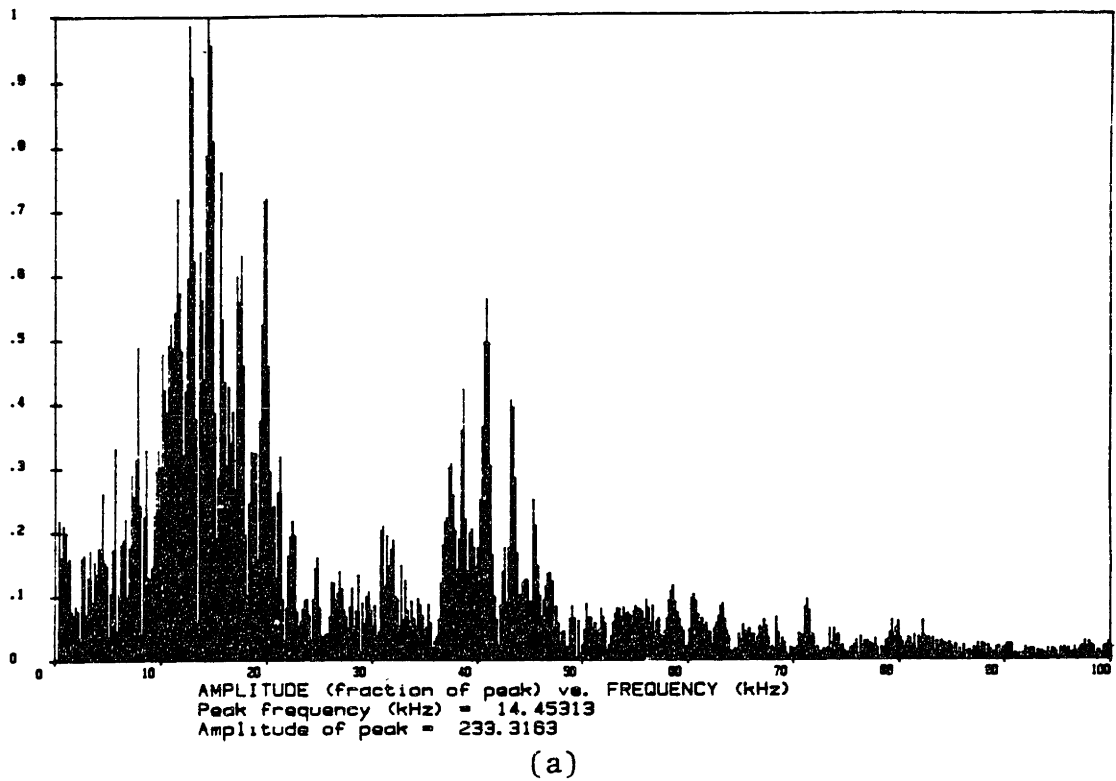


Fig. 6.7 Fast Fourier Transform Results of the Vibration of the Beds : (a) Composite Bed ; (b) Cast Iron Bed

the stiffness and damping of the composite bed were both increased at least 50 % compared to those of the cast iron bed.

7. DISCUSSIONS AND CONCLUSIONS

The spindle bearing system of a lathe was built using graphite epoxy composites to increase the natural frequency and damping of the spindle bearing system. A steel spindle which has the same flexural rigidity (EI) as the graphite epoxy composite spindle was also built in order to compare performance characteristics.

The graphite epoxy composite spindle bearing system is better than the steel spindle bearing system in maintaining the bearing preload at higher bearing temperatures, satisfies the noise limitation requirements, and is capable of transmitting the required torque in metal cutting operations.

The manufactured graphite epoxy composite spindle bearing system was observed to have a fundamental natural frequency at 1.09 kHz which is rigid body motion and the second natural frequency at 1.50 kHz which is bending motion of spindle. The steel spindle has its fundamental natural frequency at 0.94 kHz and the second natural frequency at 1.61 kHz. The fundamental natural frequency of the graphite epoxy composite spindle bearing system is higher by 16 % but its second natural frequency is decreased by 7 % because of the shear effect of the graphite epoxy composite material. However, the damping of the graphite epoxy composite spindle

bearing system at the second mode was increased by about 50 %.

The metal cutting ability of the graphite epoxy composite spindle increased by only 23 % : the first natural frequency cannot be increased dramatically due to the large spindle nose mass of the lathe even when the composite spindle has very low mass density.

In order to improve the metal cutting performance of the spindle bearing system, it is necessary to increase its fundamental natural frequency because the damping of the lateral vibration of the bearing is approximately proportional to the natural frequency [76] and the metal cutting ability of the machine tool is approximately proportional to the damping of the machine tool (See Appendix E).

In order to further improve the performance of the graphite epoxy composite spindle bearing system, the optimal design procedure of the spindle bearing system was developed.

The optimal design procedure implies that it is necessary to reduce the spindle nose mass as well as the spindle mass in order to increase the first natural frequency of the spindle bearing system. Therefore, the graphite epoxy composite spindle bearing system is suitable for a spindle bearing system which has a small spindle nose mass. If we designed optimally a high speed milling machine using graphite epoxy composites, the metal cutting performance would

increase by 50 % over that for a steel spindle bearing system.

In the metal cutting test of Chapter 3, the chatter in the metal cutting test appeared only when the negative rake angle cutting tool and 45 degree cutting angle were used. If the manufactured spindle bearing system were a high speed grinding or milling machine, the second mode of vibration might appear easily and the graphite epoxy composite spindle might perform much better than the steel spindle bearing system in the second mode of the vibration because of the high damping of the graphite epoxy composite spindle bearing system at this mode.

Since the graphite epoxy composite spindle is very light and has high material damping, this spindle is suitable for both the high speed air bearing and the magnet bearing. These two bearings have little damping and require the highly damped spindle materials. The damping of the graphite epoxy composite will play a major role in these high speed and low cutting force machine tools.

The model of the polymer concrete composite bed has very stiff structures because of its box type cross section. Its damping property is superior to that of the cast iron bed.

The machine tool has many complex shaped components which are attached to the bed. However, this complexity can be reduced by changing the design [9].

There are several advantages in manufacturing a polymer concrete composite bed which uses polymeric material as a bonding agency. We can use one mold repeatedly to manufacture many composite beds, but cast iron beds require the same number of molds as beds. In addition, the polymer concrete composite bed can be cast at room temperature without causing any air pollution.

The cost of epoxy is about 10 times greater than that of cast iron. The manufacturing cost of the composite bed is competitive because only 10 % epoxy is required, while the other ingredients are very inexpensive ; moreover these ingredients need only be mixed, while cast iron would require melting at high temperatures, which is expensive process.

In conclusion, the graphite epoxy composite spindle bearing system for a high speed milling machine or a high speed grinding machine and the prototype polymer concrete bed are recommended for production.

REFERENCES

- [1] The Machine Tool Industry Research Association, A Dynamic Performance Test for Lathes, July, 1971, 1-86.
- [2] F. P. Wardle, S. J. Lacey and S. Y. Poon, "Dynamic and Static Characteristics of a Wide Speed Range Machine Tool Spindle", Precision Engineering, 1983, 175-183.
- [3] F. Koenigsberger and J. Tlustý, Machine Tool Structures, Pergamon Press, Vol.1, 1970, Sect.2.
- [4] N. H. Cook, Manufacturing Analysis, Addison-Wesley Publishing Company, 1966, Chap.3, Chap.7.
- [5] H. E. Merritt, "Theory of Self-Excited Machine-Tool Chatter", Journal of Engineering for Industry, Transactions of ASME, 1965, 447-454.
- [6] D. B. Welbourn and J. D. Smith, Machine Tool Dynamics, Cambridge University Press, 1970, Chap.1, Chap.5, Chap.8.
- [7] J. Martin, "Diamond-Turned Telescope Mirrors", American Machinist, March, 1983, 106-109.
- [8] George Fisher Catalog, George Fisher Limited, CH-8201 Schaffhausen, P. O. Box 685, Schaffhausen, Switzerland.
- [9] H. Schultz and R. G. Nicklau, "Designing Machine Tool Structures in Polymer Concrete", Industrial and Production Engineering, 1982, 74-77.

- [10] E. Kirlikovali, "Polymer/Concrete Composite - A Review", Polymer Engineering and Science, Vol.21, No.8, 1981, 507-509.
- [11] J. Peters, "Damping in Machine Tool Construction", Proceedings of the 6th International M.T.D.R. Conference, 1965, 191-210.
- [12] J. Slavicek and J. G. Bollinger, "Design and Application of a Self-Optimizing Damper for Increasing Machine Tool Performance", Proceedings of the 10th International M.T.D.R. Conference, 1969, 71-80.
- [13] M. I. Chowdhury, M. M. Sadek and S. A. Tobias, "The Dynamic Characteristics of Epoxy Resin Bonded Machine Tool Structures", Proceedings of the 15th International M.T.D.R. Conference, 1974, 237-243.
- [14] B. J. Stone, "The State of Art in the Measurement of the Stiffness and Damping of Rolling Element Bearings", Annals of the CIRP, Vol.31/2, 1982, 529-538.
- [15] W. J. Hammill and C. Andrew, "Vibration Reduction with Continuous Damping Inserts", Proceedings of the 14th International M.T.D.R. Conference, 1973, 495-502.
- [16] P. J. Torvik, "The Analysis and Damping of Constrained Layer Damping Treatments", Damping Applications for Vibration Control, ASME, AMD-Vol.38.
- [17] S. H. Ko, "Flexural Wave Baffling by Use of a Viscoelastic Material", Journal of Sound and Vibration,

- 75(3), 1981, 347-353.
- [18] T. Lekszycki and N. Oihoff, "Optimal Design of Viscoelastic Structures under Forced Steady-State Vibration", *J. Struct. Mech.*, 9(4), 1981, 363-387.
- [19] N. R. Rao and K. V. Valsarajan, "Some Results of the Finite Deflection Analysis of Clamped Skew Sandwich Plates", *J. Struct. Mech.*, 10(2), 1982, 135-144.
- [20] E. M. Kerwin, Jr., "Damping of Flexural Waves by a Constrained Viscoelastic Layer", *The Journal of the Acoustical Society of America*, Vol.31, 1959, 952-962.
- [21] D. J. Mead and S. Markus, "The Forced Vibration of a Three-Layer, Damped Sandwich Beam with Arbitrary Boundary Conditions", *Journal of Sound and Vibration*, 10(2), 1969, 163-175.
- [22] D. J. Mead and S. Markus, "Loss Factors and Resonant Frequencies of Encastre Damped Sandwich Beams", *Journal of Sound and Vibration*, 12(1), 1978, 99-112.
- [23] D. J. Mead, "The Damping Properties of Elastically Supported Sandwich Plates", *Journal of Sound and Vibration*, 24(3), 1972, 275-295.
- [24] M. J. Yan and E. H. Dowell, "Governing Equations for Vibratory Constrained-Layer Damping Sandwich Plates and Beams", *Journal of Applied Mechanics, Transactions of ASME*, 1972, 1041-1046.
- [25] R. A. Ditaranto, "Theory of Vibratory Bending for Elastic and Viscoelastic Layered Finite-Length Beams",

- Journal of Applied Mechanics, Transactions of ASME, 1965, 881-896.
- [26] R. A. Ditaranto and J. R. McGraw, Jr., "Vibratory Bending of Damped Laminated Plates", Journal of Engineering for Industry, Transactions of ASME, 1969, 1081-1090.
- [27] C. V. Ramanchandra Reddy, "Response of Clamped Sandwich Panels with Viscoelastic Core under Random Acoustic Excitation", Journal of Sound and Vibration, 75(4), 1981, 481-494.
- [28] D. W. James, "High Damping Metals for Engineering Applications", Matr. Sci. Eng., Vol.4, 1969, 1-8.
- [29] V. Vandeuren, R. Snoeys and J. Peters, "Additive Damping Treatments for Mechanical Structures", Annals of the CIRP, Vol.30/1, 1981, 269-274.
- [30] R. G. Hannam, "A Case Study on a Use of an Aneorobic Adhesives in Machine Tool Assembly", Proceedings of the 22nd International M.T.D.R. Conference, 1981, 109-117.
- [31] M. Yoshimura, "Computer-Aided Design Improvement of a Machine Tool Structure Incorporating Joint Dynamics Data", Annals of the CIRP, Vol.28/1, 1979, 241-244.
- [32] T. Sata and et al, "Development of Machine Tool Structure Analsis Program (MASAP)", Annals of the CIRP, Vol.25/1, 1976, 287-290.
- [33] Y. Ito and M. Tsutsumi, "Determination of Mathematical Models in Structural Analysis of

- Machine Tool", Bulletin of the JSME, Vol.24, No.198, 1981, 2234-2239.
- [34] R. H. Thornley and K. Lees, "Some Static and Dynamic Characteristics of Bonded, Machined Joint Faces", Proceedings of the 13th International M.T.D.R. Conference, 1972, 79-86.
- [35] Y. Ito, "A Contribution of the Effective Range of the Preload on a Bolted Joint", Proceedings of the 14th International M.T.D.R. Conference, 1973, 503-507.
- [36] S. N. Shoukry and R. H. Thorney, "Theoretical Expressions for the Normal and Tangential Stiffness of Machine Tool Joints", Proceedings of the 22nd International M.T.D.R. Conference, 1981, 131-138.
- [37] R. E. Schofield, "The Damping Effect of Joints Formed from Machined Surfaces—the State of Art", Proceedings of the 13th International M.T.D.R. Conference, 1972, 75-77.
- [38] N. Back, M. Burdekin and A. Cowley, "Review of the Research on Fixed and Sliding Joints", Proceedings of the 13th International M.T.D.R. Conference, 1972, 87-97.
- [39] R. E. Schofield and R. H. Thornley, "Calculating the Elastic and Plastic Components of Deflection of Joints Formed from Machined Surfaces with Flatness Errors", Proceedings of the 13th International M.T.D.R. Conference, 1972, 67-73.

- [40] C. Dekoninck, "Experimental Study of the Normal Static Stiffness of Metallic Contact Surfaces of Joints", Proceedings of the 13th International M.T.D.R. Conference, 1972, 61-66.
- [41] A. C. Aubert, E. F. Crawley and K. J. O'Donnell, Measurement of the Dynamic Properties of Joints in Flexible Space Structures, Engineers Degree Thesis, Aeronautics and Astronautics Dept., MIT, Sept., 1983.
- [42] Y. Shuzi, "A Study of the Static Stiffness of Machine Tool Spindles", Int. J. Mach. Tool Des. Res., Vol.21, No.1, 1981, 23-40.
- [43] S. C. Singhvi, C. Balasubrahmanyam, N. K. Seth and A. K. Gungopadhyay, "Functional Optimization of Spindle Bearing Systems", Annals of the CIRP, Vol.29/1, 1980, 263-268
- [44] F. Ismail and J. Tlustý, "Dynamics of a Workpiece Clamped on a Lathe", Proceedings of the 8th North American Manufacturing Research Conference, 1980, 388-394.
- [45] C. Reugg and J. Habermeir, "Composite Propeller Shafts Design and Optimization", Advances in Composite Materials, ICCM3, 3rd International Conference on Composite Materials, Paris, France, 1980, Vol.2, 1740-1755.
- [46] J. C. Heine, The Stress and Frequency Dependence of Material Damping in Some Engineering Alloys, Ph.D.

- Thesis, Mech. Engineering Dept., MIT, 1966.
- [47] P. L. Vorlicek, Material Damping of Aluminum and Graphite/Epoxy in a Simulated Zero-Gravity Environment, S.M. Thesis, Aeronautics and Astronautics Dept., MIT, 1981.
- [48] R. D. Adams, "The Damping Characteristics of Certain Steels, Cast Irons and Other Metals", *Journal of Sound and Vibration*, Vol.23, 1972, 199-216.
- [49] E. F. Crawley and D. G. Mohr, "Experimental Measurements of Material Damping in Free Fall with Tuneable Excitation", Presented at AIAA/ASME/ASCE/AHS Structures. Structural Dynamics and Materials Conference Paper No.83-0858-CP.
- [50] R. M. Jones, Mechanics of Composite Materials, McGraw-Hill, Inc., 1975, Chap.1, Chap.2.
- [51] Air International (Weekly Magazine) GG70383, Vol.26, No.4, 1984.
- [52] Aviation Week and Space Technology (Weekly Magazine), April 30, 1984.
- [53] R. R. Craig, Jr., Structural Dynamics, John Wiley and Sons, 1981, Chap.10, Chap.4.
- [54] Hercules Composite Structures, Hercules Product Report.
- [55] J. C. Snowdon, Vibration and Shock in Damped Mechanical Systems, John Wiley and Sons Inc., 1968, Chap.1.
- [56] O. A. Johnson, Design of Machine Tools, Chilton Book Company, 1971, 229-235.

- [57] SNFA Bearing Catalog, 58th Street, Woodside, NY
11377, 2nd Edition, 32-35
- [58] Rahman and Y. Ito, "Some Necessary Conditions for the
Dynamic Performance Test Proposed by the MTIRA", Int.
J. Mach. Tool Des. Res. Vol.21, No.1, 1981, 1-10.
- [59] G. W. Long and J. R. Lemon, "Structural Dynamics
In Machine-Tool Chatter", Journal of Engineering for
Industry, Transactions of the ASME, November 1965,
455-463.
- [60] R. L. Kegg, "Cutting Dynamics In Machine Tool
Chatter", Journal of Engineering for Industry,
Transactions of the ASME, November 1965, 464-470
- [61] J. R. Lemon and P. C. Ackermann, "Application of
Self-Excited Machine-Tool Chatter Theory", Journal of
Engineering for Industry, Transactions of the ASME,
November 1965, 471-479.
- [62] F. M. Dimentberg, Flexural Vibrations of Rotating
Shafts, Butterworths, 1961, Chap.5.
- [63] E. J. Gunter, Jr., Dynamic Stability of Rotor-Bearing
Systems, NASA SP-113, 1963.
- [64] S. H. Crandall and et al, An Introduction to the
Mechanics of Solids, McGraw-Hill, Inc., 1972, Chap.3.
- [65] S. Timoshenko, Strength of Materials, Part 1, D. Van
Nostrand Company, Inc., 1963, 170-174.
- [66] G. R. Cowper, " The Shear Coefficient in Timoshenko's
Beam Theory", Journal of Applied Mechanics,

- Transactions of ASME, June, 1966, 335-340.
- [67] S. B. Dong, K. S. Pister and R. L. Taylor, "On the Theory of Laminated Anisotropic Shells and Plates", Journal of the Aerospace Sciences, Vol.29, 1962, 969-975.
- [68] M. Stein, "Nonlinear Theory for Laminated and Thick Plates and Shells Including the Effects of Transverse Shearing", AIAA/ASME/ASCE/AHS 26th Structures, Structural Dynamics and Material Conference, April 15-17, 1985, 259-266.
- [69] S. B. Dong, "Free Vibration of Laminated Orthotropic Cylindrical Shells", The Journal of the Acoustical Society of America, Vol.44, No.6, 1968, 1629-1635.
- [70] K. N. Shivakumar and A. V. Krishna Murty, "Vibrations of Multifiber Composite Shells - Some Numerical Results", J. Struct. Mech., 4(4), 1976, 379-393.
- [71] J. D. Ferry, Viscoelastic Properties of Polymers, John Wiley and Sons, Inc., 1980, 606-609.
- [72] P. S. Houghton, Ball and Roller Bearings, Applied Science Publishers LTD, London, 1976, 102.
- [73] D. F. Wilcock and E. R. Booser, Bearing Design and Application, McGraw-Hill Book Company, 1957, Chap.4.
- [74] F. Koenigsberger, Design Principles of Metal-Cutting Machine Tools, The Macmillan Company, 1964, 44-45.

- [75] S. H. Crandall, "The Role of Damping in vibration Theory", Journal of Sound and Vibration, 11(1), 1970, 3-18.
- [76] T. L. H. Walford and B. J. Stone, "Some Damping and Stiffness Characteristics of Angular Contact Bearings Under Oscillating Radial Load", I Mech E Conference Publications, 1980-4, 1980, 157-162.

Appendix A : Definitions of Damping Parameters

Several commonly encountered damping parameters are defined in this appendix, as are the relationships among them.

1. The damping factor, loss factor or loss coefficient, η is defined as

$$\eta = \frac{\Delta U}{2\pi U_{\max}}$$

ΔU being the energy dissipated per cycle and U_{\max} , the maximum potential energy stored in the system.

2. The quality factor, Q also called the dynamic amplification factor is the inverse of the damping factor, or

$$Q = \frac{2\pi U_{\max}}{\Delta U}$$

3. The specific damping capacity ψ is defined as

$$\psi = \frac{\Delta U}{U_{\max}}$$

4. The fraction (or ratio) of critical damping, ζ is one half the damping factor

$$\zeta = \frac{\Delta U}{4\pi U_{\max}}$$

5. The log decrement, δ is the logarithm of the ratio of two response peaks of a system undergoing free vibration

$$\delta = \frac{1}{n} \log \frac{x_m}{x_{m+n}}$$

where x_m and x_{m+n} are amplitudes of the m and $m+n$ th peaks, respectively and n is the number of cycles between these peaks. It can be shown for a simple spring-mass-damper system that δ and the fraction of critical damping ζ are thus related.

$$\delta = \frac{2\pi\zeta}{\sqrt{1-\zeta^2}}$$

For $\zeta \ll 1$, the above expression reduces to

$$\delta \approx 2\pi\zeta$$

6. For systems with potential energy stored in the form of strain energy, the complex modulus E' can be used to express both energy stored and dissipated, since

$$E' = E + i E''$$

where E is the real or elastic modulus and E'' is the loss or dissipation modulus. The damping factor is related to E' thus

$$\eta = \frac{E''}{E}$$

Finally, the relationship among the various parameters is

$$\eta = \frac{1}{Q} = \frac{\psi}{2\pi} = \frac{E''}{E} = 2\zeta \approx \frac{\delta}{\pi}$$

Appendix B : Calculation of the Material Properties of the Graphite Epoxy Composite Spindle

B.1 The General Theory

The graphite fiber used for the spindle is high modulus Cellon G-50 : Its tensile modulus is 345 GPa. The epoxy used in making the composite is Fiberite 9481. When 40 % epoxy resin is added, the composite has the following engineering properties.

$$E_L = 207 \text{ GPa (30 Mpsi)} \quad (\text{B.1})$$

$$E_T = 7.85 \text{ GPa (1.14 Mpsi)} \quad (\text{B.2})$$

$$\nu_{LT} = 0.28 \quad (\text{B.3})$$

$$G_{LT} = 4.48 \text{ GPa (0.65 Mpsi)} \quad (\text{B.4})$$

$$\alpha_{11}^* = -0.54 \times 10^{-6}/\text{K} \quad (-0.3 \times 10^{-6}/^{\circ}\text{F}) \quad (\text{B.5})$$

$$\alpha_{22}^* = 25.2 \times 10^{-6}/\text{K} \quad (14 \times 10^{-6}/^{\circ}\text{F}) \quad (\text{B.6})$$

$$\alpha_{12}^* = 0 \quad (\text{B.7})$$

$$\rho = 1.6 \times 10^3 \text{ kg/ m}^3 \quad (\text{B.8})$$

From these properties, the unidirection ply properties can be calculated by the Classical Composite Laminate Theory [B.1, B.2].

$$v_{TL} = \frac{v_{LT} E_T}{E_L} = 0.0106 \quad (\text{B.9})$$

$$E_{1111}^* = \frac{E_L}{1 - v_{LT} v_{TL}} = 207 \text{ GPa} \quad (30.1 \text{ Mpsi}) \quad (\text{B.10})$$

$$E_{2222}^* = \frac{E_T}{1 - v_{LT} v_{TL}} = 7.85 \text{ GPa} \quad (1.14 \text{ Mpsi}) \quad (\text{B.11})$$

$$E_{1122}^* = \frac{v_{LT} E_T}{1 - v_{LT} v_{TL}} = 2.20 \text{ GPa} \quad (0.32 \text{ Mpsi}) \quad (\text{B.12})$$

$$E_{1212}^* = G_{LT} = 4.48 \text{ GPa} \quad (0.65 \text{ Mpsi}) \quad (\text{B.13})$$

From the above results the invariant properties of the ply are as follows :

$$I_1 = \frac{1}{4} (E_{1111}^* + E_{2222}^* + 2E_{1122}^*) = 54.9 \text{ GPa} \quad (7.97 \text{ Mpsi}) \quad (\text{B.14})$$

$$I_2 = \frac{1}{8} (E_{1111}^* + E_{2222}^* - 2 E_{1122}^* + 4 E_{1212}^*) = 28.6 \text{ GPa} \quad (4.15 \text{ Mpsi}) \quad (\text{B.15})$$

$$R_1 = 1/2 (E_{1111}^* - E_{2222}^*) = 99.8 \text{ GPa} \quad (14.48 \text{ Mpsi}) \quad (\text{B.16})$$

$$R_2 = 1/8 (E_{1111}^* + E_{2222}^* - 2 E_{1122}^* - 4 E_{1212}^*) = 24.1 \text{ GPa} \quad (3.50 \text{ Mpsi}) \quad (\text{B.17})$$

The Young's moduli of the composite ply with angle θ are as follows.

$$E_{1111}^{[\theta]} = I_1 + I_2 + R_1 \cos(2\theta) + R_2 \cos(4\theta) \quad (\text{B.18})$$

$$E_{2222}^{[\theta]} = I_1 + I_2 - R_1 \cos(2\theta) + R_2 \cos(4\theta) \quad (\text{B.19})$$

$$E_{1122}^{[\theta]} = I_1 - I_2 - R_2 \cos(4\theta) \quad (\text{B.20})$$

$$E_{1212}^{[\theta]} = I_2 - R_2 \cos(4\theta) \quad (\text{B.21})$$

$$E_{1112}^{[\theta]} = 1/2 R_1 \sin(2\theta) + R_2 \sin(4\theta) \quad (\text{B.22})$$

$$E_{2212}^{[\theta]} = 1/2 R_1 \sin(2\theta) - R_2 \sin(4\theta) \quad (\text{B.23})$$

Table B.1 shows the Young's moduli of the ply with several winding angles

The tensor for stretching are defined as follows.

$$A_{\alpha\beta\gamma} = \sum_i t_{ply}^{[\theta_i]} E_{\alpha\beta\gamma}^{[\theta_i]} \quad (B.24)$$

The thermal expansion coefficients of plies are expressed as

$$\alpha_{11}^{[\theta]} = \alpha_{11}^* \cos^2 \theta + \alpha_{22}^* \sin^2 \theta \quad (B.25)$$

$$\alpha_{22}^{[\theta]} = \alpha_{11}^* \sin^2 \theta + \alpha_{22}^* \cos^2 \theta \quad (B.26)$$

$$\alpha_{12}^{[\theta]} = (\alpha_{11}^* - \alpha_{22}^*) \sin \theta \cos \theta \quad (B.27)$$

The ply thermal influence coefficients are defined as

$$\Gamma_{\alpha\beta}^{[\theta]} = E_{\alpha\beta\gamma}^{[\theta]} \alpha_{\sigma\gamma}^{[\theta]} \quad (B.28)$$

The laminate thermal influence coefficients are expressed as

$$\gamma_{\alpha\beta}^L = \sum_i \Gamma_{\alpha\beta}^{[\theta_i]} t_{ply}^{[\theta_i]} \quad (B.29)$$

Then the thermal expansion coefficients of a laminate are expressed as

$$\alpha_{\alpha\beta}^L = A_{\alpha\beta\gamma}^{-1} \gamma_{\sigma\gamma}^L \quad (B.30)$$

Table B.1 Young's Moduli of the Plies with Several Winding Angles

| GPa | 0° | 5° | 10° | 15° | -5° |
|--------------------|------|-------|------|------|--------|
| $E_{1111}[\theta]$ | 207 | 205 | 196 | 182 | 205 |
| $E_{2222}[\theta]$ | 7.85 | 7.92 | 8.20 | 9.16 | 7.92 |
| $E_{1122}[\theta]$ | 2.20 | 3.65 | 7.85 | 14.3 | 3.65 |
| $E_{2112}[\theta]$ | 4.48 | 5.93 | 10.1 | 16.5 | 5.93 |
| $E_{1112}[\theta]$ | 0.0 | 16.9 | 32.6 | 45.8 | -57.4 |
| $E_{2212}[\theta]$ | 0.0 | 0.413 | 1.58 | 4.07 | -0.413 |

B.2 Numerical Examples

(1) IF we use $[\pm 5]_s$ winding angle, the several properties can be calculated as follows ($t_{\text{ply}} = 0.135 \text{ mm}$).

$$A_{1111} = 2 \times 0.135 \text{ mm} \times 2 \times 205 \text{ GPa} = 111 \text{ MN/m} \quad (0.618 \text{ Mlb/in})$$

$$A_{2222} = 2 \times 0.135 \text{ mm} \times 2 \times 7.92 \text{ GPa} = 4.28 \text{ MN/m} \quad (0.024 \text{ Mlb/in})$$

$$A_{1122} = 2 \times 0.135 \text{ mm} \times 2 \times 3.65 \text{ GPa} = 1.97 \text{ MN/m} \quad (0.011 \text{ Mlb/in})$$

$$A_{1212} = 2 \times 0.135 \text{ mm} \times 2 \times 5.93 \text{ GPa} = 3.20 \text{ MN/m} \quad (0.018 \text{ Mlb/in})$$

$$A_{1112} = A_{2212} = 0$$

Then the laminate engineering properties are calculated

as follows.

$$E_L^L = \frac{1}{h} \left[A_{1111} - \frac{(A_{1122})^2}{A_{2222}} \right] = 205 \text{ GPa} \quad (29.7 \text{ Mpsi})$$

$$E_T^L = \frac{1}{h} \left[A_{2222} - \frac{(A_{1122})^2}{A_{1111}} \right] = 7.85 \text{ GPa} \quad (1.14 \text{ Mpsi})$$

$$G_{LT}^L = \frac{1}{h} A_{1212} = 5.93 \text{ GPa} \quad (0.86 \text{ Mpsi})$$

$$\alpha_{11}^L = -0.70 \times 10^{-6} / \text{K}$$

$$\alpha_{22}^L = 24.8 \times 10^{-6} / \text{K}$$

$$\alpha_{12}^L = 0$$

(2) By the same method, if we use $[\pm 10]_s$ winding angle, the laminate engineering properties are calculated as follows :

$$A_{1111} = 106 \text{ MN/m} \quad (0.591 \text{ Mlb/in})$$

$$A_{2222} = 4.43 \text{ MN/m} \quad (0.025 \text{ Mlb/in})$$

$$A_{1122} = 4.24 \text{ MN/m} \quad (0.024 \text{ Mlb/in})$$

$$A_{1212} = 5.48 \text{ MN/m} \quad (0.031 \text{ Mlb/in})$$

$$A_{1112} = A_{2212} = 0$$

$$E_L^L = 188 \text{ GPa} \quad (27.3 \text{ Mpsi})$$

$$E_T^L = 7.99 \text{ GPa} \quad (1.16 \text{ Mpsi})$$

$$G_{LT}^L = 10.3 \text{ GPa} \quad (1.49 \text{ Mpsi})$$

$$\alpha_{11}^L = -1.22 \times 10^{-6} / \text{K}$$

$$\alpha_{22}^L = 23.9 \times 10^{-6} / \text{K}$$

$$\alpha_{12}^L = 0$$

(3) If we use $[\pm 15]_s$ winding angle, the laminate engineering properties as follows :

$$A_{1111} = 98.3 \text{ MN/m} \quad (0.549 \text{ Mlb/in})$$

$$A_{2222} = 4.95 \text{ MN/m} \quad (0.028 \text{ Mlb/in})$$

$$A_{1122} = 7.72 \text{ MN/m} \quad (0.043 \text{ Mlb/in})$$

$$A_{1212} = 0.027 \text{ MN/m} \quad (0.050 \text{ Mlb/in})$$

$$A_{1112} = A_{2212} = 0$$

and

$$E_L^L = 160 \text{ GPa} \quad (23.2 \text{ Mpsi})$$

$$E_T^L = 8.13 \text{ GPa} \quad (1.18 \text{ Mpsi})$$

$$G_{LT}^L = 16.5 \text{ GPa} \quad (2.40 \text{ Mpsi})$$

$$\alpha_{11}^L = -1.98 \times 10^{-6} / \text{K} \quad (-1.1 \times 10^{-6} / ^\circ\text{F})$$

$$\alpha_{22}^L = 22.3 \times 10^{-6} / \text{K} \quad (12.4 \times 10^{-6} / ^\circ\text{F})$$

$$\alpha_{12}^L = 0$$

REFERENCES :

- [B.1] R. M. Jones, Mechanics of Composite Materials, McGraw-Hill, Inc., 1975.
- [B.2] S. W. Tsai and H. T. Hahn, Introduction to Composite Materials, Technomic Publishing Company, Westport, Connecticut 06880, 1980.

Appendix C : Calculation of the Power and Torque Capability of Adhesive Bonded Joint

The theoretical model, which was developed by R. D. Adams [69], is used to calculate the power and torque capability of the epoxy adhesive bonded joint.

The joint under consideration is shown in Fig. C.1. The adhesive shear stress is given by Equation (C.1).

$$\tau_a = \frac{T\alpha}{2\pi a^2} \left[\left(\frac{1-\psi(1-\cosh\alpha l)}{\sinh\alpha l} \right) \cosh\alpha z - \psi \sinh\alpha z \right] \quad (C.1)$$

where

$$\delta = \frac{2\pi a^2 r_1 G_a}{G_1 J_1 t} \quad (C.2)$$

$$\psi = \frac{G_2 J_2 r_1}{r_2 G_1 J_1 + r_1 G_2 J_2} \quad (C.3)$$

$$\alpha = \left(\frac{\delta}{\psi} \right)^{\frac{1}{2}} \quad (C.4)$$

$$a = \frac{r_1 + r_2}{2} \quad (C.5)$$

The maximum stress in the adhesive which occurs at $z=0$ and $z=l$ is expressed by Equation (C.6).

$$\tau_a = \frac{T}{2\pi a^2} \frac{1-\psi(1-\cosh\alpha l)}{\sinh\alpha l} \quad (C.6)$$

The torque capability is calculated from Equation (C.6).

$$T = \frac{2\pi a^2 \tau_a}{\alpha} \frac{\sinh\alpha l}{\psi \cosh\alpha l + 1 - \psi} \quad (C.7)$$

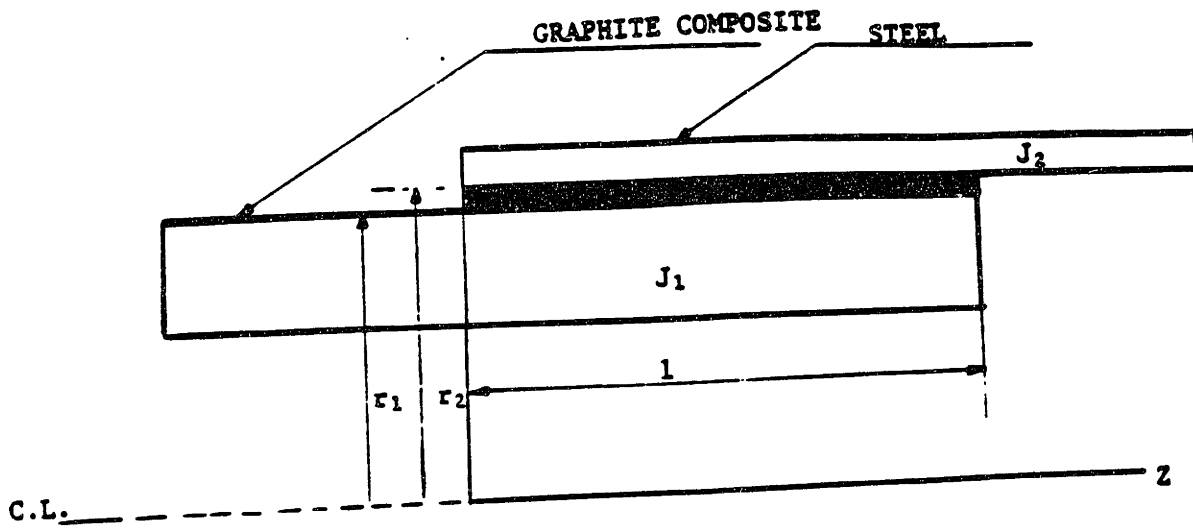


Fig. C.1 Theoretical Model of the Epoxy Adhesive Bonded Joint

Fig. C.2 shows the shear stress distribution, which are the result of applying a torque to the joints. In addition to the closed-form theory (Equation C.1), the shear stress distribution, which are calculated by the finite element method with different shapes and boundary conditions of the joint, are presented in Fig. C.2 also.

The numerical results with the design values of the graphite epoxy composite spindle are as follow.

- (1) If we use the graphite epoxy composite which is wound [± 15]s,

$$G_a = 1.03 \text{ GPa} \quad (1.5 \times 10^5 \text{ psi})$$

$$\tau_a = 34.5 \text{ MPa} \quad (5.0 \times 10^3 \text{ psi})$$

$$t = 0.203 \text{ mm} \quad (0.008 \text{ in})$$

$$r_1 = 31.29 \text{ mm} \quad (1.232 \text{ in})$$

$$r_2 = 31.32 \text{ mm} \quad (1.233 \text{ in})$$

$$a = \frac{r_1 + r_2}{2} = 31.31 \text{ mm} \quad (1.2325 \text{ in})$$

$$G_1 = 16.5 \text{ GPa} \quad (2.4 \times 10^6 \text{ psi})$$

$$G_2 = 68.9 \text{ GPa} \quad (10 \times 10^6 \text{ psi})$$

$$J_1 = \frac{\pi}{2} (31.29^4 - 21.34^4) = 1.18 \times 10^6 \text{ mm}^4 \quad (2.836 \text{ in}^4)$$

$$J_2 = \frac{\pi}{2} (33.34^4 - 31.50^4) = 3.94 \times 10^5 \text{ mm}^4 \quad (0.930 \text{ in}^4)$$

$$l = 66.7 \text{ mm} \quad (2.625 \text{ in})$$

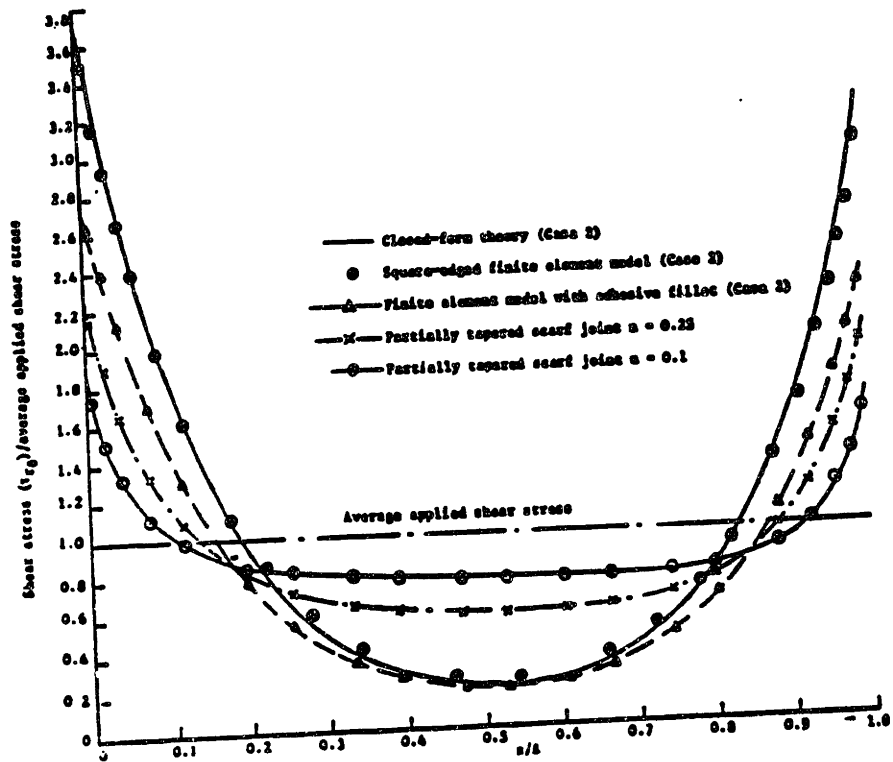


Fig. C.2 Shear Stress Distributions in Tubular Lap and Scarf Joints Subjected to Torque

$$\text{Then } \delta = \frac{2\pi a^2 r_1 G_a}{G_1 J_1 t} = 4.61 \times 10^{-2} / \text{mm}^2 \quad (29.75 / \text{in}^2)$$

$$\psi = \frac{G_2 J_2 r_1}{r_2 G_1 J_1 + r_1 G_2 J_2} = 0.5748$$

$$\alpha = \left(\frac{\delta}{\psi}\right)^{1/2} = 0.283 / \text{mm} \quad (7.194 / \text{in})$$

$$T = \frac{2\pi a^2 \tau_a}{\alpha} \cdot \frac{\sinh \alpha l}{\psi \cosh \alpha l + 1 - \psi} = 1.31 \times 10^3 \text{ N m} \quad (9.689 \times 10^2 \text{ lb ft})$$

If the motor speed is 1000 rpm, the horse power is

$$\text{HP} = T \cdot \omega = 138 \text{ kW} \quad (185 \text{ HP})$$

(2) If we use the graphite epoxy composite which is wound $[\pm 10]_s$,

$$G_1 = 10.3 \text{ GPa} \quad (1.5 \times 10^6 \text{ psi})$$

$$\delta = 7.43 \times 10^{-2} / \text{mm}^2 \quad (47.92 / \text{in}^2)$$

$$\psi = 0.686$$

$$\alpha = 0.329 / \text{mm} \quad (8.360 / \text{in})$$

$$T = 9.44 \times 10^2 \text{ N m} \quad (0.836 \times 10^4 \text{ lb in})$$

If the motor speed is 1000 rpm, the horse power is

$$\text{HP} = T \cdot \omega = 99.2 \text{ kW} \quad (133 \text{ HP})$$

(3) If we use the graphite epoxy composite which is wound [+ 5]s,

$$G_1 = 5.93 \text{ GPa} \quad (0.86 \times 10^6 \text{ psi})$$

$$\delta = 0.129/\text{mm}^2 \quad (83.02 / \text{in}^2)$$

$$\psi = 0.790$$

$$\alpha = 0.404/\text{mm} \quad (10.25 / \text{in})$$

$$T = 6.71 \times 10^2 \text{ N m} \quad (0.594 \times 10^4 \text{ lb in})$$

If the motor speed is 1000 rpm, the horse power is

$$HP = T \cdot \omega = 70.9 \text{ kW} \quad (95 \text{ HP})$$

From the above results, we can see that the power transmitting capability of the epoxy adhesive joint becomes lower as we decrease the winding angle of the graphite fiber. However, the power transmitting capability can be increased if we reduce the torsional stiffness of the steel sleeves or design the tapered scarf sleeves.

Appendix D : Properties of Hysol EA9309.2 Adhesive

EA 9309.2 High Tensile Shear and Peel Strength at Moderate Temperatures

DESCRIPTION

HYSOL Adhesive EA 9309.2 consists of a white epoxy paste (Part A), and a blue liquid curing agent (Part B). EA 9309.2 bonds metal skins and honeycomb core to yield tough permanently flexible joints that resist humidity, water and most common fluids. Its outstanding feature is high shear and peel strength on aluminum bonds at moderate temperatures.

PROPERTIES

Viscosity at 77°F:

Part A — approximately 4,000 poise (Brookfield, HBT, #7 Spindle, 20 Rpm)

Part B — approximately 0.5 poise (Brookfield, LVF, #1 Spindle, 60 Rpm)

Storage Stability:

At least 1 year at 77°F for separate components.

TYPICAL CURED PROPERTIES

The following data were obtained on chromic acid etched 2024-T3 clad aluminum. The adhesive was cured for 5 days at 77°F. Specimens employed the following metal thicknesses:

Tensile Lap Shear: 0.063 inch, 0.5 inch overlap bond, one inch wide.

90° Bell-Peel: 0.025 to 0.063 inch, 0.5 inch wide.

180° T-Peel: 0.020 inch, 1 inch wide.

Climbing Drum: 0.020 to 0.063 inch, 1 inch wide.

Lap Shear Strength vs. Temperature.

| | | | | | |
|-----------------------------|------------|-----------|------------|------------|------------|
| <u>Test Temperature °F:</u> | <u>-67</u> | <u>77</u> | <u>180</u> | <u>250</u> | <u>350</u> |
| Lap shear strength (psi): | 4,700 | 5,000 | 1,150 | 720 | 600 |

Peel Strength vs. Test Method. The effects of three test methods are compared below for room temperature performance:

| | | | |
|---------------------|-----------------|---------------|----------------------|
| <u>Test Method:</u> | <u>90° Peel</u> | <u>T-Peel</u> | <u>Climbing Drum</u> |
| Peel Value at 77°F: | 69 pli | 42 pli | 75 in. lb./in. |

Peel Strength vs. Temperature. Effect of temperature on T-Peel strength is shown below:

| | | | |
|-----------------------------|------------|-----------|------------|
| <u>Test Temperature °F:</u> | <u>-67</u> | <u>77</u> | <u>180</u> |
| Strength, lb./in. | 10 | 42 | 9 |

Appendix E : Dependence of the Metal Cutting Performance on the Damping and Stiffness of a Machine Tool [4].

The geometry of a two-dimensional, or orthogonal, cutting operation is shown simplified in Fig. E.1. The relative displacements of the tool and the workpiece are $x(t)$ and $y(t)$, respectively. The + x-direction is taken as the outwardly directed normal to the finished surface. Thus, the vibrating machine tool produces a surface undulation equal to $x(t)$.

In Fig. E.2, the resultant cutting force $R(t)$ is shown resolved into its two components $F_p(t)$ and $F_q(t)$. There is good reason to believe that the thermoplasticity relationships which define the dependence of $R(t)$ on $x(t)$ and $y(t)$ will involve only x , \dot{x} and \dot{y} and not \ddot{x} , \ddot{y} , etc. Hence, for the variation of forces, we will write

$$dF_p = \frac{\partial F_p}{\partial x} dx + \frac{\partial F_p}{\partial \dot{x}} d\dot{x} + \frac{\partial F_p}{\partial \dot{y}} d\dot{y}$$

Since the vertical force F_p can be written

$$F_p = uDs$$

where

u = energy per unit volume, psi

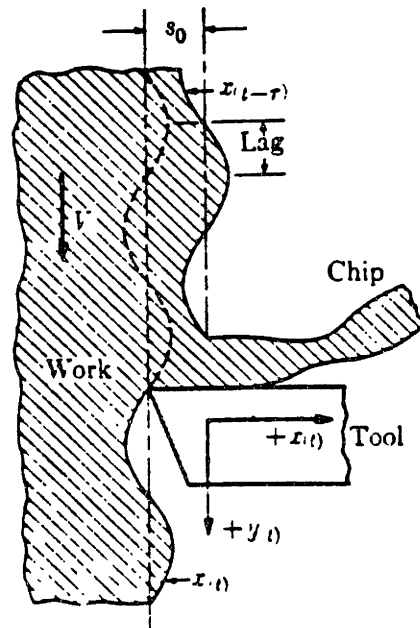


Fig. E.1 Geometry of an Idealized Dynamic Cutting Process

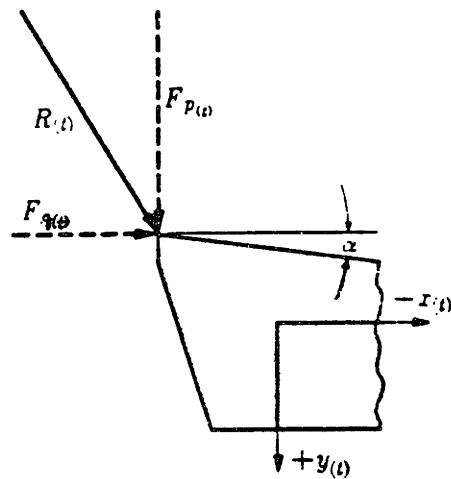


Fig. E.2 Force Relationships for Vibrating Machine Tool

D = width of cut, inch

s = feed rate, inch

Therefore,

$$\frac{\partial F_p}{\partial s} = D \left(u + s \frac{\partial u}{\partial s} \right)$$

In general u varies as the -0.2 power of the feed s ;
hence, $s \frac{\partial u}{\partial s} = -0.2u$, and

$$\frac{\partial F_p}{\partial s} = \frac{\Delta F_p}{\Delta x} = 0.8 Du$$

When only x is varied, $\dot{x} = \dot{y} = 0$, the direction R is essentially constant. Since $F_p \approx R$ in the metal cutting process, we can write

$$\frac{\Delta R}{\Delta x} \approx 0.8 Du$$

From the vibration theory for the one degree of freedom,

$$\frac{\Delta A}{\Delta R} = \frac{1}{k \sqrt{[1 - (\omega/\omega_n)^2]^2 + (2\zeta\omega/\omega_n)^2}}$$

where A is the amplitude of the vibration in the direction of R and k is the stiffness in the same direction. If $\omega/\omega_n = 1$ for the instability

$$\Delta A/\Delta R = 1/(2\zeta k)$$

If the angle between the resultant displacement and the x-direction is γ ,

$$x = \cos\gamma \cdot A$$

Therefore,

$$\frac{\Delta A}{\Delta R} = \frac{\Delta x}{\cos\gamma \cdot \Delta R} \approx \frac{1}{0.8 \Delta u} \cdot \frac{1}{\cos\gamma} = \frac{1}{2\zeta k}$$

$$\text{hence, } D_{\max} \approx \frac{2\zeta k}{0.8 u \cdot \cos\gamma} \quad (D_{\max} \equiv D)$$

BIOGRAPHY

Dai Gil Lee was born in Korea on January 19, 1952.

He graduated from Seoul National University in Korea with a B.S. in mechanical engineering in February, 1975. He received a M.S. in mechanical engineering from Korea Advanced Institute of Science and Technology in February 1977. He remained at the Institute for a year as a Ph. D student to conduct research in fluid mechanics.

After this study, Dai Gil taught fluid mechanics, thermodynamics and engineering mathematics at Busan National University in Korea as a full time instructor (March 1977 - March 1981) and an assistant professor (April 1981 - December 1981).

He returned to Korea Advanced Institute of Science and Technology and worked as a research scientist from January 1982 to August 1982.

Dai Gil came to MIT in September 1982 on an United Nations Fellowship.

Dai Gil Lee has been married to Og Heul since 1978 and has a son, Dong Gyu.